

THE STRESS STRAIN RESPONSE OF CONCRETE LATERALLY CONFINED
WITH LOW AND HIGH PERFORMANCE FIBER- REINFORCED CEMENTS
AND POLYMER COMPOSITES
A COMPARATIVE EXPERIMENTAL AND THEORETICAL STUDY

A Thesis
Presented to
The Faculty of Engineering
At Notre Dame University-Louaize

In Partial Fulfillment
Of the Requirements for the Degree of
Masters of Science in Civil Engineer

By
Rawan Osmat Sarieldine

July 2020

© COPYRIGHT

By

Ms. Rawan O. Sarieldine

Dr. Sary A. Malak

2020

All Rights Reserved

Notre Dame University - Louaize
Faculty of Engineering

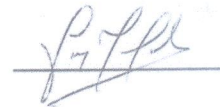
Department of Civil and Environmental Engineering

We hereby approve the thesis of

Rawan Osmat Sarieldine

Candidate for the Masters of Science in Civil Engineering

Signature



Dr. Sary Malak

Supervisor, Chair

Signature



Dr. Talal Salem

Committee Member

Signature



Dr. Gerard-Philippe Zehil.

Committee Member

DEDICATED TO

“My family, loved ones, committee NDU members who have encouraged me throughout the journey; at the end I want to dedicate this thesis to my supervisor Dr. Malak Sary who helped me achieve and gain all this knowledge that I hold today.”

ACKNOWLEDGEMENTS

I would like to thank my thesis advisor Dr. Sary A. Malak for his work and effort. His office door was always open whenever I have run into troubles, spot or had questions about my research. He consistently steered me in the right direction whenever he thought I needed it. In addition, holding the deepest gratitude, for helping in providing the required materials needed for the research.

Thanks to Ms. Yara Maalouf and Mr. Elie Lahoud for their unlimited assistance and efforts during the laboratory experiments, Mr. Ghassan G. Hachem,; representative of Fibrwrap Company, for his help regarding fiber reinforced polymer products and application process, and Baekert, and Holcim for supplying the steel fibers and micro silica, superplasticizers additives, respectively.

Further thanks goes to the committee members; Dr. Talal Salem and Dr. Gerard-Philippe Zehil for their contributions to the improvement of my research proposal and my thesis.

At the End, I would like to add a special thanks to NDU family that has accepted my GTA scholarship throughout my Master's program. I am gratefully indebt for their financial support, because without this help I would not be able to hold my graduate degree today.

ABSTRACT

While concrete, steel and Fiber Reinforced Polymer (FRP) jackets are the most commonly used types of jackets in the industry to confine columns, the focus of this research is to study and compare the compressive behavior of concrete cylinders confined with different types of fibrous composites; including Fiber Reinforced Concrete (FRC), Fiber Reinforced Mortar (FRM), and Slurry Infiltrated Fiber Concrete (SIFC). This study will provide a broad understanding of the behavior of the different confinement types used to retrofit columns to resist detrimental loads including blast and impact. The study will compare the compressive stress-strain response of different fibrous confinements to the commonly used ones such as FRP and spirals (SP), by developing empirical models to be used in design.

The confinements are classified as either continuous or discrete. Continuous confinement is when the composite is wrapped continuously around the structural members such as FRP, FRC, FRM, and SIFC while in discrete confinements they are spaced at a specific pitch such as spirals (SP) and wire mesh (WIM). The purpose of studying different types of fibrous confinements such as FRC and SIFC is to better understand their response with respect to the continuity and orientation of fibers. As for studying WIM confinement, was to understand the effect of two-fiber orientation as well as their interaction (WIM being the “bounding” case with “fibers” being oriented only in the vertical and the horizontal direction).

The ultimate goal of this research is to investigate, understand, and develop the overall stress-strain and load-displacement (i.e. resistance and ductility) response model of columns confined with different fibrous composites. The developed compressive stress-strain behavior will be compared to the existing Spiral Reinforcement (SP) and FRP

confinement used commonly in the industry, to be able to select the most suitable, and appropriate retrofit technique, and to be able to design from an engineering standpoint.

This research is achieved through an experimental and analytical investigation

Models developed in this work have shown good agreement with experimental data.

High Performance Fiber Reinforced Concrete (HPFRC) jackets made with continuous fibers exhibited debonding and multiple cracking leading to softening effects beyond peak and higher strains at rupture, which translates into an increase in ductility, and energy dissipation of the confined column. Varying orientation of fibers in FRC and FRM jackets produce radial tensile stresses on the concrete core resulting in partial confinement, thus weakening the concrete core and developing peak stresses lower than unconfined concrete. However due to fiber pull-out, they have higher ductility and maintain softening effects beyond peak and rupture strains better than unconfined concrete.

Keywords: Continuous composites, discrete composites, high performance composites, low performance composites, stress-strain response, first crack stress and strain, lateral confinement, multiple cracking, and activation region.

TABLE OF CONTENTS

I.	INTRODUCTION	1
II.	LITERATURE REVIEW	3
2.1	EXPERIMENTAL LITERATURE REVIEW	3
2.2	ANALYTICAL MODELING LITERATURE REVIEW.....	15
III.	EXPERIMENTAL PROGRAM	21
3.1	MATERIAL PROPERTIES	23
3.1.1	Fiber Reinforced Polymers	24
3.1.2	Steel Fiber Reinforcement	25
3.1.3	Wire Mesh.....	26
3.1.4	Spiral Reinforcement	27
3.2	TASKS & METHODOLOGY.....	28
3.2.1	Material Sampling/Mix Design.....	31
IV.	EXPERIMENTAL RESULTS.....	34
4.1	TYPICAL STRESS STRAIN CURVE OF CONFINED CONCRETE	34
4.1.1	Confinement Region	40
4.1.2	Transition Region	41
4.1.3	First Crack / Multiple Cracking Region of Composite	43
4.1.4	The fiber Debonding or Fiber Pull-Out Region.....	43
4.1.5	The Concrete Core First Crack Region.....	44
4.2	DISCUSSION OF CONFINED CONCRETE WITH DIFFERENT COMPOSITES	44
4.2.1	Low Performance Brittle Failure Composites (LPBF)	44
4.2.2	Low Performance Ductile Failure Composites (LPDF).....	46
4.2.3	High Performance Brittle Failure Composites (HPBF).....	47
4.2.4	High Performance Ductile Failure Composites (HPDF)	48
4.3	EXPERIMENTAL RESULTS AND DISCUSSION.....	49
4.3.1	Low Performance Brittle Failure Composites (LPBF)	52
4.3.2	Low Performance Ductile Failure Composites (LPDF).....	54
4.3.3	High Performance Brittle Failure Composites (HPBF).....	56
4.3.4	High Performance Ductile Failure Composites (HPDF)	58
4.3.5	Confinement Composites Analysis and Discussion.....	60
V.	THEORETICAL RESULTS.....	61
5.1	MODEL DEVELOPMENT.....	61
5.2	THEORETICAL RESULTS AND DISCUSSION	86

VI.	COMPARISON OF EXPERIMENTAL AND ANALYTICAL DATA	90
VII.	CONCLUSION AND RECOMMENDATION	99
VIII.	LIST OF NOTATIONS	106
IX.	REFERENCE	111
X.	APPENDIX I: EXPERIMENTAL RESULTS: GRAPHICAL AND TABULAR RESULTS	114
XI.	APPENDIX II: TENSILE STRESS STRAIN EQUATIONS FOR FIBROUS COMPOSITE CONFINEMENTS	138
XII.	APPENDIX III: GENERAL STRESS STRAIN MODEL FOR DISCRETE AND CONTINUOUS CONFINEMENTS	142
XIII.	APPENDIX IV: LOCATION OF THE PLASTIC CENTROID AND LATERAL STRESS FOR PARTIAL CONFINEMENT	147

LIST OF TABLES

Table II-1: Experimental Results-(Houssam et.al, 1999).....	6
Table III-1: CONC Mix Design I.....	28
Table III-2: FRM & SIFC Mix Design II	29
Table III-3: FRC Mix Design III	29
Table IV-1: Pre peak experimental data for longitudinal stress and strain of confined.....	50
Table IV-2: Post-peak experimental data for longitudinal stress and strain of confined concrete (symbols in parenthesis represent the composite parameters) (0.15 Ksi=1 MPa).....	50
Table IV-3: Pre-peak experimental data for longitudinal and transverse strains of confined concrete (symbols in parenthesis represent the composite parameters).....	51
Table IV-4: Post-peak experimental data for longitudinal and transverse strains of confined concrete (symbols in parenthesis represent the composite parameters) (0.15 Ksi=1 MPa).....	51
Table V-1: Factors used for peak stress and strain for confined concrete (0.15 Ksi=1 MPa) .	65
Table V-2: Fiber and matrix properties of lateral confinement (0.15Ksi=1 MPa, 1in.=2.54 cm)	70
Table V-3: Composite properties of lateral confinement (0.15 Ksi=1 MPa).....	70
Table V-4: Optimized thickness and spacing and related parameters (0.15Ksi=1 MPa, 1in.=2.54 cm).....	75
Table V-5: Parameters for regression lines for longitudinal strain versus transverse strain....	77
Table V-6 Pre-peak theoretical data for longitudinal stress and strain of confined concrete (0.15 Ksi=1 MPa)	88
Table V-7: Post-peak theoretical data for longitudinal stress and strain of confined concrete (symbols in parenthesis represent the relative composite parameters) (0.15 Ksi=1 MPa)	89
Table V-8: Pre-peak theoretical data for longitudinal and transverse strain of confined concrete (symbols in parenthesis represent the relative composite parameters).....	89
Table V-9: Post-peak theoretical data for longitudinal and transverse strain of confined concrete (symbols in parenthesis represent the relative composite parameters) (0.15 Ksi=1 MPa).....	90
Table X-1: Pre peak experimental data for longitudinal stress and strain of LPBF confined concrete specimens (0.15Ksi=1 MPa)	114
Table X-2: Post peak experimental data for longitudinal stress and strain of LPBF confined concrete specimens (0.15 Ksi=1 MPa)	115
Table X-3: Pre-peak experimental data for longitudinal and transverse strains of LPBF confined concrete specimens (symbols in parenthesis represent the composite parameters)(0.15 Ksi=1 MPa).....	116
Table X-4: Post-peak experimental data for longitudinal and transverse strains of LPBF confined concrete specimens (symbols in parenthesis represent the composite parameters)(0.15Ksi=1 MPa).....	117
Table X-5: Pre peak experimental data for longitudinal stress and strain of LPDF confined concrete specimens (0.15Ksi=1 MPa)	122
Table X-6: Post peak experimental data for longitudinal stress and strain of LPBF confined concrete specimens (0.15 Ksi=1MPa)	123
Table X-7: Pre-peak experimental data for longitudinal and transverse strains of LPDF confined concrete specimens (symbols in parenthesis represent the composite parameters)(0.15 Ksi=1MPa).....	124

Table X-8: Post-peak experimental data for longitudinal and transverse strains of LPDF confined concrete specimens(symbols in parenthesis represent the composite parameters)(0.15 Ksi=1 MPa).....	124
Table X-9: Pre peak experimental data for longitudinal stress and strain of HPBF confined concrete specimens (0.15 Ksi=1 MPa)	129
Table X-10: Post peak experimental data for longitudinal stress and strain of HPBF confined concrete specimens (0.15 Ksi=1 MPa)	130
Table X-11: Pre-peak experimental data for longitudinal and transverse strains of HPBF confined concrete specimens(symbols in parenthesis represent the composite parameters)(0.15 Ki=1MPa)	130
Table X-12: Post-peak experimental data for longitudinal and transverse strains of HPBF confined concrete specimens (symbols in parenthesis represent the composite parameters) (0.15 Ksi=1MPa)	131
Table X-13: Pre peak experimental data for longitudinal stress and strain of HPDF	134
Table X-14: Post- peak experimental data for longitudinal stress and strain of HPDF confined concrete specimens (0.15 Ksi=1 MPa)	135
Table X-15: Pre-peak experimental data for longitudinal and transverse strains of HPDF confined concrete specimens (symbols in parenthesis represent the composite parameters)(0.15 Ksi=1 MPa).....	135
Table X-16: Post-peak experimental data for longitudinal and transverse strains of HPDF confined concrete specimens (symbols in parenthesis represent the composite parameters)(0.15Ksi=1 MPa).....	135

LIST OF FIGURES

Figure II-1: Confining action of composite strap (Mander et.al., 1988).....	4
Figure II-2: Stress-Strain curve for FRP confined concrete column, (ACI440, 2018)	5
Figure III-1: MATEST; LVDT Setup	22
Figure III-2: (a)Fiber reinforced polymer, (b) Spiral wire, (c) wire mesh, and (d) steel fibers materials.....	23
Figure III-3: Fiber reinforced polymer application technique	25
Figure III-4: Confinement application for both (a) wire mesh (b) and spiral reinforcement..	27
Figure III-5: Sulfur capping application	31
Figure III-6: SIFCON confinement application technique (a) pre-layed fibers (b) Rough Surface	34
Figure IV-1: (a) Typical longitudinal stress-strain curves for fully confined concrete (b) Typical longitudinal stress-strain curves for partially confined concrete	36
Figure IV-2: (a) Typical Longitudinal stress-transverse strain curves for fully confined concrete (b) Typical longitudinal stress-transverse strain curves for partially confined concrete.....	37
Figure IV-3: (a) Typical Longitudinal strain-transverse strain curves for confined concrete (b) Typical longitudinal stress- strain curves in tension for composites	38
Figure IV-4 (a) Typical failure of concrete specimen (b) Typical failure of concrete specimen confined with FRM with 1 percent fibers (c) Typical failure of spiral reinforced concrete specimen	45
Figure IV-5 (a) Typical failure of concrete specimen confined with wire mesh (b) Typical failure of concrete specimen confined with FRC with 2 percent fibers (c) Typical failure of concrete specimen confined with carbon FRP	47
Figure IV-6:(a) Typical failure of concrete specimen confined with glass FRP (b) Typical failure of concrete specimen confined with SIFCON with 12 percent fibers	48
Figure IV-7: Stress strain-longitudinal-LPBF (0.15Ksi=1 MPa).....	52
Figure IV-8: Longitudinal strain-transverse-LPBF (0.15Ksi=1MPa).....	53
Figure IV-9: Stress strain-transverse-LPBF (0.15Ksi=1MPa).....	53
Figure IV-10: Stress strain-longitudinal-LPDF (0.15Ksi=1MPa)	55
Figure IV-11: Stress strain-Transverse-LPDF (0.15Ksi=1 MPa)	55
Figure IV-12: Longitudinal strain-Transverse-LPDF (0.15Ksi=1 MPa)	56
Figure IV-13: Stress strain-Longitudinal -HPBF (0.15Ksi=1 MPa).....	57
Figure IV-14: Stress strain-Transverse -HPBF (0.15Ksi=1 MPa).....	57
Figure IV-15: Longitudinal strain-Transverse -HPBF (0.15Ksi=1 MPa).....	58
Figure IV-16: Stress strain-Longitudinal -HPDF (0.15Ksi=1 MPa).....	59
Figure IV-17: Stress strain-Transverse -HPDF (0.15Ksi=1 MPa).....	59
Figure IV-18: Longitudinal strain-Transverse -HPDF (0.15Ksi=1 MPa).....	60
Figure V-1: (a) Elevation of cylinder with wire mesh (b) Wire mesh model	71
Figure V-2: Multiple cracking model in SIFC.....	86
Figure V-3: (a) Ascending portion of the stress-strain curve for full confinement (b) Ascending portion of the stress-strain curve for partial confinement	88
Figure VI-1: (a) Stress versus Longitudinal strain (b) Stress versus Transverse strain (c) Longitudinal versus Transverse strain – LPBF-(THEO+EXP)	93

Figure VI-2: (a) Stress versus Longitudinal strain (b) Stress versus Transverse strain (c) Longitudinal versus Transverse strain – LPDF-(THEO+EXP)	94
Figure VI-3: (a) Stress versus Longitudinal strain (b) Stress versus Transverse strain (c) Longitudinal versus Transverse strain - HPBF (Carbon)-(THEO+EXP)	96
Figure VI-4: (a) Stress versus Longitudinal strain (b) Stress versus Transverse strain (c) Longitudinal versus Transverse strain – HPBF (Glass)-(THEO+EXP)	97
Figure VI-5: (a) Stress versus Longitudinal strain (b) Stress versus Transverse strain (c) Longitudinal versus Transverse strain – HPDF-(THEO+EXP).....	98
Figure X-1: Stress versus longitudinal strain -7CONC	117
Figure X-2: Longitudinal versus transverse strain -7CONC	118
Figure X-3: stress versus transverse strain -7CONC	118
Figure X-4: Stress versus longitudinal strain -6FRM	119
Figure X-5: Stress versus Transverse strain -6FRM.....	119
Figure X-6: Longitudinal versus Transverse strain -6FRM.....	120
Figure X-7: Stress versus longitudinal strain - 6SP3	120
Figure X-8: Stress versus transverse strain - 6SP3	121
Figure X-9: Longitudinal versus transverse strain - 6SP3	121
Figure X-10: Stress versus longitudinal strain – 7FRC	125
Figure X-11: Stress versus Transverse strain – 7FRC	125
Figure X-12: Longitudinal versus Transverse strain – 7FRC	126
Figure X-13: Stress versus Longitudinal strain – 5MESH.....	126
Figure X-14: Stress versus Transverse strain – 5MESH.....	127
Figure X-15: Longitudinal versus Transverse strain – 5MESH.....	127
Figure X-16: Stress versus Longitudinal strain – 6SP2	128
Figure X-17: Stress versus Transverse strain – 6SP2	128
Figure X-18: Longitudinal versus Transverse strain – 6SP2	129
Figure X-19: Stress versus Longitudinal strain – 6FPC	131
Figure X-20: Stress versus Transverse strain – 6FPC.....	132
Figure X-21: Longitudinal versus Transverse strain – 6FPC.....	132
Figure X-22: Stress versus Longitudinal strain – 5FPG	133
Figure X-23: Stress versus Transverse strain – 5FPG	133
Figure X-24: Longitudinal versus Transverse strain – 5FPG	134
Figure X-25: Stress versus Longitudinal strain – 6SIFC	136
Figure X-26: Stress versus Transverse strain – 6SIFC	136
Figure X-27: Longitudinal versus Transverse strain – 6SIFC	137
Figure XII-1: (a) Mohr circle for lateral confining stresses (b) Mohr circle for lateral confining Strains	146
Figure XIII-1: (a) Location of plastic centroid of composite (b) Partial confinement stresses in FRM and FRC.....	150

I. INTRODUCTION

Jacketing is a technique used to rehabilitate an existing building to increase its strength, and capacity to withstand blast and impact loading. Thus, confinement increases strength and improves both static and dynamic response. The longitudinal and transverse compressive stress-strain response of laterally confined concrete is essential in developing the strength of a structural column subjected to loadings including blast and impact ^{1,2}.

Extensive use of FRP's has been implemented in the industry to confine existing columns; however very limited knowledge of other composites has been provided and how it compared to FRP in particular for blast and impact loads. Existing research ^{3,4,5,6,7} clearly indicate that fiber composites; such as Fiber Reinforced Concrete (FRC) and High-Performance FRC (HPFRC), WIM, and SIFC can be successfully used for concrete confinement; but no generalized and complete compressive stress-strain design curve models exist. Thus, comprehensive and generalized empirical stress-strain models should be considered to compare and assess the full compressive behavior of confined columns with different fibrous composites other than conventional confinements (steel, concrete, and FRP) for design purposes. Such models are needed to design, recommend and select the most suitable, and appropriate retrofit technique from a technical standpoint (stress-strain curves response). Accuracy of the developed models is evaluated using experimental data.

Consequently, this study will provide a comprehensive comparative overview and understanding of the compressive behavior of concrete confined with different fibrous composites, through developing stress-strain models. Thus, this research provides a complete and generalized compressive stress-strain response models for different

fibrous composite and compares their behavior to the commonly used FRP and Spiral confinements (SP). The stress strain longitudinal and transverse response shall be utilized in developing confined column strength, ductility, stiffness and energy absorption. This will allow the structural engineer to recommend the most suitable retrofitting technique from a theoretical and technical engineering standpoint.

The confinement types are categorized in the study based on their stress-strain response (strength), strains at failure (ductility), and toughness (energy absorption). The dilatation behavior (stress-strain response in transverse (radial) direction) will assist in establishing cratering and breaching effects, stand-off requirements, and mitigation recommendations to establish safe stand-offs from specific threats^{1,2}. Thus, the confinement types will be divided as follows: Low Performance Brittle/Ductile Failure (LPBF/LPDF), and High Performance Brittle/Ductile Failure (HPBF/HPDF). In addition to further classifying the models into full/partial and continuous/discrete confinements that are later explained in the study.

Consequently, two different types of confined models were developed in the presented research:

- For the case of continuous confinement, such as Concrete Filled Tubes (CFT) or jackets, proposed models are based on a modified ACI 440⁸-model approach.
- For the case of discrete confinement, proposed models are based on conventional concrete models that have been modified to account for the discrete-confinement effect of spirals and/or wire mesh (e.g. Todechine model⁹).

II. LITERATURE REVIEW

2.1 EXPERIMENTAL LITERATURE REVIEW

One of the major causes of damage on concrete structures, due to the 1971 San Fernando earthquake, the 1987 Whittier earthquake, and the 1989 Loma Prieta earthquake¹⁰, was the inadequate detailing of their structural components. Inadequate detailing of concrete columns (insufficient: starter bar lap lengths, lateral ties) were the major contributors to the insufficiency in resisting earthquake forces¹⁰. The work of many researchers¹⁰ have indicated that increasing the confinement in the potential plastic hinge regions of the column will increase the compressive strength and the ultimate compression strain and ductility of the concrete core. Therefore, strengthening techniques were implemented that typically involved methods for increasing the confining forces either in the potential plastic hinge regions or over the entire column. Studies and researches¹¹ have demonstrated that confinement significantly enhances concrete's compressive strength (resist higher design loads) and ductility.

Many concrete structures require repairing/retrofitting techniques due to durability issues (corrosion of internal steel reinforcement)^{3,12}, damage due to blast loads¹, increase in the design loads (changes and updates in the design codes and standards), as well as functional changes and construction errors^{3,12}. Consequently, assessments and structural upgrading of concrete infrastructures (bridges and tunnels) are required constantly. Thus, to avoid social costs related to the demolition and reconstruction of new structures and to improve column member behavior, jacketing is recommended⁴. The outward expansion of the core concrete is prevented by the confining action of the composite strap placed in circumferential tension, as illustrated in Figure II-1. The confinement lateral pressure increases the compressive strength of the concrete in both

the core and shell regions, and provide the longitudinal bars with support against buckling.

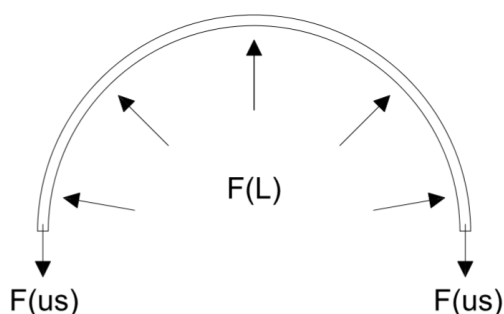


Figure II-1: Confining action of composite strap (Mander et.al., 1988)

The confinement constrains the lateral strain, producing a tri-axial stress field in the concrete that results in improving the compressive strength, maximum strain, and ductility¹³.

Traditionally, retrofitting of existing concrete structures has been accomplished using conventional materials and construction techniques, i.e. externally bonded steel plates, steel or concrete jackets and external post-tensioning⁸.

Researches⁴ have shown that steel plate jacketing technique improves the flexural strength, shear capacity, stiffness, and ductility of concrete elements. However, steel jacketing may result in excessive capacity increase, which creates unexpected failure modes; such as buckling and brittle failure at ultimate strength. Other disadvantages of steel jacketing are handling difficulties, low corrosion resistance as it is not suitable in harsh environments.

Composite materials made of fibers in a polymeric resin, also known as Fiber Reinforced Polymers (FRP) have emerged as an alternative to traditional materials and techniques⁸. Confined concrete columns with (FRP) has rapidly gained acceptance as an effective rehabilitation and strengthening technique. However to date, considerable

research¹⁴ efforts are being performed to investigate the performance of concrete members externally confined with (FRP) materials. FRP confined concrete substantially differs from that of steel confined concrete due to differences in constitutive law between FRP and steel¹⁴. Both types of confining systems provide passive confinement, as their transverse action is engaged, due to the lateral dilation of the axially loaded member¹⁴. As for FRP stress-strain behavior, a linear-elastic stress-strain response is obtained, where the confining stresses increases throughout the load history until jacket failure. Failure happens in a sudden and brittle manner (absence of yielding)¹⁴, as presented in Figure II-2⁸. In case of steel confined concrete, confining stresses remain approximately constant after transverse yielding point. This allows a ductile failure behavior, sufficient warning signs are provided prior to failure. Consequently, FRP jackets do not bear any load in the longitudinal direction, compared to steel tubes. Thus, FRP jacket is more suitable for analyzing the influence of loading path on axial stress and axial strain¹¹.

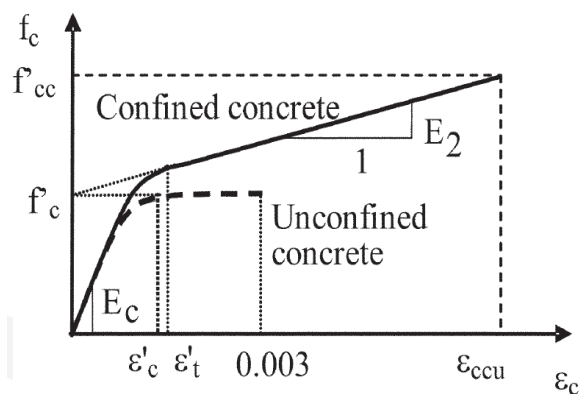


Figure II-2: Stress-Strain curve for FRP confined concrete column, (ACI440, 2018)

The growing use of FRP composites as confinement elements is attributed to the important mechanical and chemical properties of these materials. Fibers in a FRP composite material are the main load-carrying constituent; their type, orientation, and their quantity primarily govern the tensile properties of composite thus affecting

compressive strength of confined concrete columns⁸. FRP composites with their low density (typically one-fifth that of steel), adds less weight to the existing structures, and significantly simplifies the construction procedure and reduces cost¹⁰. FRP are characterized as esthetic materials—do not alter the structural appearance (increase in cross-sectional area), and will not disturb the integrity of the existing structure¹⁰. Thus, FRP materials can be used to confine areas with limited access, where traditional techniques are difficult to implement⁸.

Researches¹⁵ have shown that the axial strain and stress of the confined concrete columns increase with the increasing thickness (t) of the tube, as illustrated in Table II.1. The observed increase in axial stress over the unconfined specimen ranged from 51 to 137 percent for the concrete-filled glass FRP tube, and 57 to 177 percent for the concrete-filled carbon FRP tube, respectively. For the glass FRP tube-confined concrete, the increase in the ultimate axial strain ranged from 660 to 1100 percent, whereas columns confined with carbon FRP tubes exhibited lower axial strain that ranged from 300 to 788 percent. This was due to the fact that the ultimate strain of the carbon fiber is lower than that of the glass fiber.

Table II-1: Experimental Results-(Houssam et.al, 1999)

Specimen	Ultimate strength, MPa (Ksi)	Ultimate strain percent (%)	Increase in strength, percent (%)	Increase in strain, percent(%)
Plain	35(5.07)	0.25	-	-
GE1	52.8(7.66)	1.9	51	660
GE2	66(9.6)	2.47	89	888
GE3	83(12)	3	137	1100
C1	55(8)	1	57	300
C2	68(9.9)	1.6	94	540
C3	97(14)	2.22	177	788

GE(t)= Glass FRP polymer t layer; C(t)=Carbon polymer t layer

Alternatively, numerous experimental studies¹⁵ have shown that a significant increase in strength and ductility of concrete could be achieved by confining spirally reinforced (SP) columns with Glass Fiber Reinforced Polymer (GFRP) tubes. Increasing the number of polymer layers with same volumetric SR ratio caused an increase in ultimate compressive strength and strain. Consequently, increasing the volumetric SR ratio with the same FRP confinement result in increased maximum actual lateral confining pressures of GFRP tubes.

Unlike the explosive process observed in GFRP confined concrete cylinders, the failure process of GFRP–SR confined concrete was quiet with a good residual compressive strength after GFRP rupture. The inelastic energy absorbed by confined concrete cylinders (GFRP-SR) corresponding to failure exceeds the elastic energy absorbed. Thus, the presence of spiral reinforcement SR helped in confining the lateral deformation of the core concrete, and increasing the confinement action of the GFRP tubes.

Thus, the application of externally bonded fiber reinforced polymer FRP systems is a convenient and well-established solution to strengthen, confine, repair and retrofit structural concrete members⁸. This evidence was translated into design guidelines and codes of practice; ACI440⁸ in the USA and CSA¹⁶ in Canada, respectively.

On the other hand, FRP composites (wrap, wire, rope, or tape) holds many disadvantages; low fire resistance capability, application difficulty on damaged concrete element i.e. requiring surface column repair¹⁷, marginal increase in lateral stiffness of a structure i.e. ineffective in many retrofitting cases¹⁸. The confinement

effectiveness of FRP composites decreases when the concrete column is under eccentric axial loading or a combination of axial load and moment, which is usually the case in concrete columns¹⁸. FRP composite materials also experience a creep-rupture failure. As the ratio of the sustained tensile stress (short-term strength) of the FRP laminate increases, endurance time decreases. The endurance time also decreases under adverse environmental conditions, thus affecting its confinement effect.

Alternatively, Concrete jacketing technique is a well-established and conventional solution to repair, retrofit, and strengthen existing structures⁴. Concrete jacketing can improve the flexural and shear capacity as well as stiffness of concrete elements. A concrete jacket provides a protection layer against internal reinforcement corrosion; hence, it is a favorable retrofitting method for structures in marine and coastal environments, compared to FRP wrapping and steel jacketing⁴. However, the conventional concrete jacketing method is not an influential technique owing to some of its disadvantages related to its high thickness around concrete core. This leads to a significant increase in the dead load and decrease in the available space in the retrofitted structure. Furthermore, the retrofitted structure with conventional concrete jacketing exhibits durability issues related to concrete shrinkage; owing to additional stresses induced in the retrofitted concrete, resulting in jacket cracking and debonding. Therefore, finding an alternative jacketing material is required, to effectively minimize the crack width, and improve the durability of core concrete⁴.

With the development of concrete jacketing techniques, thin fiber-reinforced concrete (FRC) jackets (which can be in the form of shotcrete or cast-in-situ) made with ultra-high performance strain hardening cementitious material (UHP) and engineered cementitious composite (ECC) have been considered as a promising alternative to the conventional concrete jacket in the retrofit of concrete structures⁴. FRC jacket made

with ECC or UHP develops a larger strain capacity than the conventional concrete jacket, and can effectively protect the internal reinforcement from corrosion, and the core concrete from carbonation (owing to the lower porosity and permeability of the ECC and UHP than those of normal concrete)⁴.

Previous research¹⁹ found that the addition of steel fibers confinement has been regarded as an alternative solution to the use of transverse hoops. The addition of fibers confinement can lead to increased peak loads by delaying initial cover spalling, and to improved ductility by providing some additional confinement. As specified in ACI 318–17¹⁹ for the use of steel fiber as an alternative to minimum shear reinforcement, the flexural toughness of Steel Fiber Reinforced Concrete (SFRC) can be a significant index to determine the number of transverse hoops that can be eliminated when steel fiber is included in the confined concrete. The compressive toughness also can be used as index to determine the confinement ability of SFRC.

Another research⁵ has compared the confining effect of both spiral reinforced (SP) concrete and steel fiber reinforced concrete (SFRC) specimens. The volume fraction and aspect ratio of steel fibers, 1.5 percent and 70, respectively, were the same for all the confined SFRC specimens. It was noted that, as the volumetric ratio (spiral reinforcement) of the confining reinforcement increases, the ultimate load also increases in both confined reinforced concrete and confined SFRC specimens. However, the percentage increase of ultimate load seems to be higher in confined SFRC specimens than in confined reinforced concrete specimens. Note also that in confined SFRC specimens, strains at ultimate load are significantly higher than in reinforced concrete specimens⁵.

For lower levels of confinement in SFRC there exist equivalent higher levels of confinement in reinforced concrete. Hence, some amount of confining reinforcement can be replaced by the addition of short, randomly oriented steel fibers. This eases the situation in seismic-resistant, where high confinement requirements lead to congestion of steel. Apart from the improvement in strength and ductility noticed in confined SFRC, other aspects, such as durability, integrity, and dimensional stability can be achieved by the addition of steel fibers to confined reinforced concrete⁵.

Strength and ductility are the two important factors to be considered in the design of seismic-resistant reinforced concrete structures. Under seismic conditions, the structures may be subjected to large deformations. In the case of reinforced concrete columns, the behavior depends largely on the amount of confinement provided to the core concrete because of spalling effect of concrete cover at compressive strains of about 0.004⁵. Thus, FRC behavior makes it ideal for retrofitting concrete members subjected to large inelastic deformation demands and harsh environments⁵. Therefore, due to the superior mechanical properties of FRC jacket compared to a conventional concrete jacket, and its superior durability benefits compared to those of the FRP wrap and steel jacket, FRC has a great potential to serve as a high performance confinement material in structural applications.

Recent research⁷ have studied the confinement effects of ultra-high performance fiber reinforced cement (UHPFRC) jacket in comparison with GFRP jacket, on reinforced concrete (RC) columns. Four different interface treatments were employed to prepare the contact surface between the substrate concrete column and the UHPFRC jackets: longitudinal grooving (LG), horizontal grooving (HG), sandblasting (S), and abrasion (A); *Refer to the referenced paper⁷ for illustration.*

It was noted that, specimens confined with UHPFRC (1.5 % hooked steel fibers), LG and HG, exhibited increase of 176% and 145%, respectively, in their peak loads. While, the specimens confined with 1.5% synthetic (barchip) macro-fibers, LG and HG, recorded increase of 144% and 89%, respectively, in their peak loads relative to the reference column (normal reinforced concrete column)⁷.

As for the specimens confined with UHPFRC 1.5% hooked steel fibers with interface treatment: sandblasting (S) and abrasion (A), indicated increase of 131% and 121%, respectively. However, specimens confined with UHPFRC 1.5% barchip steel fibers with surface treatment: S and A, indicated increases of 67% and 38%, respectively, relative to the reference column (normal reinforced concrete column)⁷.

Finally, the specimens lacking internal reinforcement, confined with 1.5% hooked steel and 1.5% barchip fibers, experienced the highest increase of about 276% and 225%, respectively, in their load-carrying capacity⁷.

Obviously, the effect of longitudinal grooving (LG) in strengthened columns on increasing peak load was superior to that of horizontal grooving (HG). Moreover, the columns strengthened with UHPFRC jackets with hooked steel fibers displayed a higher load capacity than did those strengthened with synthetic (barchip) macro fibers⁷.

As for the ultimate axial strain, the specimen with LG interface treatment confined with UHPFRC hooked steel fibers recorded an increase of 91% in its ultimate axial strain relative to LG confined with barchip fibers. This difference may be attributed not only to the mechanical properties (tensile strength) of steel fibers that are superior to those of barchip fibers but also to the double-ended hook shape of the steel fibers that creates a better bond with the concrete⁷.

As for GFRP confinement, where F signifying GFRP jacket, F-W, FIW1, and FIW2 recorded increases of about 115%, 53%, and 64%, respectively, in the peak load relative to the measured reference⁷.

F-W corresponds to full GFRP hoop confinement wraps while the remaining two designated as F-IW1 and F-IW2 were strengthened with intermittent GFRP hoop wraps 50 mm (1.97in.) and 10 mm (0.39 in.) in width, respectively. The FRP strips were oriented in the hoop direction; *Refer to the referenced paper⁷ for illustration*

Thus, strengthening the RC column with 15 intermittent GFRP wraps 10mm (0.39ich) in width led to a reduction of 60% in the consumption of GFRP composites but the peak load dropped by 31% relative to that of the specimen strengthened with full GFRP wraps. This indicates that intermittent GFRP along the column height may be economic for a target loading level⁷.

However, the need to obtain higher strength and ductile material structures that can resist blast and impact loads, has led to Slurry Infiltrated Fiber Concrete (SIFC) material development. It was noted, that the percentage increase of fiber in the cementitious matrix has caused the formation of a very high durable material, called Slurry Infiltrated Fiber Concrete (SIFC). Thus, with additional development of fiber reinforced concrete (FRC) jackets, SIFC have been considered as the next promising alternative to the conventional concrete jacket in the retrofitting concrete structures by infiltrating large percentage of fibers thus limiting cracks⁶.

SIFC has diverged from conventional SFRC in two respects: a higher fiber volume fraction (usually 5 to 20 volume percent), and consists of a very fine matrix (absence of coarse aggregates)²⁰. Thus, SIFC is a unique construction material

possessing high strength as well as large ductility and far exceptional potential for structural applications when sudden loads are encountered during services.

B. Abdollahi et al.⁶ looked at comparing FRP wrapping with SIFC but no models were developed and it was noted that SIFC and FRP had some similarities in their performance depending on the strength of the concrete core effectively confined by the composite.

Based on the results of the conducted study by B. Abdollahi et al.⁶, following conclusions can be drawn:

- Both Glass Fiber Reinforced Polymer (GFRP) and SIFC confinement methods enhanced strength, strain and energy absorption capacity of concrete cylinders
- The increase in the thickness of the SIFC jacket as well as increasing the GFRP layer numbers led to a significant improvement of stress–strain response of confined concrete samples. Thickness of the confining layer is found to be the most effective parameter to improve the confined concrete behavior in both methods.
- SIFC confinement technique is more effective for strengthening of the mid-strength (25MPa (3.6Ksi)), followed by the low-(15MPa (2.2Ksi)) and the higher-(40Mpa (5.8Ksi)) strength concrete. However, efficiency of GFRP wrap in confining concrete columns decreased by increasing core concrete strength. Therefore, initial concrete strength should be among other criteria to choose a better confinement technique.
- Confinement performance for higher-strength SIFC jacket is much better than mid-strength jacket, while fiber length has no significant effect on the performance of the jacket. As the fibers are placed in hoop like direction in a continuous matter, bridging micro-cracks

- GFRP behavior in confinement is very sensitive to the fiber orientation with respect to the hoop direction, as the change of fiber orientation from 0° weakened the GFRP performance.
- The stress–strain responses of GFRP-confined concrete show bilinear forms before starting failure, while SIFC curves have nonlinear behaviors throughout the test.
- In many cases, the ultimate strength and absorbed energy of SIFC-confined concrete is very similar to the results of GFRP-confined cylinders. The comparison shows that SIFC confinement method can be regarded as a competitive method with respect to the well-known FRP confinement technique.
- Passive confinement models⁶ can be used to predict compressive strength of SIFC-confined columns. Confinement coefficient depends on the unconfined concrete strength and the level of the provided confining pressure. In addition to the confinement model proposed in this study, applying some FRP confinement models result in relatively accurate prediction of SIFC confinement strength
- SIFC-confined cylinders fail due to tensile failure of the jacket along with surface delamination between the core concrete and the jacket. Similar failure mode was observed in most of GFRP-confined samples (failure due to both hoop fiber rupture and delamination, with intact concrete and FRP jacket above and below the failure region)
- Size effects on SIFC-confined columns are predicted to be similar to GFRP jackets; (significant effect on the confined concrete strength, a less significant effect on the stress–strain behavior and a slight effect on failure modes).

However, the ratio of SIFC fiber length to shell thickness may also affect the behavior of jacket through changing the tensile strength of the material.

- Failure in GFRP-confined cylinders is a drastic reduction in the stress level; such significant stress decay was not observed in SIFC-confined cylinder.
- The stress–strain response of SIFC-confined concrete shows a strain softening behavior after peak stress, while the GFRP-confined concrete demonstrates a plateau response or a strain hardening with a distinct bilinear behavior in which a reduction in stiffness is experienced after reaching an axial stress higher than the unconfined strength.

Thus, the results have shown that SIFC confinement application can be regarded as a competitive method with respect to the well-known FRP confinement method.

2.2 ANALYTICAL MODELING LITERATURE REVIEW

Limited research^{3, 4, 5, 6, 7} have developed comprehensive empirical models for SIFC, FRC, Fiber Reinforced Mortar (FRM), and WIM similar to that of FRP confinement. Most research^{10, 11, 14, 15, 21} has been focused on one typical FRP confinement, and very few publications^{6, 7, 22} have provided a comparison between the compressive stress-strain responses of laterally confined concrete with different fibrous composites. B. Abdollahi et al.⁶ looked at comparing FRP wrapping with SIFC, Liang Huang et al.²² studied the compressive behavior of concrete confined with glass fiber reinforced polymers and spirals, Sayyed A. D. et al.⁷ studied the compressive behavior of ultra-high performance fiber reinforced concrete (UHPFRC) and GFRP confinement, but no specific comprehensive models were developed.

Thus, the ultimate goal of the current research was to investigate and develop a model capable of predicting the complete stress-strain response of confined concrete necessary

for predicting complete load-displacement response of column confined with various fiber composites.

Two classes of stress-strain models were used in the presented research: (a) models for discretely confined concrete (e.g., models for concrete confined by spirals (SP) or mesh reinforcement (WIM)), and (b) models for continuously confined concrete (FRC, FRM, SIFC).

Continuous confinement is when the composite is wrapped continuously around the structural members while in discrete confinements they are spaced at a specific pitch

a- **Discrete Confinement Models:** The following Todechini⁹ stress-strain model for unconfined concrete was used in the presented research.

$$\sigma_{lu} = \frac{2\sigma'_c \left(\frac{\varepsilon_{lu}}{\varepsilon'_c} \right)}{1 + \left(\frac{\varepsilon_{lu}}{\varepsilon'_c} \right)^2} \quad 0 < \varepsilon_{lu} < \varepsilon_{lur} \quad \text{Eq. II. 1}$$

$$\varepsilon'_c = \frac{1.71\sigma'_c}{E_c} \quad \text{Eq. II. 2}$$

Where $\sigma'_c, \varepsilon'_c$ are the stress and strain at peak of unconfined concrete, respectively. ε_{lur} is the strain at rupture of unconfined concrete, E_c is the modulus of elasticity of unconfined concrete and , $\sigma_{lu}, \varepsilon_{lu}$ are the longitudinal stress and strain of unconfined concrete.

b- **Continuous Confinement Models:** Most of the existing models^{6, 10,11,13,14,15,21,22} were developed for FRP jacketed concrete. These include: (1) the ACI 440⁸ model and (2) the model by Saadatmanesh et. al.¹⁰. The key difference between the two is that ACI 440⁸ model predicts stress-strain behavior only up to the maximum load, while the model by Saadatmanesh et. al.¹⁰ predicts the full stress-strain response. It should also

be noted that neither models predicts the maximum stress, but instead, both use the following relationship for triaxially confined concrete, developed by Mander et al²³ :

$$\sigma_{lccu} = \sigma'_c + 4.1\sigma_{2cu} \quad \text{Eq. II. 3}$$

Where σ'_c is the peak stress of unconfined concrete, σ_{lccu} is the peak stress of confined concrete

$$\sigma_{2cu} = \frac{2\sigma_{lxxxcu}A_{st}}{D_c s_{xxx}} \quad \text{Eq. II. 4}$$

where A_{st} is the area of the composite strap, D_c is the diameter of the concrete core (i.e. central portion of the column effectively confined by the composite), s_{xxx} is the pitch of the lateral confinement, σ_{lxxxcu} is the tensile stress of composite at peak and σ_{2cu} is the lateral peak stress.

1. **ACI 440 Model:** ACI 440⁸ uses the following model for predicting the ascending behavior of concrete confined with FRP jackets.

$$\sigma_{lc} = E_c \varepsilon_{lc} - \frac{(E_c - E_{lc2})^2 \varepsilon_{lc}^2}{4\sigma'_c} \quad 0 < \varepsilon_{lc} < \varepsilon_{lcco} \quad \text{Eq. II. 5}$$

$$\sigma_{lc} = \sigma'_c + E_{lc2} \varepsilon_{lc} \quad \varepsilon_{lcco} < \varepsilon_{lc} < \varepsilon_{lccu} \quad \text{Eq. II. 6}$$

$$E_{lc2} = \frac{\sigma_{lccu} - \sigma'_c}{\varepsilon_{lccu}} \quad \text{Eq. II. 7}$$

$$\varepsilon_{lcco} = \frac{2\sigma'_c}{E_c - E_{lc2}} \quad \text{Eq. II. 8}$$

$$\sigma_{lccu} = \sigma'_c + \psi_f 3.3k_a \sigma_{2cu} \quad \text{Eq. II. 9}$$

$$\varepsilon_{lccu} = \varepsilon'_c \left(1.5 + 12k_b \frac{\sigma_2}{\sigma'_c} \left(\frac{\varepsilon_{IFRPcu}}{\varepsilon'_c} \right)^{0.45} \right) \quad \text{Eq. II. 10}$$

$$\sigma_{2cu} = \frac{2E_{IFRP} n t_{FRP} \varepsilon_{IFRPcu}}{D_c} \quad \text{Eq. II. 11}$$

Where σ_{lc} and ε_{lc} are the longitudinal stress and strain of confined concrete, σ_{lccu} and ε_{lccu} are longitudinal stress and strain at peak. ε_{lcco} is the confinement stress at the point at which the slope of the stress-strain curve equals E_{lc2} ; where E_{lc2} is the in-elastic modulus of stress strain curve during activation of the composite (i.e., the point of the initiation of tensile stresses in the composite due to lateral expansion of the column). E_c is the modulus of unconfined concrete. ψ_f is a reduction factor =0.95. k_a and k_b are coefficient factors equal to 1 for circular sections. σ_{2cu} is the concrete core lateral stress at peak, n is the number of layers of FRP, t_{FRP} is the thickness of the FRP composite, ε_{lFRPcu} is strain at peak stress, E_{lFRP} is the tensile modulus of the FRP composite, and D_c is the diameter of the concrete core effectively confined by the composite.

2. **Model by H. Saadatmanesh et. al.:** It represents the full stress-strain model developed by H. Saadatmanesh et. al¹⁰ for concrete confined with FRP straps.

Refer to the referenced paper for illustration..

$$\sigma_{lc} = \frac{\sigma_{lccu} x^r}{r - 1 + x^r} \quad 0 < \varepsilon_{lc} < \varepsilon_{lcr} \quad \text{Eq. II. 12}$$

$$x = \frac{\varepsilon_{lc}}{\varepsilon_{lccu}} \quad \text{Eq. II. 13}$$

$$\varepsilon_{lccu} = \varepsilon'_c \left[1 + 5 \left[\frac{\sigma_{lccu}}{\sigma'_c} - 1 \right] \right] \quad \text{Eq. II. 14}$$

$$r = \frac{E_c}{E_c - \frac{\sigma_{lccu}}{\varepsilon_{lccu}}} \quad \text{Eq. II. 15}$$

$$\sigma_{lccu} = \sigma'_c \left[-1.254 + 2.254 \sqrt{\left(1 + \frac{7.94 \sigma'_{2cu}}{\sigma'_c} \right) - \frac{2 \sigma'_{2cu}}{\sigma'_c}} \right] \quad \text{Eq. II. 16}$$

$$\sigma'_{2cu} = \sigma_{2cu} \frac{A_e}{A_{cc}} \quad \text{Eq. II. 17}$$

$$\sigma_{2cu} = \frac{2\sigma_{IFRPCu}A_{st}}{D_c s_{FRP}} \quad \text{Eq. II. 18}$$

Where ϵ_{lcr} is the strain at rupture of confined concrete and previously defined parameters are the same, while

$$A_{cc} = A_g(1 - \rho_{cc}) \quad \text{Eq. II. 19}$$

is the effective area of concrete enclosed by composite strap

A_g is the gross area of concrete, ρ_{cc} is the ratio of longitudinal reinforcement to gross area of concrete, A_e is the area of effectively confined concrete core, σ_{IFRPCu} is the tensile stress of FRP composite at peak, A_{st} is the area of the FRP strap which is equal to $t_{FRP}s_{FRP}$ for the case of continuous confinements. D_c is the diameter of column, and s_{FRP} is the width of FRP strap, t_{FRP} is the thickness of FRP strap.

Furthermore, H. Saadatmanesh et. al¹⁰ proposed an approach based on the concept of balance of energy to calculate the longitudinal compressive strain of confined concrete at failure ϵ_{cu} . In this approach, the additional ductility available when concrete is confined is considered to be due to energy stored in the confining composite straps.

$$U_{st} = U_{cc} + U_{sl} - U_{co} \quad \text{Eq. II. 20}$$

Where U_{co} = ultimate strain energy per unit volume of unconfined concrete given by

$$U_{co} = A_c \int_0^{2\epsilon_{co}} \sigma_{uc} d\epsilon_c \quad \text{Eq. II. 21}$$

U_{sl} = energy required to maintain yield in longitudinal steel in compression given by

$$U_{sl} = \rho_{cc} A_c \int_0^{\epsilon_{cu}} \sigma_{sl} d\epsilon_{sl} \quad \text{Eq. II. 22}$$

U_{cc} = ultimate strain energy per unit volume of confined concrete

$$U_{cc} = A_c \int_0^{\varepsilon_{cu}} \sigma_c d\varepsilon_c \quad \text{Eq. II. 23}$$

U_{st} = ultimate strain energy per unit volume of composite strap given by

$$U_{st} = \rho_s A_c \int_0^{\varepsilon_{us}} \sigma_{st} d\varepsilon_{st} \quad \text{Eq. II. 24}$$

Then the ultimate compression strain of concrete at the point of fracture of the confining composite strap can be calculated, resulting in complete determination of the stress strain curve of the confined concrete throughout the entire range of loading, up to the fracture of composite strap and consequent failure of the column.

3. **Model by Sayyed A.D. et. al.⁷**: The following represents the stress-strain model of reinforced concrete (RC) columns confined with ultra-high performance fiber reinforced concrete (UHPFRC) jackets. However, this model was not used in our research.

$$\sigma = \frac{\frac{\sigma_{cc}\varepsilon}{\varepsilon_{cc}} n}{n - 1 + \left(\frac{\varepsilon}{\varepsilon_{cc}}\right)^n} \quad \text{for } \varepsilon < \varepsilon_{cc} \quad \text{Eq. II. 25}$$

$$n = \frac{E_0}{E_0 - \frac{\sigma_{cc}}{\varepsilon_{cc}}} \quad \text{Eq. II. 26}$$

$$\sigma = \frac{\sigma_{cc} - \sigma_{cu}}{\varepsilon_{cc} - \varepsilon_{cu}} (\varepsilon - \varepsilon_{cu}) + \sigma_{cu} \quad \text{for } \varepsilon > \varepsilon_{cc} \quad \text{Eq. II. 27}$$

Where, σ_{cc} is the compressive strength of the confined concrete, ε_{cc} represents the longitudinal compressive strain of the concrete, E_0 is the slope of the first portion, and ε denotes the longitudinal strain, σ_{cu} are the ultimate stress and the corresponding axial strain, and n is the number of data (1,2,3...)

III. EXPERIMENTAL PROGRAM

The testing was done according to ASTM C49/C49M-1416 “Standard Test Method for Static Modulus of Elasticity and Poisson’s Ratio of Concrete in Compression”²⁴. Testing apparatus consists of compressive MATEST machine set at rate control of 0.2 mm/sec (0.0078 in. /sec). Figure III-1 shows the MATEST setup; Two LVDT’s were placed vertically and diametrically opposite the test cylinder to measure the longitudinal strains (LVDT 1&2). A third LVDT was placed horizontally along the circumference to measure the Poisson’s ratio; (LVDT3). For measuring transverse strains, the apparatus has a pivot at one end of the cylinder and measurements are taken at the other end of the cylinder diametrically opposite. A fourth LVDT was attached to the cross head of the testing machine in order to confirm the set control rate for the test. The stroke control LVDT was used only to measure the modulus of elasticity of the sample specimens. The load was measured through the built in load cell.

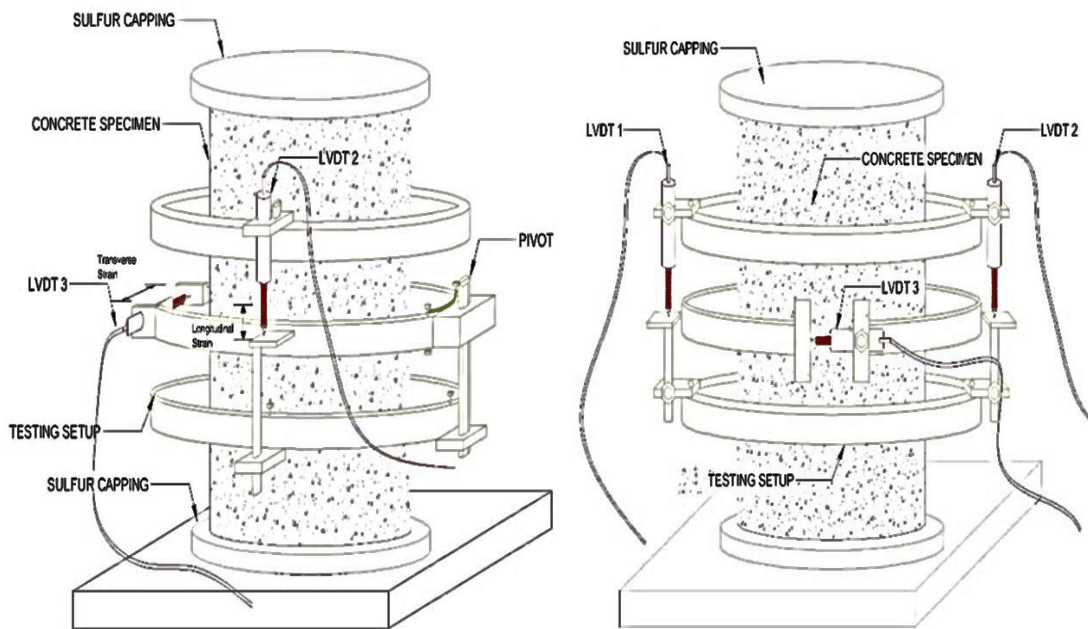


Figure III-1: MATEST; LVDT Setup

3.1 MATERIAL PROPERTIES

In this chapter, materials used in this study, consists of fifty samples, divided among different confinement's products illustrated in FigureIII-2(a, b, c, d). Further detailed discussion is presented in the upcoming section.

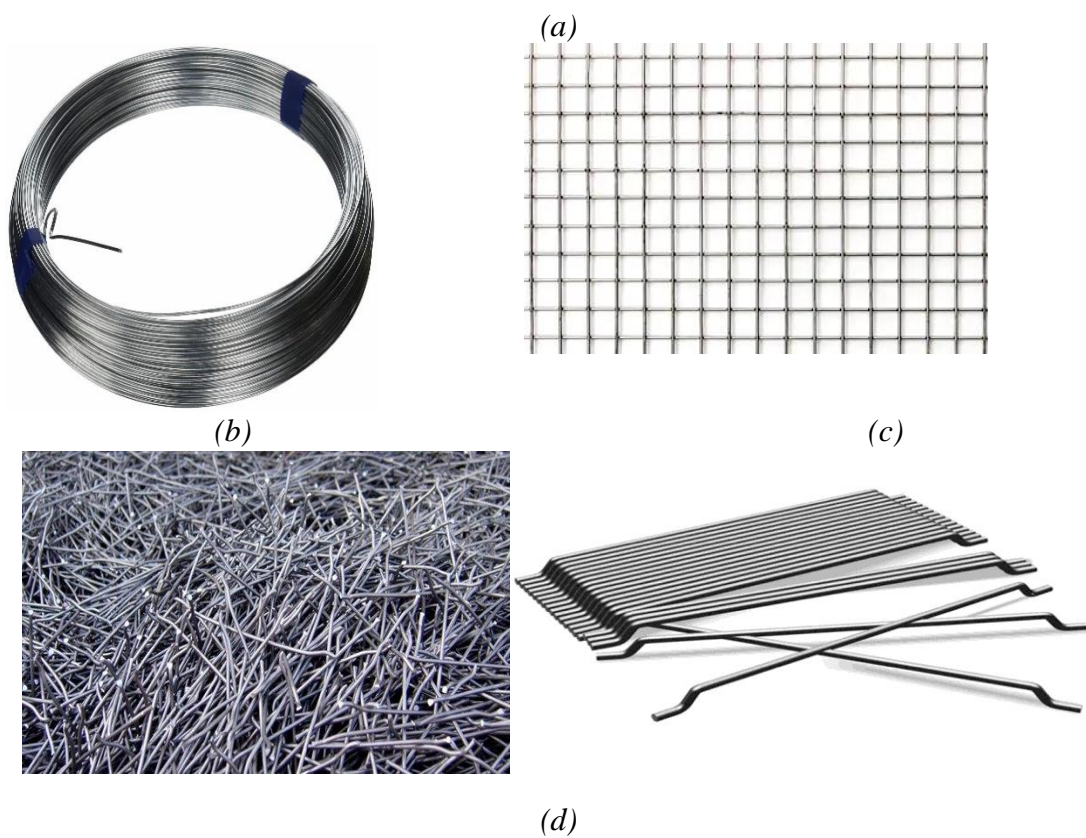


Figure III-2: (a)Fiber reinforced polymer, (b) Spiral wire, (c) wire mesh, and (d) steel fibers materials

3.1.1 Fiber Reinforced Polymers

FRP composites are made up of short fibers or filaments of glass, carbon, etc., bonded together with a resin matrix as shown in Figure III-3. The fibers provide the composites with their unique structural properties. The matrix serves only as a bonding agent. Two major types of resin-impregnated unidirectional composite straps are used in this study; Fiber Glass Polymer (FGP), and Fiber Carbon Polymer (FCP) with different layers²⁵. From FGP, Tyfo® SEH-51A²⁵ material was used; however, from FCP, Tyfo® SCH-11UP²⁵ and Tyfo® SCH-41²⁵ materials were used.

Tyfo® SEH-51A²⁵ is a custom weave, uni-directional glass fabric. The glass material is orientated in the 0° direction with additional yellow glass cross fibers at 90°; However, as for the Tyfo® SCH-11UP²⁵ & Tyfo® SCH-41²⁵, both are custom, uni-directional carbon fabric orientated in the 0-degree direction

Mechanical properties of Tyfo® SEH-51A²⁵; glass fiber, and Tyfo® SCH-11UP²⁵, Tyfo® SCH-41²⁵; carbon fiber fabric materials along with the resin Tyfo® S Epoxy²⁵ used are presented in Fyfe Europe data sheet²⁵. In general, the tensile strength and modulus of elasticity of composites, i.e., resin and fiber, based on gross cross-sectional area, are smaller than the strength and modulus of the constituent fiber itself.



Figure III-3: Fiber reinforced polymer application technique

3.1.2 Steel Fiber Reinforcement

Steel fiber is a metal reinforcement usually intermixed with concrete (low percentage fibers), or infiltrated with slurry (high percentage fibers). Steel fiber for reinforcing concrete is defined as short, discrete lengths of fibers with an aspect ratio (ratio of length to diameter) from about 20 to 100, with different cross-sections. They are sufficiently small to be randomly dispersed in an unhardened concrete mixture using the usual mixing procedures. A certain amount of steel fiber in concrete can cause qualitative changes in concrete's mechanical property, greatly increasing resistance to cracking, impact, fatigue, bending, tenacity, durability, and other properties. Steel fiber can be

categorized into five groups, depending on the manufacturing process and its shape and/or section: cold-drawn wire, cut sheet, melt-extracted, mill cut, and modified cold-drawn wire²⁶.

The fiber used in the study is a hooked shape fiber of length 50mm (1.97in.) and diameter 1.05mm (0.04in.); aspect ratio (l/d) =45 as shown in Figure III-2(d)

The reason for using hooked steel fibers in this study; as previous studies have found that hooked-end fiber is more effective than straight or crimped fiber in improving the tensile behavior of concrete²⁰. Consequently, through statistical analysis of fibers production all over the world, Katzer²⁷ reported that 67.1% are the hooked type. Thus, Katzer²⁷ study clearly indicates that hooked-end steel fiber is the most popular and effective type of reinforcing fiber for concrete.

According to ASTM A820²⁸, the tensile strength of steel fibers is 1.115N/mm^2 (161.7lb/inch^2) with tolerances $\pm 7.5\%$ average. Young modulus records $\pm 200\text{ N/mm}^2$ (29kip/inch^2)

3.1.3 Wire Mesh

The wire mesh (WIM) used in the study is a square shape steel wire mesh. It consists of wire strands electrically welded together to form a high strength mesh. WIM is available in two formats: Rolled mesh and rigid mesh. The study is based on rolled, thin, flexible, zinc coated steel wire with axial gaps. (WIM) reinforcement was tested to better understand contribution of fibers placed at various angles to the jacketed column; “fibers” being oriented only in the vertical and the horizontal direction.

Mesh used in the study has a diameter of 1mm (0.04inch) with modulus of elasticity 40,000 MPa (5,802 Ksi), Yield strength of 1,600 MPa (232 Ksi), with brittle failure at 0.04 strain. The horizontal wire pitch, i.e. the distance between two horizontal wire

strands is 10mm (0.39inch), and the vertical wire pitch, i.e. the distance between two vertical wire strands is 10mm (0.39inch) as shown in Figure III-4(a).

3.1.4 Spiral Reinforcement

Spiral reinforcement is also termed as helical reinforcement, which is used, only in the circular column. Spiral reinforcement contribute to bind the longitudinal reinforcements, make the column stiff against buckling due to axial loading or eccentric moment or lateral loading, and provides resistance against shear in column, though shear is small in magnitude. This confinement provides the column (which works mainly in compression) with both more capacity and ductility. Spiral reinforcement was tested as presenting a typical confinement used through ages.

Wire spiral reinforcement used in this study consists of galvanized steel wire with a 3mm diameter, a modulus of elasticity 5,000MPa (725Ksi) and yield strength of 500MPa (72.5Ksi). As for further mechanical properties, refer to ANBAO Corp., Wire & Wire Products ²⁹.

Two pitch sample criteria were used-a 20mm (0.79inch) and 30mm (1.18inch) pitch; each made up six samples for testing; as shown in Figure III-4(b)



(a)

(b)

Figure III-4: Confinement application for both (a) wire mesh (b) and spiral reinforcement

3.2 TASKS & METHODOLOGY

The following section presents the material sampling and mix designs proportions used in the study. As previously discussed, the aim of this study is to develop complete stress-strain models for fibrous composites: (FRC, SIFC, WIM, FRM), investigate, compare their behavior to existing FRP, and SP confined concrete.

Regular Concrete (CONC)

The regular concrete mix design is similar for all regular/control specimens and core concrete of confined specimens. A consistence concrete strength was used for comparison reasons only. Mix design proportions are presented in Table III-1 for a targeted concrete strength of 40MPa (5.8Ksi). Concrete samples (CON) consisted of Type I Portland cement, 19 mm (3/4 in.) coarse aggregate, fine aggregate (sand) and water in the proportions of 1: 2: 2: 0.4 by weight, respectively.

Table III-1: CONC Mix Design I

Material	Weight of material Kg(lb);proportion	% of Cement (weight)
Cement	24(53); W_c	100%
Sand	48(105.8); $2W_c$	200%
Aggregate (3/4'')	48 (105.8); $2W_c$	200%
Water	10(22); $0.4W_c$	42%

Fiber Reinforced Mortar (FRM), Slurry Infiltrated Concrete (SIFC)

As for fiber reinforced mortar (FRM) and slurry infiltrated fiber concrete (SIFC), the slurry mix design was based on a study done by Naaman et al²⁰ for having an optimized (maximum) tensile strength of SIFC. However, Krstulovic-Opara et.al³⁰ and Sary A.M.³¹ have modified these proportions based on excessive research in order to attain the optimized slurry mix design proportions; giving a maximum tensile strength of

fibrous composites; Mix design proportions are presented in Tables III-2. The slurry for (FRM) and (SIFC) consisted of Portland cement type I, silica sand, micro silica, water and superplasticizer of portions by weight of cement of 1: 0.5, 0.5, 0.3, 0.01, respectively.

Table III-2: FRM & SIFC Mix Design II

Material	Weight of material Kg(lb);proportion	% of Cement (weight)
Cement	59.5(131.2); W_c	100%
Water	17.8(39.2); $0.3W_c$	30%
Silica Sand	29.74(65.6); $0.5W_c$	50%
Micro silica	29.74(65.6); $0.5W_c$	50%
Superplasticizer	0.59(1.3); $0.01W_c$	1%

Fiber Reinforced Concrete (FRC)

As for Fiber Reinforced Concrete, the concrete mix design was based on studies done by Lee et.al³² and Naaman et.al³³ for having an optimized (maximum) tensile stress-strain properties of FRC, presented in TableIII-3. The concrete mix for (FRC) consisted of Portland cement type I, 9.5 mm (3/8 in.) coarse aggregate, fine aggregate (sand), and water of proportions by weight of cement of 1: 2, 2, 0.4, respectively. A 3/8 in. coarse aggregate was used to simplify casting in a 25.4mm (1-inch) confinement.

Table III-3: FRC Mix Design III

Material	Weight of material Kg(lb);proportion	% of Cement (weight)
Cement	24(53); W_c	100%
Sand	48(105.8); $2W_c$	200%
Aggregate (3/8")	48 (105.8); $2W_c$	200%
Water	10(22); $0.4W_c$	42%

It should be noted no material testing was made: sieve analysis, (coarse and fine aggregates), water absorption capacity, water content, density, etc. This gap has contributed for having a marginal experimental error.

Hooked Steel Fibers Percent

An important action of fibers in cement composites, is to stop and redirect the propagation of internal flaws (e.g., micro cracks) under increasing stresses³⁴. Thus increasing the fibers percentage increases the confined matrix tensile strength. Engineered Cementitious Composites (ECC)³⁵ currently employs 2% volume content of random hooked short fibers that has achieved a maximum composite ductility, with a minimum percent of fibers. Based on studies by Lee et.al³² and Naaman et.al³³, 2% fiber volume is the maximum percent of fibers that can be used in concrete mixture, avoiding fiber balling effect. Based on that a 2% fiber volume fraction will be used in Fiber Reinforced Concrete (FRC) matrix.

As for Fiber Reinforced Mortar (FRM) a 1% fiber volume fraction will be used, based on research and studies done by Naaman et.al³³ that have introduced the optimized % fiber volume fraction in mortar matrix, 1%, as mixing difficulties and segregation will be encountered at higher fiber contents (1 percent), which will lead to a harsh mix.

As for Slurry Infiltrated Fiber Concrete (SIFC), a 12% fiber volume fraction was used based on study done by Naaman et.al²⁰ on stress-strain properties of SIFC in both compression and tension. It was noticed that a 12% hooked steel fiber gives an optimized (maximum) tensile strength. For practical placement of fibers in a hoop direction, a 25.4mm (1-inch) confinement was selected for all specimens.

3.2.1 Material Sampling/Mix Design

Continuous confinement was provided by: (a) wrapping Fiber Reinforced Polymer (FRP), jackets made using fiber polymer carbon (FPC) or fiber polymer glass (FPG) composites. (b) Fiber Reinforced Concrete (FRC) composites with 2% steel fiber volume fraction. (c) Fiber Reinforced Mortar (FRM) composites made with 1% steel fiber volume fraction, and (d) Slurry Infiltrated Concrete (SIFC) composites made with 12% steel fiber volume fraction.

While discrete confinement was provided by: (a) spiral re-bar spaced at a 20mm (0.78 in.) pitch (SP2), (b) a spiral re-bar spaced at 30mm (1.18 in.) pitch (SP3), and (c) wire mesh (WIM) that was cast within the cylinder. All cylinders were sulfur capped at top and bottom to insure a level surface during load application as shown in Figure III-5.



Figure III-5: Sulfur capping application

The following samples were considered and classified as follows in the experimental investigation; partial/full confinement classification are later explained in the subsequent text:

Low Performance Brittle Failure Composites (LPBF):

- (CON) Regular concrete – Eight Specimens-(discrete no confinement)

Eight concrete samples (CON) consisted of type I Portland cement, 19 mm (3/4 in.) coarse aggregate, fine aggregate (sand) and water. The samples were poured in 150 mm x 300 mm (6 in. x 12 in.) cylinder molds. Mix design I was used in material proportions, as shown in TableIII-1

- (SP3) Spiral reinforcement – Six Specimens-(discrete no confinement)

For (SP3), spirals²⁹ of diameter 3 mm (0.118 in.) were placed in the molds at a pitch of 30 mm (1.18 in.) and a cover of 7.5 mm (0.29 in.) prior to pouring the concrete. Mix Design I was used in material proportions, as shown in TableIII-1

- (FRM) Fiber reinforced mortar–Six Specimens-(continuous partial confinement)

In (FRM) samples²⁸, the original concrete samples were first cured for 28 days. The surface concrete was roughened to insure proper bonding as shown in Figure III-6 (b), and then a 25.4 mm (1 in.) confinement was poured consisting of a slurry mix intermixed with 1% hooked steel fibers²⁸ of length 50 mm (1.97 in.) and diameter 1.05 mm (0.041 in.) respectively. The slurry materials and proportions for (FRM) is presented in Mix design II, as shown in TableIII-2.

Low Performance Ductile Failure composites (LPDF):

- (SP2) Spiral reinforcement –Six Specimens-(discrete full confinement)

For (SP2), spirals²⁹ of diameter 3 mm (0.118 in.) were placed in the molds at a pitch of 20 mm (0.78 in.) and a cover of 7.5 mm (0.29 in.) prior to pouring the concrete. Mix design I was used in material proportions, as shown in TableIII-1

- (WIM) Wire mesh reinforcement –Six Specimens-(discrete full confinement)

For (WIM), a wire mesh steel grid 10mm x 10mm (0.39 in. x 0.39 in.) of diameter 1 mm (0.039 in.) was placed along the circumference of the molds to provide

confinement; no concrete cover. The same control concrete was poured in the molds. Mix design I was used in material proportions, as shown in TableIII-1

- (FRC) Fiber reinforced concrete-Six Specimens-(continuous partial confinement)
Same fibers²⁸ as in (FRM) were poured in a 25.4 mm (1 in.) confinement width but with 2% fiber volume fraction. The concrete surface was roughened as for FRM, shown in Figure III-6(b). The concrete mix for (FRC) proportions is presented in Mix design III, as shown in TableIII-3

High Performance Brittle Failure (HPBF):

- (FPC) Fiber polymer carbon –Six Specimens-(continuous full confinement)
For (FPC)²⁵, six control specimens are poured and cured in water for 28 days. Samples were wrapped with carbon fiber polymers. Thickness of the layers was varied.

- › 2-SCH-41²⁵ with one layer $t_{FPC} = 1 \text{ mm (0.039 in.)}$
- › 2-SCH-41²⁵ with two layers $t_{FPC} = 2 \text{ mm (0.079 in.)}$
- › 2-SCH-11 UP²⁵ with two layers $t_{FPC} = 1.02 \text{ mm (0.04 in.)}$

- (FPG) Fiber polymer glass –Six Specimens-(continuous full confinement)
For (FPG)²⁵, six control specimens were wrapped with glass fiber polymers. Thickness of the layers were varied.

- › 3-SEH-51A²⁵ with one layer $t_{FPG} = 1.3 \text{ mm (0.051 in.)}$
- › 3-SEH-51A²⁵ with two layers $t_{FPG} = 2.6 \text{ mm (0.102 in.)}$

High Performance Ductile Failure (HPDF):

- (SIFC) Slurry infiltrated concrete-Six Specimens-(continuous full confinement)
For (SIFC), 12 percent fibers²⁸ similar to FRM and FRC, were pre-layed around the circumference within a thickness of 25.4 mm (1 in.) after attaining a rough surface concrete, as shown in Figure III-6(a, b). Slurry materials and proportions for (SIFC) is presented in Mix design II, as shown in TableIII-2.



Figure III-6: SIFCON confinement application technique (a) pre-layed fibers (b) Rough Surface

IV. EXPERIMENTAL RESULTS

4.1 TYPICAL STRESS STRAIN CURVE OF CONFINED CONCRETE

Confinement types are categorized into the following: Low Performance Brittle Failure (LPBF), Low Performance Ductile Failure (LPDF), High Performance Brittle Failure (HPBF), and High Performance Ductile Failure (HPDF), based on their stress-strain response (resistance), strains at failure (ductility) and toughness (energy absorption). The performance criterion is based on the expected level of strength. The failure criterion is based on the energy absorption and expected level of stress and strain at rupture.

Brittle failures are dictated when the longitudinal confinement strains (i.e. strains occurring before the tensile stresses in the composite occur designated as activation of the composite) are close to the peak strains where no first crack of composite is noted and concrete core has already witnessed cracks prior to any activation of the composite.

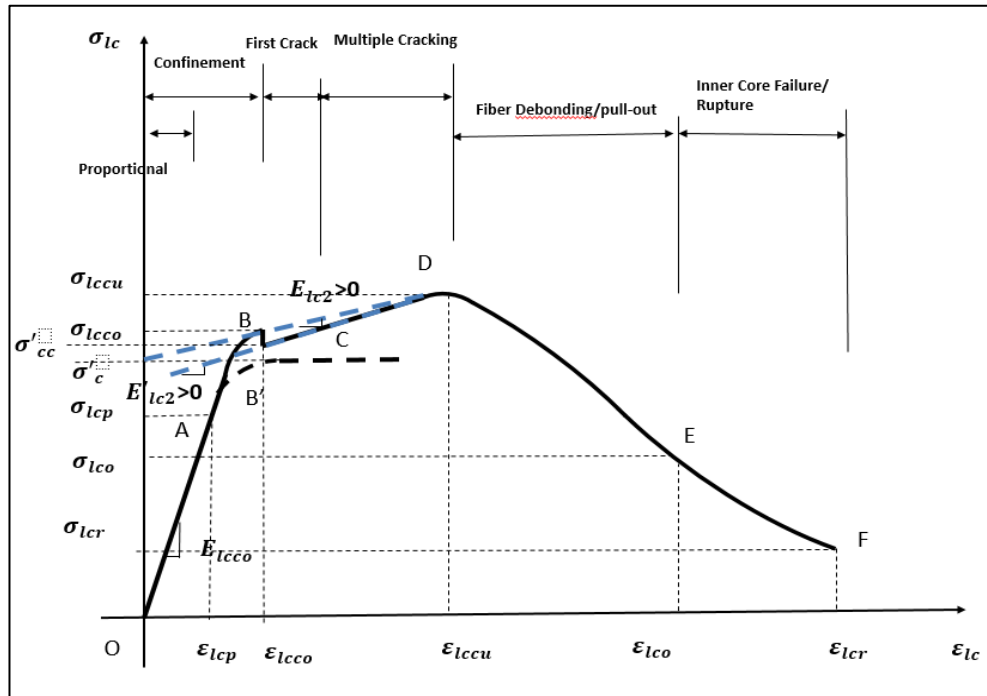
However, brittle failure is also noted when confinement strains of the composite are less than the peak axial compressive strains of the confined concrete, thus the composites are activated, however, confined concrete do not sustain axial compressive strains beyond peak (sudden rupture; explosive behavior) such as in Fiber-Reinforced Polymers (FRP).

Ductile failures are observed when the composite confinement strains are smaller than the peak axial compressive strains resulting in no surface cracks within the concrete core allowing the composite to get activated thus working to protect the concrete core. In addition, ductile failure occurs when composites allow a softening response and not a sudden failure beyond peak.

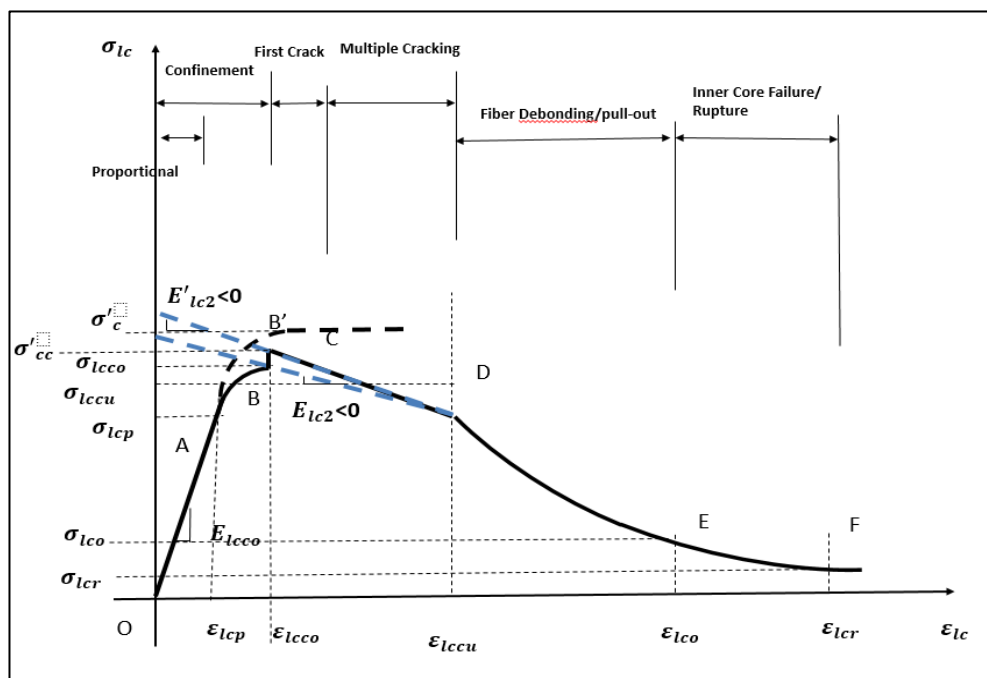
Confinements are also classified into continuous or discrete confinement/ *full* or *partial* confinement. Continuous confinement is when the composite is wrapped continuously around the structural members while in discrete confinements they are spaced at a specific pitch. Partial confinement²¹, when the peak axial stress of confined concrete is less than the confinement stress (circumferential tensile confinement stress measured at the plastic centroid, Refer to Appendix IV) and less than the strength of unconfined concrete, while full confinement is achieved when peak stresses are larger than the confinement stress, which is larger than the strength of pure concrete.

Figures IV-1 (a) and (b) represents typical graphs of confined concrete for the longitudinal stress versus the longitudinal strain for full and partial confinement. Figures IV-2 (a) and (b) represent typical graphs of confined concrete for the longitudinal stress versus the transverse strain for full and partial confinement. Figure

IV-3(a) is represented by Poisson's ratio (longitudinal strain versus transverse strain (radial) of confined concrete) of the material and Figure IV-3(b) represents a typical tensile stress strain curve of the composite or the lateral confinement.

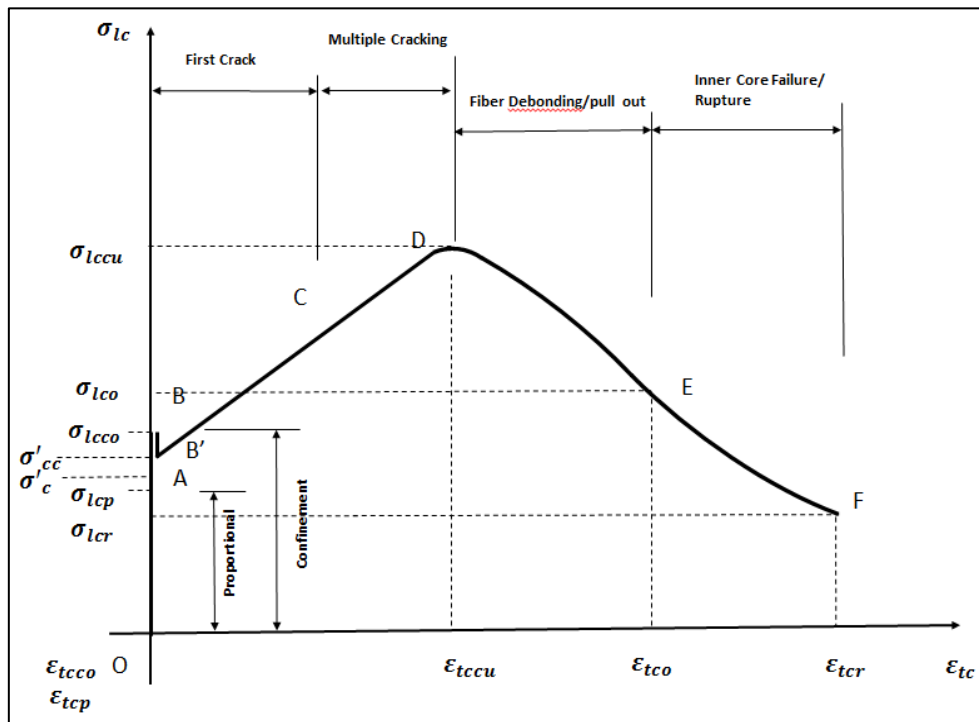


(a)

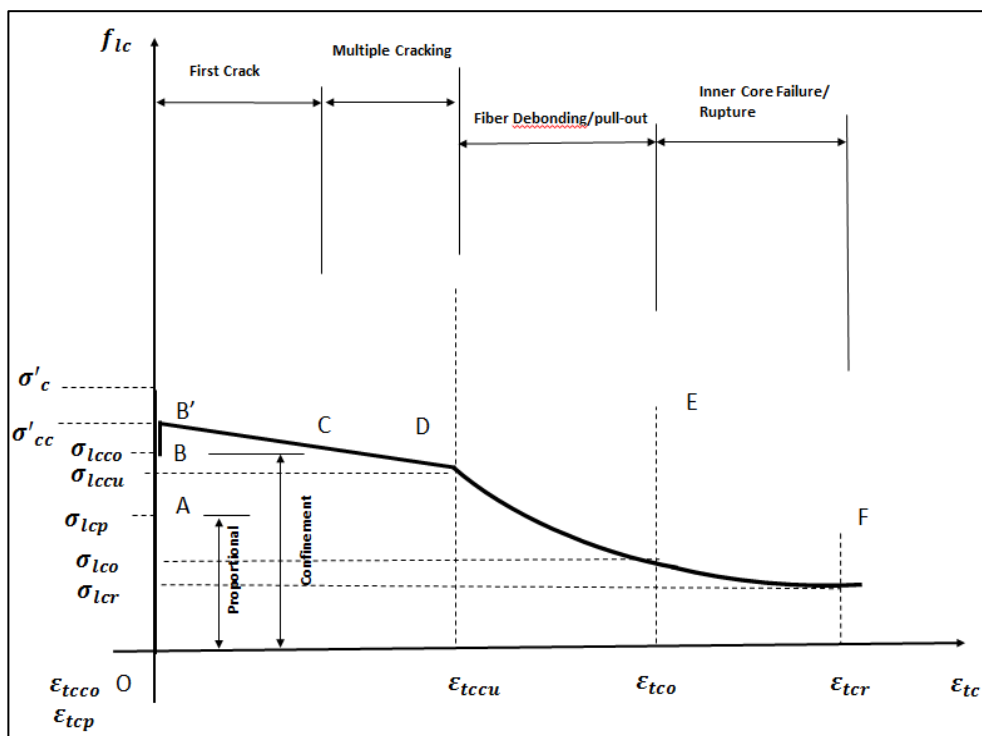


(b)

Figure IV-1: (a) Typical longitudinal stress-strain curves for fully confined concrete (b) Typical longitudinal stress-strain curves for partially confined concrete

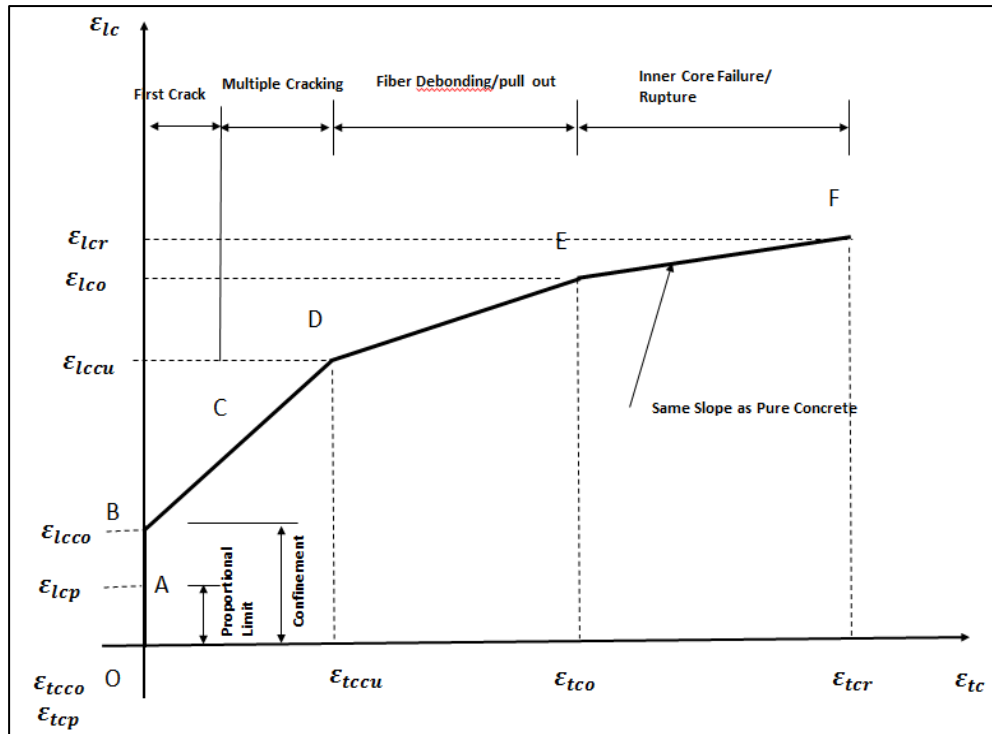


(a)

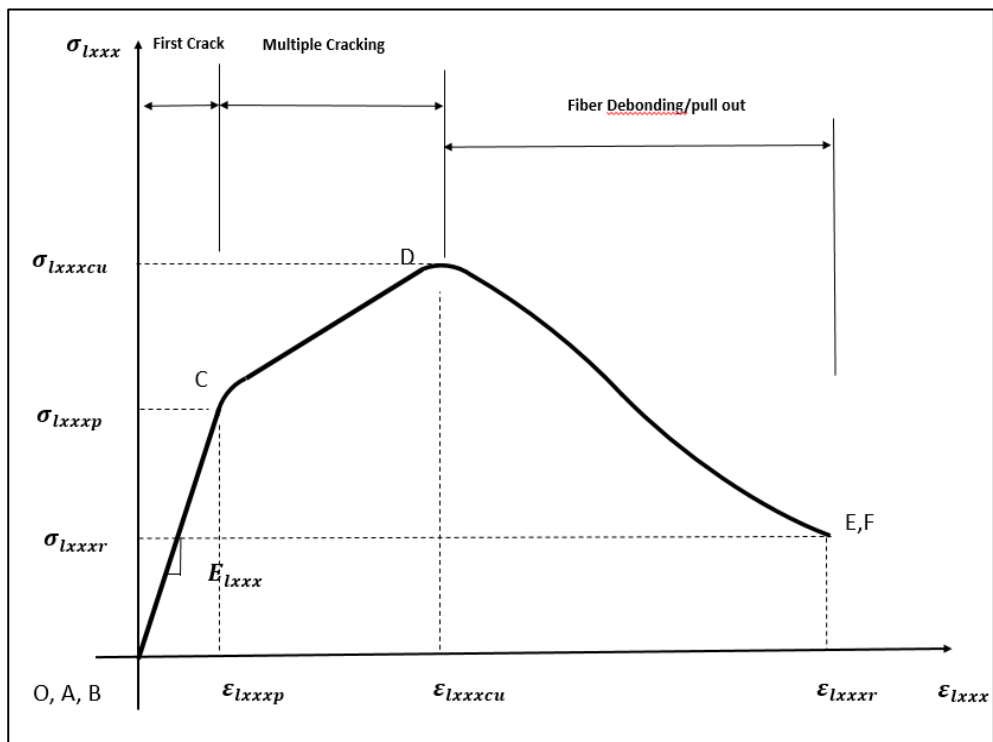


(b)

Figure IV-2: (a) Typical Longitudinal stress-transverse strain curves for fully confined concrete (b) Typical longitudinal stress-transverse strain curves for partially confined concrete



(a)



(b)

Figure IV-3: (a) Typical Longitudinal strain-transverse strain curves for confined concrete (b) Typical longitudinal stress-strain curves in tension for composites

Figures IV-1-2-3 are represented by the following different regions and behavior:

Ascending Branch

As defined the ascending branch consists of three distinct regions as shown in Figures IV (a,b):

1. *Confinement Region*: Only insignificant lateral expansion of the concrete column takes place in this region, and therefore no tensile stresses have yet developed in the confining composite. Consequently, the entire concrete as well as the confining composite carry compression. At the end of this region, stresses and strain values reach σ_{lcco} and ϵ_{lcco} .
2. *Transition Region*: The stress level in this region drops due to composite first crack. The extent of the decrease is a function of the level of confinement, i.e. the spacing or thickness of the discrete or continuous confinement respectively. The transition region represents the end of the confinement region and the onset of the composite activation region. This behavior is further discussed in the subsequent text.
3. *Composite Activation Region*: Significant lateral expansion takes place in this region, leading to the development of tensile stresses in the composite jacket. Stresses and strains in the concrete core effectively confined by the composite range between σ_{lcco} and ϵ_{lcco} and the peak values at σ_{lccu} and ϵ_{lccu} .

Descending Branch

As defined the descending branch the failure of the composite jacket starts first, followed by rupture of the concrete core. FRP confined concrete experience brittle failure (explosive rupture, no softening behavior effect). Spiral, wire mesh, FRC, FRM

and SIFC confined concrete exhibits different levels of ductile failure. Spiral, and /or wire mesh are governed by the spacing and yielding of the composite. FRC and FRM failure is governed by the fiber pull out, while SIFC failure is governed by the fiber debonding mechanism due to continuity of fibers. Specimens are classified into brittle and ductile failure based on a previously defined criteria.

Detailed explanation of presented regions:

4.1.1 Confinement Region

(OAB) represents the longitudinal strain ε_{lcco} , transverse strain ε_{tcco} and longitudinal stress σ_{lcco} of the confined concrete at end of confinement. In this region, the composite and the concrete core act as two springs in parallel, deform the same amount, and support a total load equal to the sum of the loads of each component. The elastic modulus of elasticity of the confined concrete is represented by E_{lcco} which is equal to that of pure concrete E_c for discrete composites and larger than E_c for continuous composites due to the additional effect of the modulus of the matrix in compression E_{mxxx} . The confinement region consists of a linear stage (OA) and a non-linear stage (AB). The elastic stage is represented by the following proportional limits of longitudinal strain ε_{lcp} , transverse strain ε_{tcp} and longitudinal stress σ_{lcp} of the confined concrete respectively. The non-linear stage is represented by the in-elastic modulus at E_{lc2} at the point $(\varepsilon_{lcco}, \sigma_{lcco})$ which is the slope of the line between σ'_c and σ_{lccu} where σ'_c is the ultimate strength of unconfined concrete, σ_{lccu} is the peak stress of confined concrete. It is noted that ε_{tcco} and ε_{tcp} , as shown in Figure IV-2(a) and IV-3(a), are zero during confinement and no transverse deformations are noted.

4.1.2 Transition Region

Point B is the transition point between confinement and the activation of the composite material. Composite material induces a composite tensile force that resist the lateral force within the concrete core. At this point, a sudden drop is expected because of the activation of the composite (first crack in the composite). Thus we will have a formation of two peaks; where a first peak occurs σ_{lcco} (end of confinement, activation of composite) and a second peak σ_{lccu} , that represents the strength of confined concrete. E'_{lc2} is the modulus during activation of the composite between end of confinement and peak σ_{lccu} ; which is the slope of the line between σ'_{cc} and σ_{lccu} . σ'_{cc} represents the compressive strength of the concrete core at start of composite activation. This change in slope is dependent on the thickness of the composite material for continuous confinement and the spacing for the discrete composites. There are optimized values for spacing and thickness for each type of composite above which renders the system ineffective, values and calculations presented later in the study.

When the spacing of discrete confinements is between zero and the optimized value, the point B which is the confined stress σ_{lcco} shifts downward from a higher value to reach point B'. Once the spacing reaches optimized value and larger, then point B matches point B' and the stress σ_{lcco} reaches σ'_{cc} (which is the stress at start of composite activation) and the slope E_{lc2} will equals E'_{lc2} .

$\sigma'_{cc} > \sigma'_c$ for spirals due to the cover thickness and $\sigma'_{cc} = \sigma'_c$ for wire mesh. For every spacing value, there is a different point location of B.

In the case of optimized thickness for continuous confinements, when the thickness of the composite is between zero ($\sigma'_{cc} = \sigma'_c$) and the optimized value, the point B' ($\sigma'_{cc} > \sigma'_c$) due to thickness of the composite starts moving upwards towards point B (σ_{lcco}).

For every thickness value there is a different point location of B'. Once the thickness reaches optimized value and larger, then point B' matches point B and the slope becomes E_{lc2} .

For partial confinement, the slopes are negative $E_{lc2} < 0$ and $E'_{lc2} < 0$ and the process is reversed as shown in Figures IV-1(b). Confined concrete stress (σ_{lcco}) is lower than the compressive strength of both normal concrete σ'_c and concrete core at start of composite activation σ'_{cc} . As the maximum recorded stress that can be achieved is the compressive strength of normal concrete, σ'_c . The strength shifts between confined concrete stress (σ_{lcco}) and normal concrete strength σ'_c based on the optimized spacing and thickness of the composite.

As for the ultimate/ peak strength of confined concrete σ_{lccu} it records a value lower than that of confined concrete stress (σ_{lcco}); causing negative slopes of inelastic modulus of elasticity. In other words, the confined concrete will have an ultimate strength value that is less than that of pure concrete. Such behavior is due to radial stresses caused by different fiber alignments, which is later studied in the upcoming chapters.

When the spacing of discrete confinements is between zero and the optimized value, the point B which is the confined stress σ_{lcco} shifts downward from B' (compressive strength of pure concrete) to reach point B. At zero discrete confinement the slope E_{lc2} equals E'_{lc2} and σ_{lcco} matches σ'_c . Once the spacing reaches optimized value and larger, then point B record a lower value than point B' thus stress $\sigma_{lcco} < \sigma'_{cc} < \sigma'_c$ (σ'_{cc} which is the stress at start of composite activation)

In the case of optimized thickness for continuous confinements, when the thickness of the composite is between zero ($\sigma'_{cc} = \sigma'_c$) and the optimized value, the point B due to

thickness of the composite starts moving upwards towards point B'. For every thickness value there is a different point location of B. Once the thickness reaches optimized value and larger, then point B matches point B' and the slope becomes $E'_{lc2} = E_{lc2}$.

4.1.3 First Crack / Multiple Cracking Region of Composite

This region is called the activation region. In this region (BCD) is represented by the longitudinal strain ε_{lccu} , transverse strain ε_{tccu} and longitudinal stress σ_{lccu} at peak of confined concrete. This represents the end of first crack (BC) or end of multiple cracking (CD) regions of the composite. The response of the composite separates from the concrete core and the tensile stress of the composite ($\varepsilon_{lxxxp}, \sigma_{lxxxp}, \varepsilon_{lxxxcu}, \sigma_{lxxxcu}$) as shown in Figure IV-3(b) is resisted by the lateral stress σ_2 within the core during composite activation. σ_{2cu} represents the lateral stress at peak or end of activation (end of first crack or multiple cracking of composite).

($\varepsilon_{lxxxp}, \sigma_{lxxxp}$) are the proportional strains and stresses of the composite at end of first crack for FRM, FRC and SIFC. $\varepsilon_{lxxxcu}, \sigma_{lxxxcu}$ are the strain and stress of composite at peak for FRM and FRC or end of multiple cracking for SIFC. Stresses and strains at proportional limit, peak and rupture are equal for each of SP2, SP3, WIM, FPG and FPC. The stress strain curve for these composites is a straight line. (*xxx is the index designation for the different types of composites as shown in the list of notations.*)

4.1.4 The fiber Debonding or Fiber Pull-Out Region

This region (DE) is represented by the longitudinal strain ε_{lco} , transverse strain ε_{tco} and longitudinal stress σ_{lco} at the end of fiber pull-out (FRC and FRM) or debonding SIFC. This is the final stage of fiber pull-out or debonding ($\varepsilon_{lxxxr}, \sigma_{lxxxr}$) represented by the rupture stress and strain of the fibrous composite as shown in Figure IV-3(b). Eventual exposure of the concrete core resulting in the initiation process of the first

crack of the concrete core. This region does not exist for SP2, SP3, WIM, FPG and FPC.

4.1.5 The Concrete Core First Crack Region

In this region (EF) represent the rupture longitudinal stain ϵ_{lcr} , rupture transverse strain ϵ_{tcr} and rupture longitudinal stress σ_{lcr} at end of confined concrete core failure. This is failure of the specimen where the concrete core has ruptured. The failure response is different than that of unconfined concrete due to confinement. The slope of the line in Figure IV-3(a) in that region represents a Poisson's ratio of unconfined concrete that was originally in confinement, which is larger than that of unconfined concrete.

4.2 DISCUSSION OF CONFINED CONCRETE WITH DIFFERENT COMPOSITES

4.2.1 Low Performance Brittle Failure Composites (LPBF)

CON, SP3 and FRM: This system is considered unconfined with a confinement region $(\epsilon_{lcco}, \epsilon_{tcco}, \sigma_{lcco})$ (OAB) dominated by the concrete core first crack region only whereby the column has no first or multiple cracking of composite. The 3 cm (1.18 in.) spacing in SP3 was large enough to allow for the propagation of surface cracks though the spiral reinforcement towards the concrete core. The confinement stress and strain $(\sigma_{lcco}, \epsilon_{lcco})$ are close to the stress and strain of unconfined concrete (σ_c', ϵ_c') . During confinement an elastic (OA) region exists with a modulus E_{lcco} and in-elastic regions of $E_{lc2} = E'_{lc2} = 0$ reaching the peak strain and stress $(\epsilon_{lccu}, \epsilon_{tccu}, \sigma_{lccu})$ that of unconfined concrete (BCD, BC=0 and CD=0)

In FRM due to varying orientation of fibers, tensile radial stresses occur on the concrete core thus weakening it and translating to peak stresses lower than unconfined concrete resulting in partial confinement. $E_{lc2} \neq E'_{lc2} \cdot E_{lc2} < 0$ and E'_{lc2} does not exist since the

confinement strain ε_{lcc0} is close to peak strain ε_{lccu} . Before peak stress is reached (BCD, CD=0), first crack with no multiple cracking of the composite is noted. This is related to stresses and strains of composite at first crack and peak ($\varepsilon_{IFRMp}, \sigma_{IFRMp}, \varepsilon_{IFRMcu}, \sigma_{IFRMcu}$). After peak stress and strain of the confined concrete, rupture of the composite ($\varepsilon_{lco}, \varepsilon_{tco}, \sigma_{lco}$) (DEF) will take place, due to pull-out of fibers ($\varepsilon_{IFRMr}, \sigma_{IFRMr}$) (DE), resulting in a typical stress strain failure response of the concrete core ($\varepsilon_{lcr}, \varepsilon_{tcr}, \sigma_{lcr}$) (EF). The failure is brittle due to the low percentage of fiber volume fraction and lack of presence of coarse aggregates.

Figure IV-4 (a) shows the brittle typical cone failure of concrete with splitting effect of the cylinder. Figure IV-4(b) shows fiber pull-out during the FRM confined concrete brittle failure.



(a)

(b)

(c)

Figure IV-4 (a) Typical failure of concrete specimen (b) Typical failure of concrete specimen confined with FRM with 1 percent fibers (c) Typical failure of spiral reinforced concrete specimen

4.2.2 Low Performance Ductile Failure Composites (LPDF)

SP2, WIM and FRC: The response of the system is similar to that of unconfined concrete during confinement and then a first crack of the spiral or wire mesh where the composite picks up its tensile stress

($\varepsilon_{lxxxp} = \varepsilon_{lxxxcu} = \varepsilon_{lxxxr}$; $\sigma_{lxxxp} = \sigma_{lxxxcu} = \sigma_{lxxxr}$) Where xxx is the index designation for SP2 or WIM. The tensile stress and strain at first crack and peak for FRC is represent by (ε_{lFRCp} , σ_{lFRCp} , ε_{lFRCcu} , σ_{lFRCcu}). In this region (BCD CD=0) the tensile stresses of the composite develop lateral core stresses σ_2 within the concrete core. Spalling is noted during that phase for the spiral reinforcement since the spirals have a clear cover while the wire mesh no spalling occurs. For SP2 and WIM, $E'_{lc2} = E'_{lc2}$ (curve shifts down) where the confined stress σ_{lcco} matches σ'_{cc} where $\sigma'_{cc} > \sigma'_c$ for spirals due to the presence of a concrete cover and $\sigma'_{cc} = \sigma'_c$ for wire mesh.

In (FRC), since the peak and confinement stresses are lower than pure concrete due to varying fiber orientation, partial confinement similar to FRM is considered. $E'_{lc2} \neq E'_{lc2} < 0$. The shift between B and B' is relatively significant since the confinement strains are smaller than the peak strains.

Figure IV-4(c) shows the effect of spiral confinement and spalling effects during first yield of the spirals and eventual cracking at the surface of the concrete core. Figure IV-5(a) shows limited cracking at the surface due to the smaller spacing of the wire mesh with the mesh protecting the concrete core and an eventual failure of the wire mesh. Figure IV-5(b) shows a ductile failure with limited crack width of the FRC composite compared to FRM due to the larger volume fraction of the fibers and presence of coarse aggregates in the composite mix.



(a)

(b)

(c)

Figure IV-5 (a) Typical failure of concrete specimen confined with wire mesh (b) Typical failure of concrete specimen confined with FRC with 2 percent fibers (c) Typical failure of concrete specimen confined with carbon FRP

4.2.3 High Performance Brittle Failure Composites (HPBF)

FPC, FPG: Fiber Reinforced Polymers exhibit a confinement region (OAB) and eventually a first crack of the composite (BCD, CD=0) thus initiating the stress strain response of the composite ($\varepsilon_{lxxxp} = \varepsilon_{lxxxcu} = \varepsilon_{lxxxr}$; $\sigma_{lxxxp} = \sigma_{lxxxcu} = \sigma_{lxxxr}$) where xxx is the index designation for FPC and FPG. At the transition point of the stress-strain curve, $E_{lc2} \neq E'_{lc2}$ (curve shifts up) resulting in a first and second peak response. Due to composite brittleness, initiation of first cracks in the composite and concrete core takes place simultaneously reaching peak stress and strain of confined ($\varepsilon_{lccu} = \varepsilon_{lcr}$, $\varepsilon_{tccu} = \varepsilon_{tcr}$; $\sigma_{lccu} = \sigma_{lcr}$). No fiber pull-out and no later first crack of the concrete core takes place (DEF, DE=0, EF=0). This simultaneous behavior of first crack in the composite and in the concrete core results in a brittle high explosive rupture with no softening response beyond peak as in other composites. Figure IV-5 (c) and Figure IV-6 (a) show the brittle failure of carbon and glass after first crack of the composite.

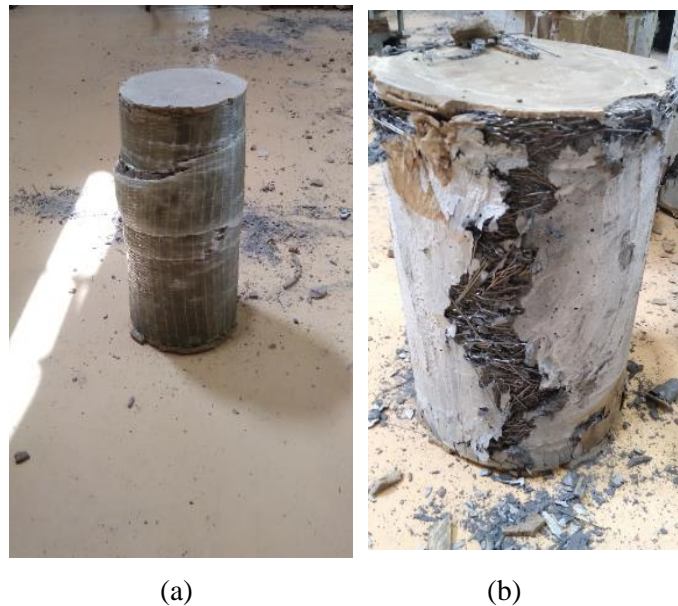


Figure IV-6:(a) Typical failure of concrete specimen confined with glass FRP (b) Typical failure of concrete specimen confined with SIFCON with 12 percent fibers

4.2.4 High Performance Ductile Failure Composites (HPDF)

Fibers are transversely aligned that will produce continuous confinement. The confinement region $(\epsilon_{lcc0}, \epsilon_{tcc0}, \sigma_{lcc0})$ (OAB), first crack (BC) $(\epsilon_{lSIFp}, \sigma_{lSIFp})$ and multiple cracking $(\epsilon_{lSIFcu}, \sigma_{lSIFcu})$ (CD) takes place due to the continuity of fibers. First cracks of the composite results and multiple cracks propagate longitudinally along the circumference of the cylinder. $E_{lc2} = E'_{lc2} > 0$ and the point B' reaches point B at $(\epsilon_{lcc0}, \sigma_{lcc0})$ which is larger than the ultimate strength of unconfined concrete. End of multiple cracking resulting in a peak stress and strain of confined concrete $(\epsilon_{lccu}, \epsilon_{tccu}, \sigma_{lccu})$. At end of multiple cracking, a localized crack is formed where fiber debonding takes place $(\epsilon_{lSIFr}, \sigma_{lSIFr})$ (DE). Through the localized crack, a crack at the surface of the concrete core is formed $(\epsilon_{lco}, \epsilon_{tco}, \sigma_{lco})$ (DE), resulting in propagation to the concrete core and eventual rupture of the concrete core and failure $(\epsilon_{lcr}, \epsilon_{tcr}, \sigma_{lcr})$ (EF). Figure IV-6 (b) shows the crack width being sustained by

the fibers during debonding due to the continuity of fibers and resulting in softening effects of the system.

4.3 EXPERIMENTAL RESULTS AND DISCUSSION

Tables IV-1 and IV-2 show experimental results for pre-peak and post-peak experiment longitudinal stress and longitudinal strain parameters of representative curves for the different composites. All parameters have been as previously defined and in the notation list. T_l, T_t represent the area under the longitudinal and transverse stress strain curve till rupture and TI_l, TI_t represent the toughness index in the longitudinal and transverse direction which is the ratio of the area of the system to that of unconfined concrete indicative of energy absorption. The parameters in parenthesis represent the associated composite parameters as previously defined. Tables IV-3 and IV-4 show experimental results for pre-peak and post-peak longitudinal strain and transverse strain parameters of representative curves for the different composites. Tables X-1 to X-16 in Appendix I shows the tabulated experimental results for all tested samples. Figure IV-7 to IV-17 represent experimental longitudinal and transverse stress-strain curves and the Poisson ratio curves for the different composites for comparison. Figures X.1 to X.27 in Appendix I show the experimental longitudinal and transverse stress-strain curves and the Poisson ratio curves for all different composites specimens. A regression analysis was performed for these graphs to develop the corresponding analytical equations for the transverse stress-strain curves.

Various experimental difficulties were faced that have led to lack of data consistency. An analysis was thus made on one typical specimen picked based on various literature review data and engineering standpoint judgement;

The following results are noted:

Table IV-1: Pre peak experimental data for longitudinal stress and strain of confined concrete (0.15 Ksi=1 MPa)

		E_{lcco} MPa (Ksi)	σ_{lcp} MPa (Ksi)	ϵ_{lcp}	E_{lc2} MPa (Ksi)	E'_{lc2} MPa (Ksi)	σ_{lcco} MPa (Ksi)	ϵ_{lcco}
LPBF	CON	27692 (4016)	36 (5.2)	0.0013	0	0	42 (6.1)	0.003
	FRM	22857 (3428)	32 (4.5)	0.0014	-2250 (-326)	NA	30 (4.4)	0.004
	SP3	25000 (3626)	35 (5.1)	0.0014	0	0	42.3 (6.13)	0.004
LPDF	FRC	23000 (3336)	23 (3.3)	0.001	-5333 (-773.48)	-16000 (-2321)	24 (3.5)	0.002
	WIM	26000 (3771)	26 (3.8)	0.001	210 (32)	210 (32)	42.42 (6.15)	0.003
	SP2	24667 (3578)	37 (5.4)	0.0015	210 (32)	210 (32)	43 (6.2)	0.003
HPBF	FPC(SCH-41-1)	28572 (4144)	40 (5.8)	0.0014	2800 (406)	3500 (508)	46 (6.7)	0.002
	FPC(SCH-41-2)	27693 (4016)	36 (5.2)	0.0013	2000 (290)	2333 (338)	48 (7)	0.003
	FPC(11UP-2)	26471 (3839)	45 (6.5)	0.0017	1125 (163)	1411.8 (204.8)	56 (8)	0.007
	FPG(SEH-1)	24667 (3839)	37 (5.4)	0.0015	136 (20)	125 (18.7)	42 (6.1)	0.006
	FPG(SEH-2)	24667 (3839)	37 (5.4)	0.0015	1684 (252.6)	1842 (276.3)	48 (7)	0.004
HPDF	SIFC	32500 (4714)	26 (3.8)	0.0008	2000 (290)	2000 (290)	42 (6.1)	0.0014

Table IV-2: Post-peak experimental data for longitudinal stress and strain of confined concrete (symbols in parenthesis represent the composite parameters) (0.15 Ksi=1 MPa)

		σ_{lccu} (σ_{lxxxp} , σ_{lxxxcu}) MPa (Ksi)	ϵ_{lccu} (ϵ_{lxxxp} , ϵ_{lxxxcu})	σ_{lco} (σ_{lxxxr}) MPa (Ksi)	ϵ_{lco} (ϵ_{lxxxr})	σ_{lcr} MPa (Ksi)	ϵ_{lcr}	T_l MPa (Ksi)	TI_l
LPBF	CON	42 (6.1)	0.0025	-	-	35 (5.1)	0.005	0.135 (0.019)	1
	FRM	33 (4.8)	0.004	32 (4.6)	0.0051	31 (4.5)	0.0057	0.14 (0.02)	1.1
	SP3	42.3 (6.13)	0.004	-	-	35 (5.1)	0.008	0.17 (0.025)	1.3
LPDF	FRC	26 (3.8)	0.003	25 (3.6)	0.007	16.5 (2.4)	0.016	0.22 (0.03)	1.6
	WIM	44 (6.4)	0.0041	-	-	30 (5.2)	0.011	0.26 (0.04)	2
	SP2	45 (6.5)	0.0043	-	-	20 (2.9)	0.02	0.59 (0.09)	4.4
HPBF	FPC (SCH41-1)	70 (10)	0.01	-	-	70 (10)	0.01	0.53 (0.08)	4
	FPC (SCH41-2)	84 (12)	0.021	-	-	84 (12)	0.021	1.35 (0.19)	10
	FPC (11UP-1)	78 (11)	0.032	-	-	78 (11)	0.025	1.7 (0.25)	12.6
	FPG (SEH-1)	45 (6.5)	0.022	-	-	45 (6.5)	0.022	0.4 (0.058)	3
	FPG (SEH-2)	80 (11.6)	0.023	-	-	80 (11.6)	0.023	1.35 (0.19)	10
HPDF	SIFC	52 (7.5)	0.004	50 (7.2)	0.0054	20 (2.9)	0.042	1.28 (0.18)	10

Table IV-3: Pre-peak experimental data for longitudinal and transverse strains of confined concrete (symbols in parenthesis represent the composite parameters)

		ϵ_{lcp}	ϵ_{tcp}	ϵ_{lcco}	ϵ_{tcco}	ϵ_{lccu} ($\epsilon_{lxxxp}, \epsilon_{lxxxcu}$)	ϵ_{tccu} ($\epsilon_{lxxxp}, \epsilon_{lxxxcu}$)
LPBF	CON	0.0013	0.00039	0.0025	0.00075	0.0025	0.00075
	FRM	0.0014	0	0.004	0.00032	0.004	0.00032
	SP3	0.0014	0.000067	0.004	0.00023	0.004	0.00067
LPDF	FRC	0.001	0	0.002	0	0.003	0.00045
	WIM	0.001	0	0.002	0	0.0041	0.0075
	SP2	0.0015	0	0.003	0	0.0043	0.0006
HPBF	FPC(SCH 41-1)	0.0014	0	0.002	0	0.01	0.0021
	FPC (SCH 41-2)	0.0013	0	0.003	0	0.021	0.004
	FPC (11UP-2)	0.0017	0	0.0065	0	0.032	0.006
	FPG (SEH-1)	0.0015	0	0.006	0	0.022	0.0078
	FPG (SEH-2)	0.0015	0	0.004	0	0.023	0.009
HPDF	SIFC	0.0008	0	0.0014	0	0.004	0.0025

Table IV-4: Post-peak experimental data for longitudinal and transverse strains of confined concrete (symbols in parenthesis represent the composite parameters) (0.15 Ksi=1 MPa)

		ϵ_{lco} (ϵ_{lxxxr})	ϵ_{tco} (ϵ_{lxxxr})	ϵ_{lcr}	ϵ_{tcr}	ν	T_t MPa (Ksi)	TI_t
LPBF	CON	-	-	0.005	0.0015	0.3	0.051 (0.00765)	1
	FRM	0.0051	0.0013	0.0057	0.002	-	0.058 (0.0086)	1.14
	SP3	-	-	0.008	0.0017	0.1	0.039 (0.0058)	0.76
LPDF	FRC	0.007	0.004	0.016	0.012	-	0.33 (0.0368)	5.88
	WIM	-	-	0.011	0.015	-	0.59 (0.089)	11.56
	SP2	-	-	0.02	0.011	-	0.335 (0.05)	6.62
HPBF	FPC(SCH 41-1)	-	-	0.01	0.0021	-	0.133 (0.019)	2.60
	FPC (SCH 41-2)	-	-	0.021	0.004	-	0.267 (0.04)	5.24
	FPC (11UP-2)	-	-	0.025	0.006	-	0.4 (0.06)	7.84
	FPG (SEH-1)	-	-	0.022	0.0078	-	0.34 (0.051)	6.67
	FPG (SEH-2)	-	-	0.023	0.009	-	0.54 (0.081)	10.64
HPDF	SIFC	0.0054	0.003	0.042	0.016	-	0.685 (0.103)	13.43

4.3.1 Low Performance Brittle Failure Composites (LPBF)

CON and SP3 are similar in their performance. The initial modulus of confinement is typical of concrete at 28000 MPa (4061 ksi). The confinement strains of SP3 and FRM are higher than CON due to confinement. The strength of SP3 is that of unconfined concrete at 42 MPa (6.3 ksi). Since there is no first crack of composite for SP3, the slopes E_{lc2} at end of confinement and E'_{lc2} during composite activation are zero.

The strength for FRM is 30 MPa (4.5 ksi) lower than 42 MPa (6.3 ksi) due to partial confinement where $E_{lc2} < 0$. Strains at peak for FRM and SP3 were at 0.004 compared to 0.0025 for CON. All lateral confinements had the same toughness index close to one. Transverse strains for SP3 reached up to 0.0017 at rupture compared to 0.0015 for CON. Transverse strains for FRM reached 0.002 due to fiber pull out. The transverse toughness indices of FRM was in the range of 1.2 times that of concrete due to the presence of fibers, However toughness indices of SP3 was approximately equal to that of normal concrete. Figures IV-7, IV-8, and IV-9 represents experimental longitudinal and transverse stress-strain curves and the Poisson ratio curves for LPBF composites.

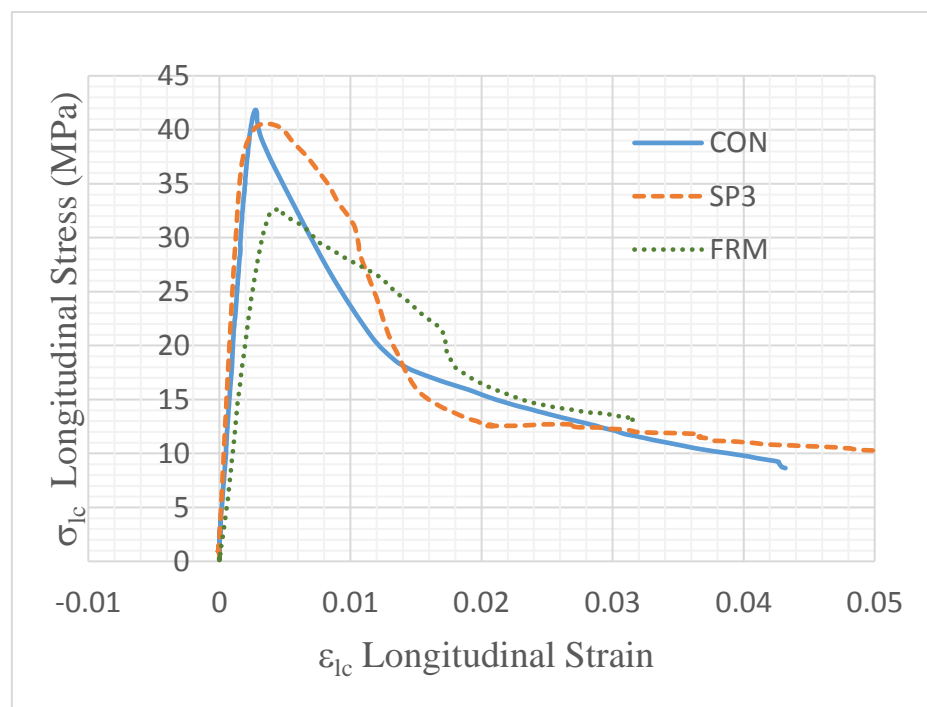


Figure IV-7: Stress strain-longitudinal-LPBF (0.15Ksi=1 MPa)

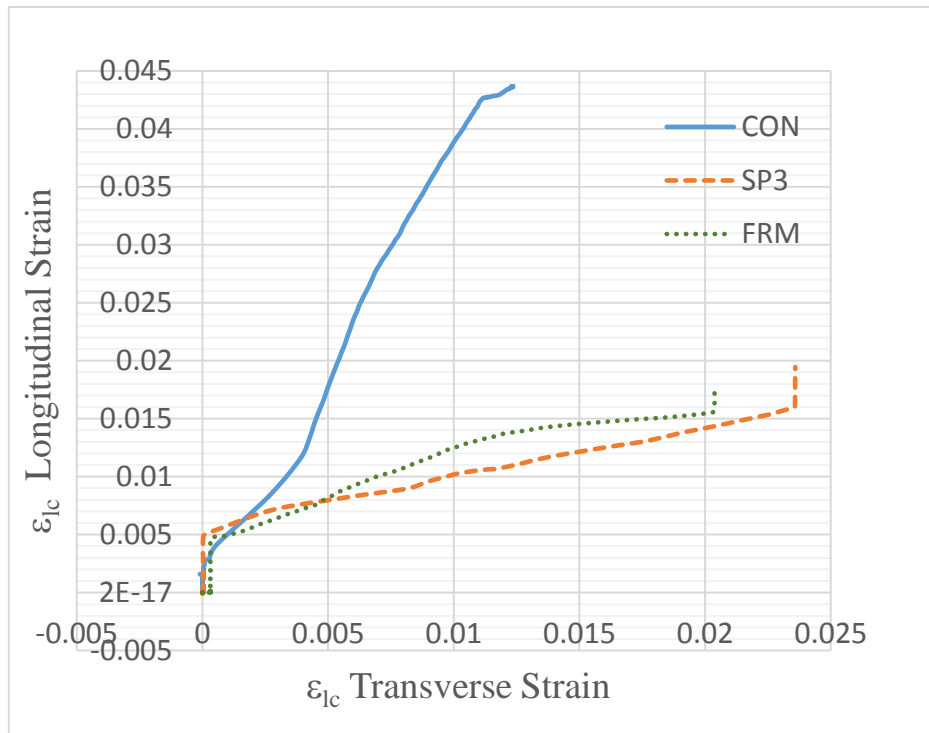


Figure IV-8: Longitudinal strain-transverse-LPBF (0.15Ksi=1MPa)

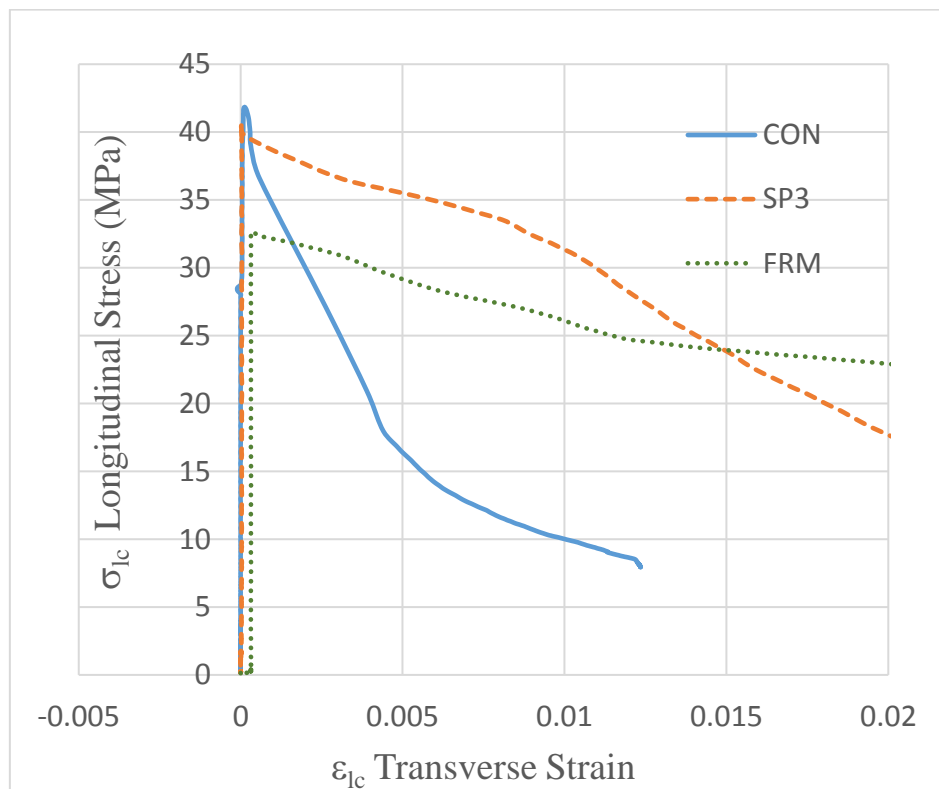


Figure IV-9: Stress strain-transverse-LPBF (0.15Ksi=1MPa)

4.3.2 Low Performance Ductile Failure Composites (LPDF)

The modulus of elasticity of the confinement remains the same at 26,000 MPa (3900 ksi) same as unconfined concrete since the spirals and wire mesh do not contribute to the elastic modulus. A slight increase in strength over unconfined concrete is noted for WIM and SP2 equal to 43 MPa (6.6 ksi). The low values of the moduli of elasticity $E_{lc2} = E'_{lc2} = 210MPa (30.5Ksi)$ indicates that the ultimate stress is close to that of unconfined concrete. FRC showed a drop in strength of 26 MPa (4 ksi) due to partial confinement with E_{lc2} and $E'_{lc2} < 0$. The rupture strain and stress for the spiral showed a better improvement than WIM and FRC with values of 0.02 compared to 0.01 and 0.016. The toughness index is double and four times that of WIM and FRC, respectively.

The transverse strains of WIM is 0.0075 at peak and 0.015 at rupture resulting in a toughness index of 11.6 compared to that of SP2 and FRC of 6 as shown in TableIV-4. The high values of the toughness are indicative of possible delamination of the wire mesh from the concrete core surface. FiguresIV-10, IV-11, and IV-12 represents experimental longitudinal and transverse stress-strain curves and the Poisson ratio curves for LPDF composites.

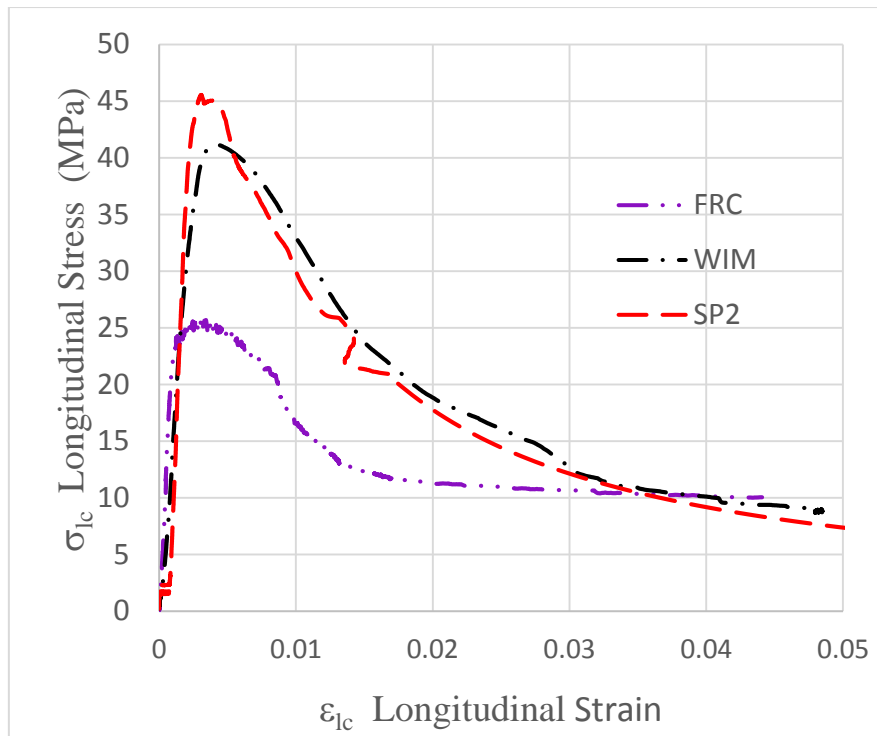


Figure IV-10: Stress strain-longitudinal-LPDF (0.15Ksi=1MPa)

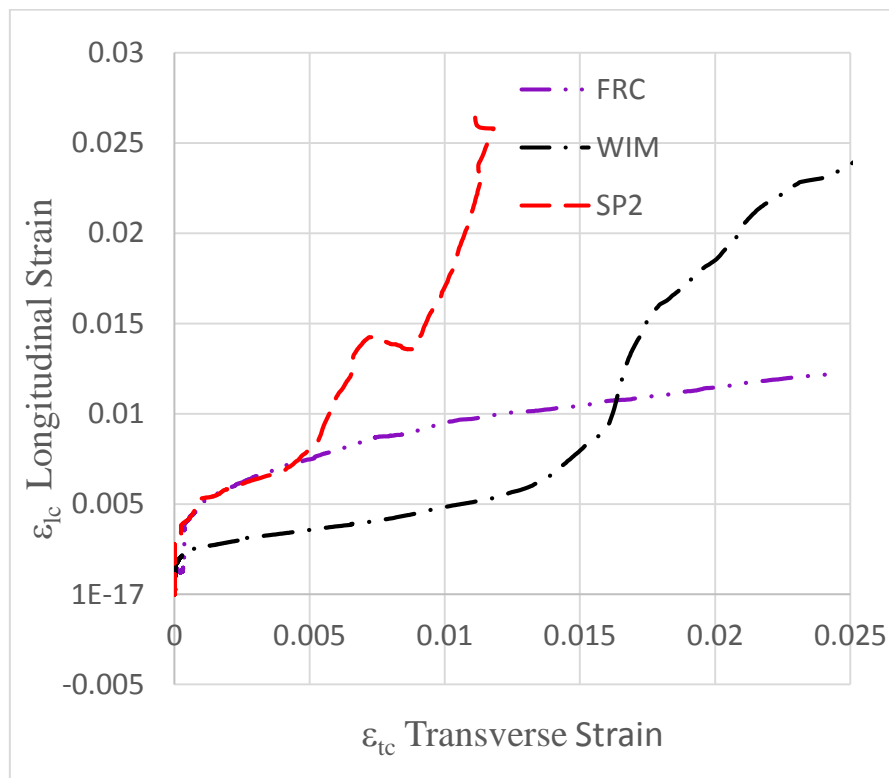


Figure IV-11: Stress strain-Transverse-LPDF (0.15Ksi=1 MPa)

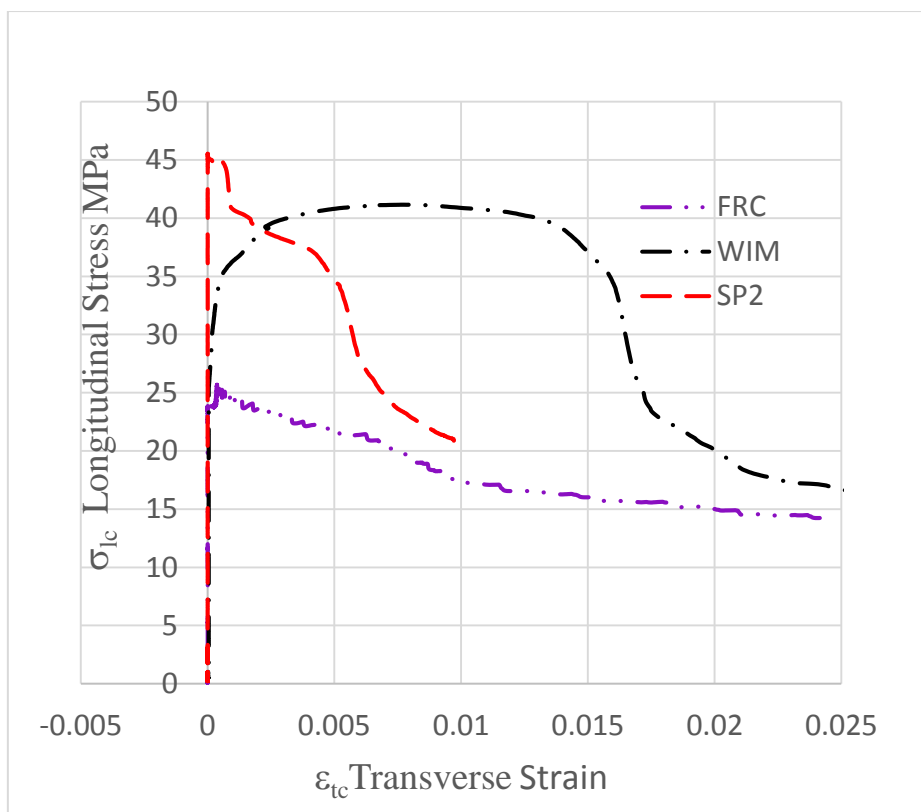


Figure IV-12: Longitudinal strain-Transverse-LPDF (0.15Ksi=1 MPa)

4.3.3 High Performance Brittle Failure Composites (HPBF)

Carbon SCH-2 layer showed the most improvement in strength compared to other carbon FRP's with a strength of 84 MPa (12.6 ksi) compared to other carbon FRP's ranging about 78 MPa (11.7 ksi) to 80 MPa (12 ksi). Glass with one layer was the weakest with strength of 50 MPa (7.5 ksi). However, the SCH-11UP had the largest strain at failure at 0.025 with toughness index of 8. The confinement stresses for all FRP's were in the range of 50 MPa (7.5 ksi) and confinement strains ranging between 0.002 to 0.007. For carbon FPC and FPG, a two-peak stress is expected since $E'_{lc2} \neq E'_{lc2} > 0$ with values shown in Table IV-1.

Transverse strains at peak and rupture were reached up to 0.009 for FPG and 0.006 for FPC-SCH-11UP and 0.004 for FPC-SCH-41. Figures IV-13, IV-14, and IV-15 represents experimental longitudinal and transverse stress-strain curves and the Poisson ratio curves for HPBF composites.

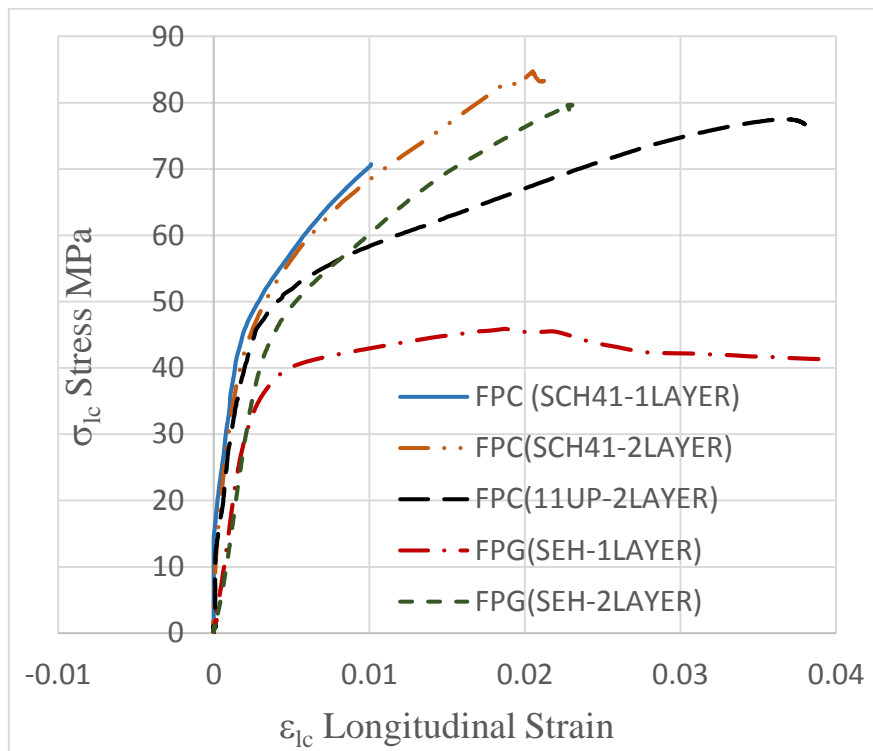


Figure IV-13: Stress strain-Longitudinal -HPBF (0.15Ksi=1 MPa)

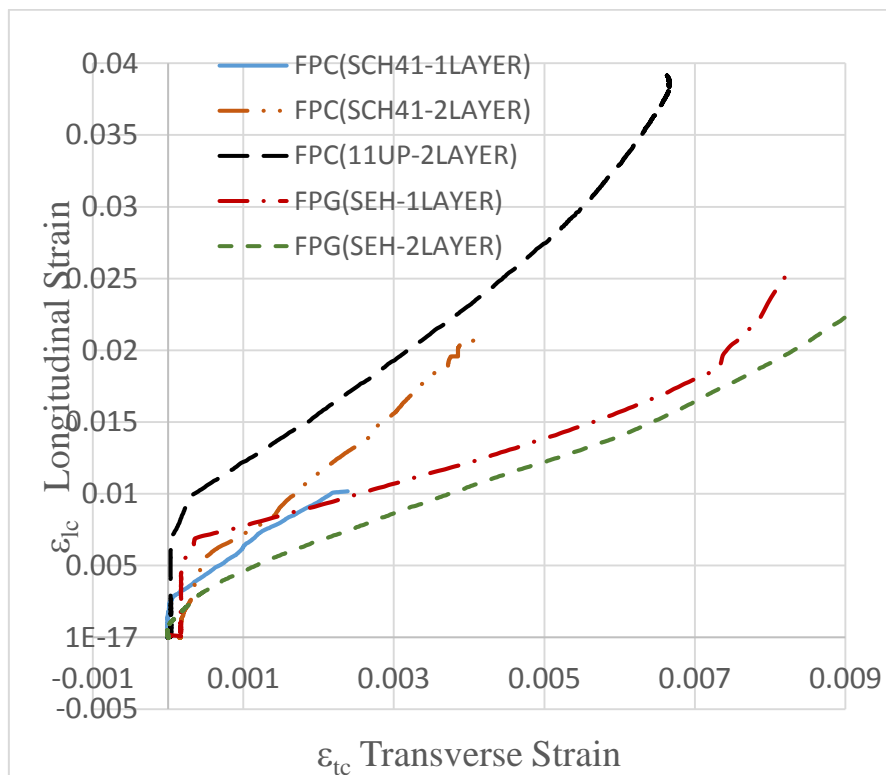


Figure IV-14: Stress strain-Transverse -HPBF (0.15Ksi=1 MPa)

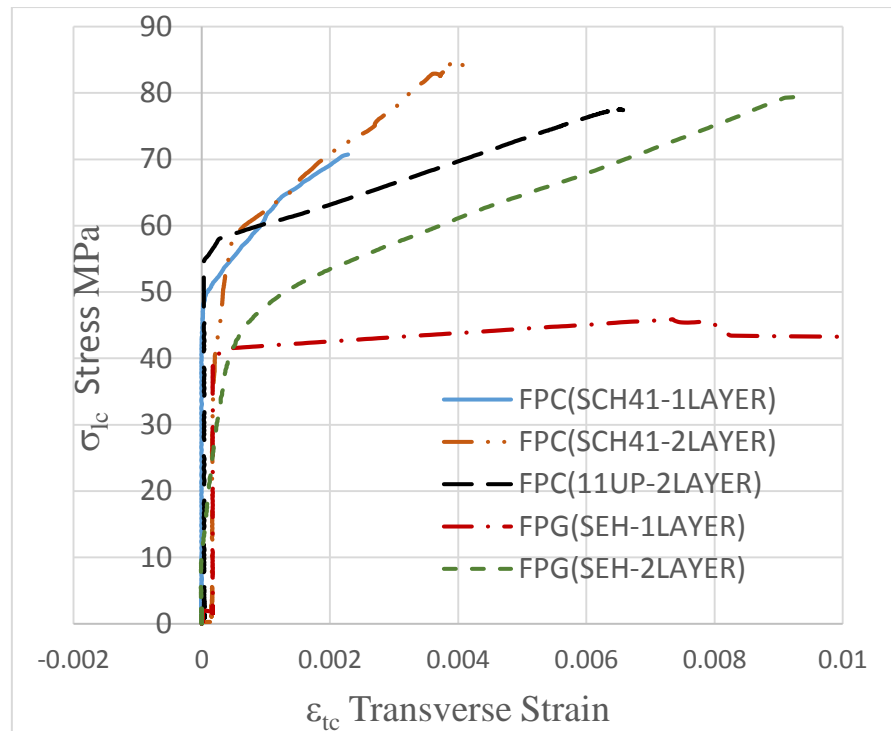


Figure IV-15: Longitudinal strain-Transverse -HPBF (0.15Ksi=1 MPa)

4.3.4 High Performance Ductile Failure Composites (HPDF)

SIFC showed some improvement in strength at 52 MPa (8.1 ksi) compared other fibrous composite. However, it reached the highest rupture strains due to continuity of fibers and debonding effects. The confinement strains were low at 0.0014 maintaining confinement and reached high peak strains at 0.005 due to multiple cracking, which is not noted in other composites that exhibited only single cracks. For SIFC no expected drop in stress at the transition point B was noted resulting in moduli $E_{lc2} = E'_{lc2} > 0$ with values shown in Table IV-1. The composite was fully effective in confinement since there was no drop in stress at the transition point. Although the toughness index is 10 close to FPC-11 UP and similar to glass FPG there was no brittle failure but a softening response at debonding. Fibers are bridging the cracks thus protecting the concrete core during the load duration as recommend for blast and impact loads¹.

Transverse strains reached the highest at 0.016 and longitudinal and lateral toughness indices of 10 and 14 due to continuity of fibers and debonding effects. Figures IV-16, IV-17, IV-18 represents experimental longitudinal and transverse stress-strain curves and the Poisson ratio curves for HPDF composites.

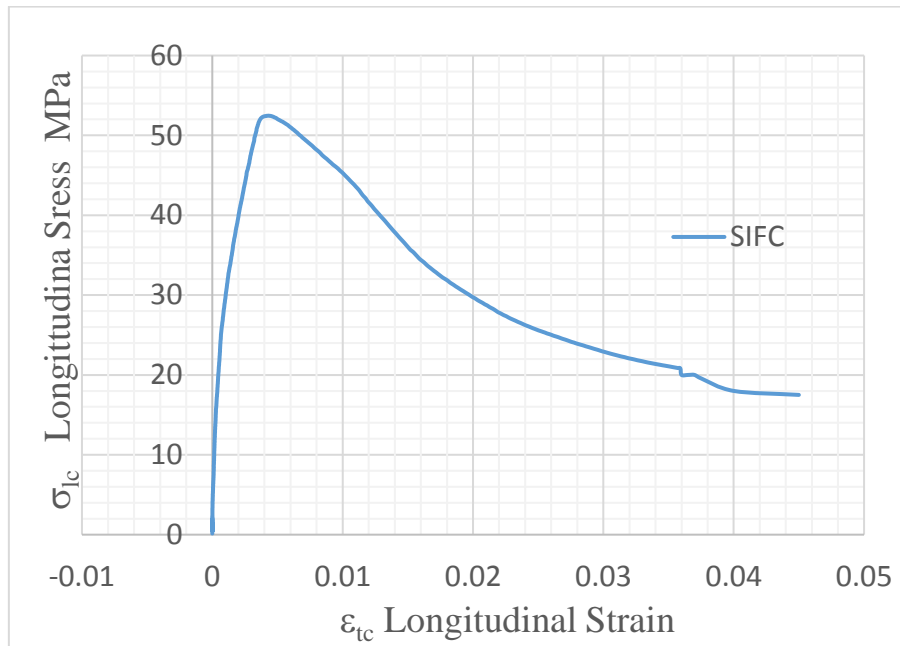


Figure IV-16: Stress strain-Longitudinal -HPDF (0.15Ksi=1 MPa)

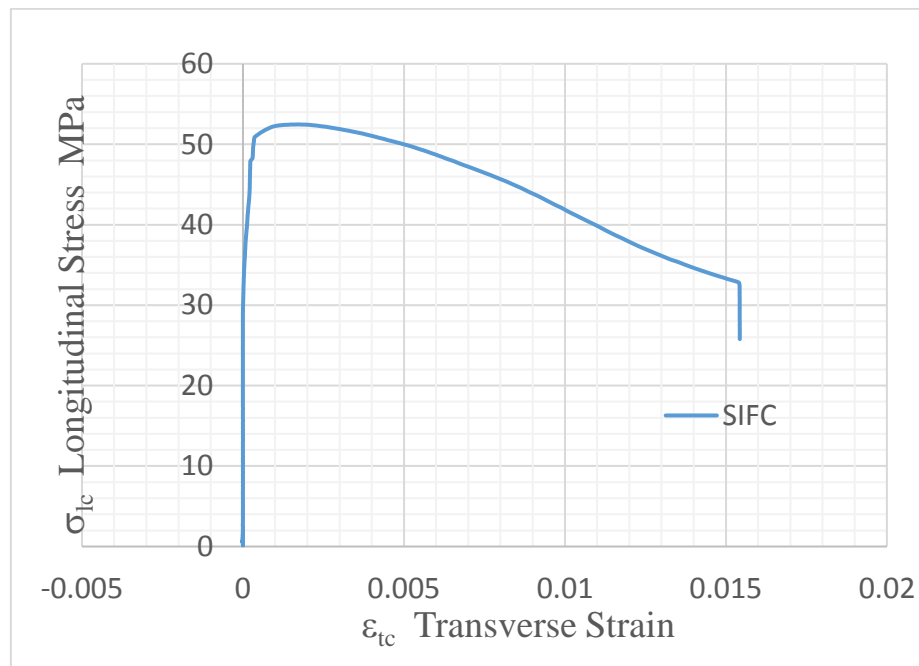


Figure IV-17: Stress strain-Transverse -HPDF (0.15Ksi=1 MPa)

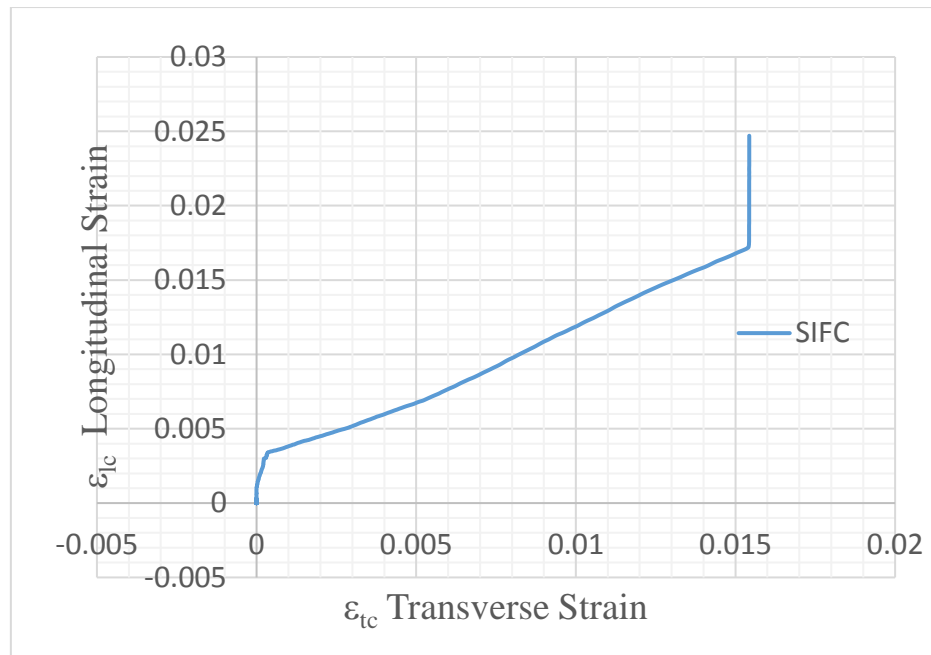


Figure IV-18: Longitudinal strain-Transverse -HPDF (0.15Ksi=1 MPa)

4.3.5 Confinement Composites Analysis and Discussion

FRP showed the highest strength compared to other composites. Carbon FPC with 2-layers showed better performance than glass FPG. Although concrete confined with FRC and FRM lead to lower strengths due to partial confinement, some ductility and softening effects beyond peak were noted due to fiber pull-out. Spirals spaced 20 mm (0.78 in.) and wire mesh showed slight improvement in the confinement of concrete with the spirals providing better ductility and larger strains at rupture than wire mesh. However, stresses at rupture for WIM were higher due to vertical tie resistance. Toughness indices of wire mesh ranged about 2.0 while spirals at 20mm (0.78 in.) spacing indices were at 4.4. Glass with 1 layer showed the same toughness index as WIM and SP2 although the strength was higher but brittle failure was expected leading to the same toughness index.

SIFC showed great improvement in confinement and had a toughness index of 10 compared to the 11UP carbon FPC at 12. The advantage of SIFC is the large

longitudinal and transverse strains at rupture and the softening effect that are beneficial for blast and impact loads where resilience is required.

Transverse strains at peak for high performance composites ranged between 0.002 and 0.009 compared to 0.0003 and 0.0006 for low performance composites with wire mesh as an exception at 0.0075 due to delamination. At rupture, the strains of high performance composites ranged between 0.002 and 0.009 except for SIFC which reached 0.016 resulting in the highest toughness index of 13 due to fiber debonding. This indicates lateral energy absorption requirements necessary for resisting blast pressures in different directions.

The large strength in FRP's are compensated for by lower strains at rupture leading to same toughness as SIFC with lower strengths. SIFC has shortcomings in its application in the industry due to its difficulty in application. Segmental pouring is necessary as well as the monitoring of the layout of fibers. On the other hand, fire protection is necessary for FRP due to its impact on the epoxy resin. Each composite has his particular use for the required loading and response. Figures IV-17 (a) IV-17(b), IV-17(c) represents experimental longitudinal and transverse stress-strain curves and the Poisson ratio curves for different composites for comparison.

V. THEORETICAL RESULTS

5.1 MODEL DEVELOPMENT

General Stress Strain Model for Discrete and Continuous Confinements

Figures IV (a) and IV (b) show the typical ascending portion of a stress-strain curve for full and partial confinement respectively. Full confinement is when the peak stress is higher than the ultimate stress of unconfined concrete while partial confined concrete

is when the peak stress is lower than the ultimate stress of unconfined concrete (further discussed in the subsequent text).

The confined model derivation differs depending on the confinement type: Discrete or Continuous

5.1.1 Discrete Confinement (CON), (SP3), (SP2) and (WIM)

The model for complete (ascending and descending) stress-strain curve of discretely confined concrete was developed using the Todechini⁹ model defined by Eq. (II-1). Key steps in the model development are:

- 1) Development of stress-strain equations for defining the ascending and descending response. Derivation of these equations includes the development of the following parameters: peak stress σ_{lccu} and strain ε_{lccu} , modified tensile strains of composite ε_{lxxx}^* in the ascending and descending branches of the curve, confinement stress σ_{lcco} and strain ε_{lcco} , modulus of elasticity of confined concrete E_{lcco} and lateral stress at peak σ_{2cu} , where the xxx index designates the composite type.
- 2) Optimization of spacing for full and partial confinement used to obtain the response at the transition region.
- 3) Development of analytical equations for longitudinal strains as a function of transverse strains. These equations, needed for defining the transverse stress-strain relationship, were obtained by the regression analysis of experimental data.
- 4) Strains at rupture of the confined concrete. This strain is the key factor for defining ductility and energy absorption capacity.

Details of each of these steps are presented as follows:

1. Longitudinal Stress-Strain Curve (Refer to Figures IV (a,b) for ascending branch of curve)

Stress strain relationships Eq.(V.1; V.5) were obtained through modifying Todechini⁹ Eq.(II.1; II.2) by replacing peak stresses and strains of unconfined concrete with values for confined concrete.

$$\sigma_{lc} = \frac{2\sigma_{lccu}(\frac{\varepsilon_{lc}}{\varepsilon_{lccu}})}{1 + (\frac{\varepsilon_{lc}}{\varepsilon_{lccu}})^2} \quad 0 < \varepsilon_{lc} < \varepsilon_{lcco} \quad \text{Eq. (V. 1)}$$

$$\sigma_{lc} = \sigma'_{cc} + E'_{lc2}(\varepsilon_{lc} - \varepsilon_{lcco}) \quad \varepsilon_{lcco} < \varepsilon_{lc} < \varepsilon_{lccu} \quad \text{Eq. (V. 2)}$$

$$\sigma_{lc} = \frac{2\sigma_{lccu}(\frac{\varepsilon_{lc}}{\varepsilon_{lccu}})}{1 + (\frac{\varepsilon_{lc}}{\varepsilon_{lccu}})^2} \quad \varepsilon_{lccu} < \varepsilon_{lc} < \varepsilon_{lcr} \quad \text{Eq. (V. 3)}$$

$$\sigma_{lccu} = A_1\sigma'_{cc} + \psi_f k_a B_1 \sigma_{2cu} \quad \text{Eq. (V. 4)}$$

$$\varepsilon_{lccu} = C_1 \varepsilon'_c + D_1 k_b \frac{\sigma_{2cu}}{\sigma'_{cc}} \frac{(\varepsilon_{lxxxcu}^*)^{E_1}}{(\varepsilon'_c)^{F_1}} \quad \text{Eq. (V. 5)}$$

$$\sigma'_{cc} = \sigma'_c \frac{A_g}{A_c} = \sigma'_c \frac{\frac{\pi(D_c + 2t_{xxx})^2}{4}}{\frac{\pi D_c^2}{4}} \quad \text{Eq. (V. 6)}$$

σ'_{cc} is the compressive stress of confined concrete at start of the activation of the composite resisted by the concrete core. $\psi_f = 0.95$, $k_a = k_b = 1$ ε_{lxxxcu}^* is the modified peak strain of the composite (further discussed in the subsequent text). Equation (V.6) is satisfied for $\sigma'_c \leq \sigma'_{cc} \leq \sigma_{lcco}$, where $\sigma'_{cc} = \sigma_{lcco}$ for ($s = 0$) and $\sigma'_{cc} = \sigma'_c$ for ($s = s_{opt}$).

Equation (V.2) represents the straight-line stress-strain curve of the composite activation region. E'_{lc2} is the slope of the stress-strain straight line for the activation region. To account for the presence of the concrete cover and the compressive strength of the concrete core at start of composite activation, Eq.(V.4) and Eq.(V.5) were developed by using ACI FRP model⁸ and replacing σ'_{cc} with σ'_c . Since the FRP

jacket thickness is insignificant compared to the diameter of the concrete core, the following approximation was introduced: $\sigma'_{cc} \cong \sigma'_c$ as noted from equation Eq.(V.6).

a) Peak Stress σ_{lccu} and Strain ε_{lccu}

Factors A_1 through F_1 in Eq.(V.4) and Eq.(V.5) were introduced into ACI 440⁸ equations to obtain generalized equations at peak stress and strain for the different types of composites.

A_1 through F_1 are the factors for the activation region. Constants A_1 to F_1 are determined by equating Eq.(V.4) and Eq.(V.5) to peak stress and strain Eq.(V.7) and Eq.(V.8), and using $G_1 = 3$, determined from the experimental data replacing the Todechini's⁹ factor $G_1 = 1.17$ for unconfined concrete. Peak stress and strain Eq.(V.7) and Eq.(V.8) are based on Mander et al.²³ and Todechini models⁹, respectively.

$$\sigma_{lccu} = \sigma'_{cc} + 4.1\sigma_{2cu} \quad \text{Eq. (V. 7)}$$

$$\varepsilon_{lccu} = \frac{G_1 \sigma_{lccu}}{E_{lcco}} \quad \text{Eq. (V. 8)}$$

σ'_{cc} replaces σ'_c in Eq. (V. 7) for reasons explained previously. Derivation of factors A_1 through F_1 is provided in Appendix XII. Final values are summarized in Table V.1.

Table V-1: Factors used for peak stress and strain for confined concrete (0.15 Ksi=1 MPa)

		A_1	B_1	C_1	D_1	E_1	F_1	G_1	$\frac{\sigma_{2cu}}{\text{MPa}}$ (Ksi)
LPBF	CON	1	4.32	1	4.32	0	-1	1.71	0 (0)
	FRM	1	100(-)	1.5	0	0.45	0.45	-	-0.137 (-0.021)
	SP3	1	4.32	1.75	7.56	0	-1	3	0 (0)
LPDF	FRC	1	50(-)	1.5	0	0.45	0.45	-	-0.27 (-0.04)
	WIM	1	4.32	1.75	7.56	0	-1	3	0.102 (0.015)
	SP2	1	4.32	1.75	7.56	0	-1	3	0.037 (0.0055)
HPBF	FPC(SCH 41-1)	1	3.3	1.5	12	0.45	0.45	-	10.25 (1.54)
	FPC (SCH 41-2)	1	3.3	1.5	12	0.45	0.45	-	12.77 (1.92)
	FPC (11UP-2)	1	3.3	1.5	12	0.45	0.45	-	14.33 (2.15)
	FPG (SEH-1)-ACI	1	3.3	1.5	12	0.45	0.45	-	6.79 (1.02)
	FPG (SEH-1)	1	1	1.5	12	0.45	0.45	-	6.79 (1.02)
	FPG (SEH-2)	1	3.3	1.5	12	0.45	0.45	-	13.57 (2.04)
HPDF	SIFC	1	1	1.5	7.5	0.45	0.45	-	4.38 (0.66)

b) Modified Tensile Strain of Composite ε_{lxxx}^*

ε_{lxxx}^* is the modified tensile strain of the composite. It is determined by introducing the strain efficiency factor, defined as the ratio of (a) the experimental transverse strain of the confined concrete, to (b) the actual tensile strain of the composite. When a cover exists between the outside perimeter and lateral confinement (e.g. case of spirals), the strain at the location of spirals is obtained by multiplying (a) strain measured at the outside perimeter of the confined concrete by (b) the ratio $\frac{D_c}{\frac{D}{2}}$. In this case, D is the cylinder diameter and D_c is the diameter of the concrete core. Two efficiency factors are considered: μ_{lxxx} during activation of the composite and ζ_{lxxx} during the descending branch of the stress strain curve. Modified tensile strains of the composite takes into account the actual strain of the composite in the peak and

post-peak regions. It should be noted that the efficiency factors are limited by the following equations:

Activation Region

$$\mu_{lxxx} = 1 \text{ if } \frac{\alpha \varepsilon_{tc} \left(\frac{D_c}{2}\right)}{\varepsilon_{lxxx}} > 1 \quad \text{Eq. (V. 9)}$$

$$\mu_{lxxx} = \frac{\alpha \varepsilon_{tc} \left(\frac{D_c}{2}\right)}{\varepsilon_{lxxx}} \text{ if } \frac{\alpha \varepsilon_{tc} \left(\frac{D_c}{2}\right)}{\varepsilon_{lxxx}} < 1 \quad \text{Eq. (V. 10)}$$

$$\varepsilon_{lxxx}^* = \mu_{lxxx} \varepsilon_{lxxx} \quad \text{Eq. (V. 11)}$$

It can be concluded from Eq. (V.11) that the modified strain at peak is

$$\varepsilon_{lxxxcu}^* = \mu_{lxxx} \varepsilon_{lxxxcu} \quad \text{Eq. (V. 12)}$$

where ε_{lxxx} and ε_{lxxx}^* are the actual and modified general tensile strains of the composite during the activation region, and ε_{lxxxcu} and ε_{lxxxcu}^* are the actual and modified peak tensile strains of the composite, ε_{tc} is the transverse strain of confined concrete.

Equation (V.9-V.12) indicate that the peak strains of confined concrete are reached when the tensile strains of the composite is less or equal its peak values. α is an experimental factor equal to 2 for low performance composites and 4 for high performance composites, that was determined using finite element models. Such models were not presented in this current study. This factor is used to related the radial experimental transverse strain to the tangential strain of the composite

Descending Branch

Similar analogy can also be used for the modified strain of the composite in the descending branch of the curve by introducing an efficiency factor ζ_{lxxx}

$$\zeta_{lxxx} = 1 \text{ if } \frac{\alpha \varepsilon_{tc} \left(\frac{D_c}{2}\right)}{\varepsilon_{lxxx}} < 1 \quad \text{Eq. (V. 13)}$$

$$\zeta_{lxxx} = \frac{\alpha \varepsilon_{tc} \left(\frac{D_c}{2}\right)}{\varepsilon_{lxxx}} \text{ if } \frac{\alpha \varepsilon_{tc} \left(\frac{D_c}{2}\right)}{\varepsilon_{lxxx}} > 1 \quad \text{Eq. (V. 14)}$$

$$\varepsilon_{lxxx}^* = \zeta_{lxxx} \varepsilon_{lxxx} \quad \text{Eq. (V. 15)}$$

It can be concluded from Eq.(V.15) that the modified strain at rupture is

$$\varepsilon_{lxxxr}^* = \zeta_{lxxx} \varepsilon_{lxxxr} \quad \text{Eq. (V. 16)}$$

where ε_{lxxxr} and ε_{lxxxr}^* are the actual and modified rupture tensile strains of the composite. Equations (V.13-V.16) indicate that the confined concrete rupture strain is greater or equal to the rupture strain of the composite. This is due to failure of the concrete core occurring with or after the composite failure.

c) Confinement Stress σ_{lcco} , Strain ε_{lcco} and Modulus of Elasticity E_{lcco}

The confining strain ε_{lcco} is the point at which the slope of the stress-strain curve equals E_{lc2} which is the tangent modulus of the system during confinement. The tangent modulus E_{lc2} is obtained by determining the derivative of Eq.(V.1) of the stress strain curve at ε_{lcco} . The following equations can be utilized to determine ε_{lcco} (see Figures IV (a,b)):

$$\frac{d\sigma_{lc}}{d\varepsilon_{lc}} @ \varepsilon_{lcco} = E_{lc2} = \frac{\sigma_{lccu} - \sigma'_c}{\varepsilon_{lccu}} \quad \text{Eq. (V. 17)}$$

σ_{lcco} is determined by resubstituting ε_{lcco} from Eq.(V.17) into Eq.(V.1).

E'_{lc2} is the slope of the stress-strain curve during composite-activation defined from Figures IV(a,b):

$$E'_{lc2} = \frac{\sigma_{lccu} - \sigma'_{cc}}{\varepsilon_{lccu} - \varepsilon_{lcco}} \quad \text{Eq. (V. 18)}$$

$$E_{lcco} = \frac{E_c A_c + E_{mxxx} A_{mxxx}}{A_c + A_{mxxx}} = E_c \quad \text{Eq. (V. 19)}$$

The confinement modulus of elasticity represents the equivalent stiffness of the core concrete and matrix in compression.

$$A_{mxxx} = \frac{\pi(D_c + 2t_{xxx})^2}{4} - \frac{\pi D_c^2}{4} \quad \text{Eq. (V. 20)}$$

where A_c is the cross-sectional area of the concrete core, A_{mxxx} is the cross-sectional area of the composite.

Equation (V.19) is obtained using the parallel-springs model approach. It is shown that the confinement modulus of elasticity equals that of unconfined concrete since (a) $t_{xxx} = 0$ for wire mesh and (b) $E_{mxxx} = E_c$ for spirals

d) Lateral Stress σ_2

The generalized lateral stress at different points during composite-activation is obtained from the condition of equilibrium where the tensile force in the composite equals the lateral confining pressure across the diameter of the concrete core (i.e., “pressure vessel” formula):

$$\sigma_2 = \frac{2\sigma_{lxxx} A_{lxxx}}{A_{cc}} \quad \text{Eq. (V. 21)}$$

For discrete confinements $A_{cc} = D_c S_{xxx}$

$$\sigma_2 = \frac{2\sigma_{lxxx} A_{lxxx}}{D_c S_{xxx}} \quad \text{Eq. (V. 22)}$$

$$\sigma_{lxxx} = E_{lxxx} \varepsilon_{lxxx}^* \quad \text{Eq. (V. 23)}$$

Lateral Stress at peak is obtained from the generalized Eq.(V.22) and (V.23) so that:

$$\sigma_{2cu} = \frac{2\sigma_{lxxx}A_{lxxx}}{D_c S_{xxx}} \quad \text{Eq. (V. 24)}$$

$$\sigma_{lxxx} = E_{lxxx} \varepsilon_{lxxx}^* \quad \text{Eq. (V. 25)}$$

Where σ_{lxxx} depends on the tensile properties of the composites. Specific tensile properties of matrix, fiber and composite for discrete confinement used in this research are summarized in Table V.2 and V.3, respectively.

Table V.2 lists the properties of the fibers and matrix obtained from different references^{32,36} including diameter and length of fibers ϕ_{xxx} , L_{xxx} , thickness of composite t_{xxx} , average shear stress between fiber and matrix τ_{xxx} , slip coefficient k_{xxx} , tensile moduli of elasticity of fiber and matrix E_{fxxx} , E_{mxxx} where xxx represent the index designation of the different types of composites refer to notation list. σ_{fxxx} , σ_{mxxx} are tensile stresses of fibers and matrix and ε_{fxxx} , ε_{mxxx} are strains of fibers and matrix. Table V.3 lists the longitudinal composite properties in tension as obtained from the stress and strain equations above. The parameters include the modulus of composite E_{lxxx} , proportional limit or first crack stresses and strains σ_{lxxxp} , ε_{lxxxp} , peak stresses and strains σ_{lxxx} , ε_{lxxx} , and rupture stresses and strain σ_{lxxxr} , ε_{lxxxr}

Table V-2: Fiber and matrix properties of lateral confinement (0.15Ksi=1 MPa, 1in.=2.54 cm)

		FIBER								MATRIX		
		L_{xxx} mm (in.)	ϕ_{xxx} mm (in.)	t_{xxx} mm (in.)	τ_{xxxu} MPa (Ksi)	k_{xxx} MPa (Ksi)	E_{fxxx} MPa (Ksi)	σ_{fxxx} MPa (Ksi)	ϵ_{fxxx}	E_{mxxx} MPa (Ksi)	σ_{mxxx} MPa (Ksi)	ϵ_{mxxx}
LPBF	CON	-	-	-	-	-	-	-	-	-	-	-
	FRM ³²	50 (1.97)	1.05 (0.04)	-	5.85 (0.87)	3.17 (0.47)	200000 (30000)	1130 (170)	0.0057	14480 (2172)	1.2 (0.175)	.000083
	SP3	-	4 (0.157)	-	-	-	5000 (750)	500 (75)	0.1	-	-	-
LPDF	FRC ³²	50 (1.97)	1.05 (0.04)	-	5.85 (0.87)	3.17 (0.47)	200000 (30000)	1130 (170)	0.0057	30460 (4569)	31.98 (4.79)	.00105
	WIM	-	1 (0.039)	-	-	-	40000 (6000)	96 (14.4)	0.0024	-	-	-
	SP2	-	4 (0.157)	-	-	-	5000 (750)	500 (75)	0.1	-	-	-
HPBF	FPC (SCH 41-1)	-	-	1 (0.039)	-	-	230000 (34500)	3790 (569)	0.016	3180 (477)	72.4 (10.86)	0.05
	FPC (SCH 41-2)	-	-	2 (0.078)	-	-	230000 (34500)	3790 (569)	0.017	3180 (477)	72.4 (10.86)	0.05
	FPC (11UP-2)	-	-	0.51 (0.02)	-	-	230000 (34500)	3790 (569)	0.017	3180 (477)	72.4 (10.86)	0.05
	FPG (SEH-1)	-	-	1.3 (0.05)	-	-	72400 (10860)	3240 (569)	0.045	3180 (477)	72.4 (10.86)	0.05
	FPG (SEH-2)	-	-	2.6 (0.1)	-	-	72400 (10860)	3240 (569)	0.045	3180 (477)	72.4 (10.86)	0.05
HPDF	SIFC ³⁶	50 (1.97)	1.05 (0.04)	-	-	-	200000	1130 (170)	0.0057	14480 (2172)	1.2 (0.175)	.000083

Table V-3: Composite properties of lateral confinement (0.15 Ksi=1 MPa)

		COMPOSITE						
		E_{lxxx} MPa (Ksi)	σ_{lxxxp} MPa (Ksi)	ϵ_{lxxxp}	σ_{lxxxu} MPa (Ksi)	ϵ_{lxxxu}	σ_{lxxxr} MPa (Ksi)	ϵ_{lxxxr}
LPBF	CON	-	-	-	-	-	-	-
	FRM ³²	14480 (2172)	1.682 (0.242)	.00012	1.128 (0.1692)	.00054	1.086 (0.163)	0.02
	SP3	-	-	-	-	-	-	-
LPDF	FRC ³²	30460 (4570)	3.84 (0.576)	.00013	2.27 (0.3405)	.00054	2.17 (0.33)	0.02
	WIM	-	-	-	-	-	-	-
	SP2	-	-	-	-	-	-	-
HPBF	FPC(SCH 41-1)	95800 (14370)	958 (144)	0.01	958 (144)	0.01	958 (144)	0.01
	FPC (SCH 41-2)	95800 (14370)	958 (144)	0.01	958 (144)	0.01	958 (144)	0.01
	FPC (11UP-2)	105400 (15810)	980 (147)	0.0093	980 (147)	0.0093	980 (147)	0.009 3
	FPG (SEH-1)	26100 (3910)	574 (86)	0.022	574 (86)	0.022	574 (86)	0.022
	FPG (SEH-2)	26100 (3910)	574 (86)	0.022	574 (86)	0.022	574 (86)	0.022
HPDF	SIFC ³⁶	13540 (2031)	1.625 (0.25)	.00012	13.1 (1.965)	0.01	12.91 (1.9)	0.02

Wire Mesh: For wire mesh, a model is developed to determine the tensile stress in the composite σ_{IWIMcu} due to the presence of the vertical ties. The model has been developed as shown in Figures V-1(a and b) to take into account the effect of vertical wires that increase resistance and produce additional stresses in the

transverse (horizontal) fibers. Guided rollers were used to account for symmetric deformation where slopes are zero.

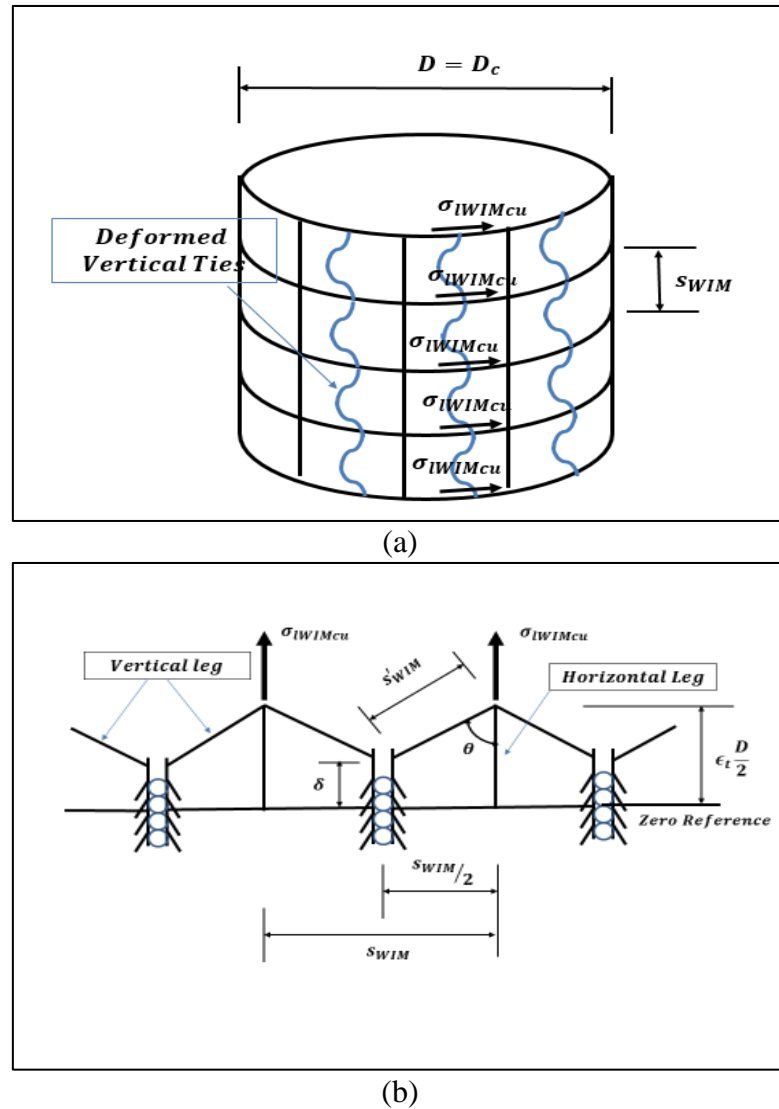


Figure V-1: (a) Elevation of cylinder with wire mesh (b) Wire mesh model

$$s'_{WIM} = \sqrt{\left(\frac{s_{WIM}}{2}\right)^2 + \left(\frac{\varepsilon_{IWIMcu}^* D}{2} - \delta\right)^2} \quad \text{Eq. (V. 26)}$$

where s_{WIM} is the spacing of the lateral ties and s' is the deformed spacing, D is the diameter of the cylinder, ε_{IWIMcu}^* is the modified peak strain of the composite, δ is the tangential displacement of the wire mesh vertical leg; maximum displacement (flexible system) at $\delta = 0$ and zero displacement (rigid

system) at $\delta = \frac{\varepsilon_{IWIMcu}^* D}{2}$. The final strain of the vertical ties after deformation

$\varepsilon_{IWIMvcu}$ is obtained using geometry:

$$\varepsilon_{IWIMvcu} = \frac{\sqrt{\left(\frac{s_{WIM}}{2}\right)^2 + \left(\frac{\varepsilon_{IWIMcu}^* D}{2} - \delta\right)^2} - \frac{s_{WIM}}{2}}{\frac{s_{WIM}}{2}} \quad \text{Eq. (V. 27)}$$

$$\varepsilon_{IWIMvcu} = \sqrt{1 + \left[\frac{2\left(\frac{\varepsilon_{IWIMcu}^* D}{2} - \delta\right)}{s_{WIM}}\right]^2} - 1 \quad \text{Eq. (V. 28)}$$

The horizontal component of the stress in the vertical ties after deformation is:

$$\sigma_{IWIMvcu} = \left\{ 2E_{IWIM} \sqrt{1 + \left[\frac{2\left(\frac{\varepsilon_{IWIMcu}^* D}{2} - \delta\right)}{s_{WIM}}\right]^2} - 1 \right\} \cos\theta \quad \text{Eq. (V. 29)}$$

$$\cos\theta = \frac{\left(\frac{\varepsilon_{IWIMcu}^* D}{2} - \delta\right)}{s'_{WIM}} \quad \text{Eq. (V. 30)}$$

Where E_{IWIM} is the tensile modulus of the wire mesh and θ is the angle the deformed shape makes with the vertical direction, while $\sigma_{IWIMvcu}$ is the horizontal component of the tensile stress in the vertical ties after deformation. Substituting s'_{WIM} from Eq.(V.26) into Eq.(V.30) and substituting Eq.(V.30) into Eq.(V.29) as well as considering that the stress in the horizontal ties equals:

$$\sigma_{IWIMhcu} = E_{IWIM} \varepsilon_{IWIMcu}^* \quad \text{Eq. (V. 31)}$$

The final stress becomes:

$$\sigma_{IWIMcu} = \sigma_{IWIMhcu} + \frac{\left\{ 2E_{IWIM} \sqrt{1 + \left[\frac{2\left(\frac{\varepsilon_{IWIMcu}^* D}{2} - \delta\right)}{s_{WIM}}\right]^2} - 1 \right\}}{\sqrt{1 + \left[\frac{s_{WIM}}{2\left(\frac{\varepsilon_{IWIMcu}^* D}{2} - \delta\right)}\right]^2}} \quad \text{Eq. (V. 32)}$$

$$\text{Let } \beta = \frac{2\left(\frac{\varepsilon_{IWIMcu}^* D}{2} - \delta\right)}{S_{WIM}} \quad \text{Eq. (V. 33)}$$

$$\sigma_{IWIMcu} = E_{IWIM} \varepsilon_{IWIMcu}^* + \frac{\left\{2E_{IWIM} \sqrt{1 + \beta^2} - 1\right\}}{\sqrt{1 + \left[\frac{1}{\beta}\right]^2}} \quad \text{Eq. (V. 34)}$$

σ_{IWIMcu} is the final tensile stress in the composite after deformation and resistance by the vertical ties and β is a factor introduced to simplify the expression.

For a rigid system:

$$\delta = \frac{\varepsilon_{IWIMcu}^* D}{2} \text{ and } \beta = 0 \quad \text{Eq. (V. 35)}$$

$$\sigma_{IWIMcu} = E_{IWIM} \varepsilon_{IWIMcu}^* \quad \text{Eq. (V. 36)}$$

For a flexible system:

$$\delta = 0 \text{ and } \beta = \frac{\varepsilon_{IWIMcu}^* D}{S_{WIM}} \quad \text{Eq. (V. 37)}$$

$$\sigma_{IWIMcu} = E_{IWIM} \varepsilon_{IWIMcu}^* + \frac{\left\{2E_{IWIM} \sqrt{1 + \left(\frac{\varepsilon_{IWIMcu}^* D}{S_{WIM}}\right)^2} - 1\right\}}{\sqrt{1 + \left[\frac{S_{WIM}}{\varepsilon_{IWIMcu}^* D}\right]^2}} \quad \text{Eq. (V. 38)}$$

2. Optimization of Spacing (Transition Region)

The optimized spacing is the limiting spacing of the composite above which the system becomes ineffective. As shown in Figure IV (a), for values between zero and the optimized value, the point B starts dropping down towards the point B'. For every spacing value, there is a different point location of B. Once the spacing is equal or larger than the optimum value (i.e., the system becomes ineffective), the point B matches the point B' at the stress of σ'_{cc}

$$\sigma_{lcco} \geq \sigma'_{cc} \quad \text{Eq. (V. 39)}$$

Where σ_{lcco} is the confining stress associated with strain ε_{lcco} at end of confinement

a) Full Confinement

For the case of discrete confinement with a wire mesh: $t_{xxx} = 0$ and $\sigma_{lcco} = \sigma'_{cc} = \sigma'_c$. For the case of discrete confinement with spirals, t_{xxx} is the cover and at optimization $\sigma_{lcco} = \sigma'_{cc} > \sigma'_c$

Using equations (V.1) and (V.39) and assuming the optimized spacing, the value of σ_{lcco} becomes

$$\sigma_{lcco} = \sigma'_{cc} = \frac{2\sigma_{lccu} \left(\frac{\varepsilon_{lcco}}{\varepsilon_{lccu}} \right)}{1 + \left(\frac{\varepsilon_{lcco}}{\varepsilon_{lccu}} \right)^2} \quad \text{Eq. (V. 40)}$$

Since at optimized spacing the slopes E'_{lc2} and E_{lc2} match at ε_{lcco} as shown in

Figure IV.a.

$$\frac{d\sigma_{lc}}{d\varepsilon_{lc}} @ \varepsilon_{lcco} = E_{lc2} = E'_{lc2} \quad \text{Eq. (V. 41)}$$

$$E'_{lc2} = \frac{\sigma_{lccu} - \sigma'_{cc}}{(\varepsilon_{lccu} - \varepsilon_{lcco})} \quad \text{Eq. (V. 42)}$$

$$\varepsilon_{lccu} = \frac{G_1 \sigma_{lccu}}{E_c} \quad \text{Eq. (V. 43)}$$

Substituting ε_{lccu} from Eq.(V.43) into Eq.(V.40) and solving for σ_{lccu} as a function of ε_{lcco} leads to

$$\sigma_{lccu} = \frac{\varepsilon_{lcco} E_c}{G_1 \sqrt{\frac{2E_c \varepsilon_{lcco}}{G_1 \sigma'_{cc}} - 1}} \quad \text{Eq. (V. 44)}$$

Equations (V.44) and (V.41) provide two conditions necessary to solve two unknowns σ_{lccu} and ε_{lcco} . Finally s_{opt} is obtained in two steps: (a) σ_{lccu} is substituted in equations (V.4) or (V.7) to determine σ_{2cu} which is then (b)

substituted in equation (V.24) to obtain the optimized confinement spacing,

s_{opt} .

In summary for full confinement, (See Figure IVa):

- $s \geq s_{opt}$ - there is no shift between B and B' and both points coincide with one peak stress σ_{lccu} and $\sigma_{lcco} = \sigma'_{cc}$ and

$$E_{lc2} = E'_{lc2} = \frac{\sigma_{lccu} - \sigma'_{cc}}{(\varepsilon_{lccu} - \varepsilon_{lcco})} \quad \text{Eq. (V.45)}$$

- $s < s_{opt}$ - there is a shift between points B and B' leading to two peaks σ_{lcco} and σ_{lccu}

The stress at point B' is σ'_{cc} . The stress at point B is σ_{lcco} with two moduli

$$\text{of elasticity } E_{lc2} = \frac{\sigma_{lccu} - \sigma'_c}{\varepsilon_{lccu}} \text{ and } E'_{lc2} = \frac{\sigma_{lccu} - \sigma'_{cc}}{(\varepsilon_{lccu} - \varepsilon_{lcco})}$$

Values for s_{opt} and the different stresses at confinement are tabulated in Table

V-4.

Table V-4: Optimized thickness and spacing and related parameters (0.15Ksi=1 MPa, 1in.=2.54 cm)

		t_{opt} mm (in.)	s_{opt} mm (in.)	t_{xxx} mm (in.)	s_{xxx} Mm (in.)	σ'_c MPa (Ksi)	σ'_{cc} MPa (Ksi)	σ_{lcco} MPa (Ksi)	σ_{lccu} MPa (Ksi)
LPBF	CON	-	-	-	-	42 (6.3)	42 (6.3)	42 (6.3)	42 (6.3)
	FRM	-	-	25 (0.98)	-	42 (6.3)	30 (4.5)	30 (4.5)	30 (4.5)
	SP3	0 (0)	-	-	30 (1.18)	42 (6.3)	42 (6.3)	42 (6.4)	42 (6.4)
LPDF	FRC	-	-	25 (0.98)	-	42 (6.3)	42 (6.3)	33 (4.95)	30 (4.5)
	WIM	-	-	-	-	42 (6.3)	42 (6.3)	42.4 (6.3)	42.4 (6.3)
	SP2	-	-	-	20 (0.78)	42 (6.3)	42 (6.3)	42.2 (6.4)	42.2 (6.4)
HPBF	FPC(SCH 41-1)	4.7 (0.71)	-	1 (0.04)	-	42 (6.3)	43 (6.45)	48 (7.2)	74 (11.1)
	FPC (SCH 41-2)	5.6 (0.22)	-	2 (0.08)	-	42 (6.3)	44 (6.6)	49 (7.35)	82 (12.3)
	FPC (11UP-2)	3.29 (0.13)	-	1.02 (0.04)	-	42 (6.3)	43 (6.45)	46 (6.9)	73 (10.95)
	FPG (SEH-1)-ACI	4.35 (0.17)	-	1.3 (0.05)	-	42 (6.3)	43 (6.45)	47 (7.05)	63 (9.45)
	FPG (SHE-1)	1.3 (0.05)	-	1.3 (0.05)	-	42 (6.3)	43 (6.45)	43 (6.45)	48 (7.2)
	FPG (SEH-2)	4.97 (0.19)	-	2.6 (0.1)	-	42 (6.3)	45 (6.75)	48 (7.2)	73 (10.95)
HPDF	SIFC	7 (0.28)	-	25 (0.98)	-	42 (6.3)	53 (7.95)	53 (7.95)	56 (8.4)

b) Partial Confinement

In the case of the partial confinement as shown in Figure IV,b, optimized spacing is obtained using the same equations as for the full confinement. The only difference between the two being (1) E_{lc2} and E'_{lc2} are both negative and (2) stresses are less than that of unconfined concrete σ'_c .

3. Longitudinal Stress and Transverse Strains

A regression analysis of experimental data was used to obtain the longitudinal versus transverse strain values, resulting in the following equations (see corresponding Figure IV-3(a)):

$$\varepsilon_{lc} = \infty \quad 0 < \varepsilon_{tc} < \varepsilon_{tcco} \quad \text{Confinement} \quad \text{Eq. (V.46)}$$

$$\varepsilon_{lc} = A_2 \varepsilon_{tc} + B_2 \quad \varepsilon_{tcco} < \varepsilon_{tc} < \varepsilon_{tccu} \quad \text{First crack/multiple cracking} \quad \text{Eq. (V.47)}$$

$$\varepsilon_{lc} = C_2 \varepsilon_{tc} + D_2 \quad \varepsilon_{tccu} < \varepsilon_{tc} < \varepsilon_{tco} \quad \text{Fiber debonding/pull-out} \quad \text{Eq. (V.48)}$$

$$\varepsilon_{lc} = E_2 \varepsilon_{tc} + F_2 \quad \varepsilon_{tco} < \varepsilon_{tc} < \varepsilon_{tcr} \quad \text{Concrete core failure} \quad \text{Eq. (V.49)}$$

$$A_2 = \frac{(\varepsilon_{lccu} - \varepsilon_{lcco})}{(\varepsilon_{tccu} - \varepsilon_{tcco})} \quad \text{Eq. (V.50)}$$

$$B_2 = \frac{(\varepsilon_{lccu} - \varepsilon_{lcco})\varepsilon_{tcco}}{(\varepsilon_{tccu} - \varepsilon_{tcco})} + \varepsilon_{lcco} \quad \text{Eq. (V.51)}$$

$$C_2 = \frac{(\varepsilon_{lco} - \varepsilon_{lccu})}{(\varepsilon_{tco} - \varepsilon_{tccu})}, \quad \text{Eq. (V.52)}$$

$$D_2 = -\varepsilon_{tccu} \frac{(\varepsilon_{lco} - \varepsilon_{lccu})}{(\varepsilon_{tco} - \varepsilon_{tccu})} + \varepsilon_{lccu} \quad \text{Eq. (V.53)}$$

$$E_2 = \frac{(\varepsilon_{lcr} - \varepsilon_{lco})}{(\varepsilon_{tcr} - \varepsilon_{tco})} \quad \text{Eq. (V.54)}$$

$$F_2 = -\varepsilon_{tco} \frac{(\varepsilon_{lcr} - \varepsilon_{lco})}{(\varepsilon_{tcr} - \varepsilon_{tco})} + \varepsilon_{lco} \quad \text{Eq. (V.55)}$$

Where all parameters are as defined in the list of notations. Obtained values of A_2 to F_2 are summarized in Table V.5. The transverse stress-strain model is obtained by (a) substituting the values of the longitudinal strains, obtained from the regression equations (V.46) to (V.49) for different values of transverse strains, into (b) the stress strain model equations (V.1) to (V.3).

Table V-5: Parameters for regression lines for longitudinal strain versus transverse strain

		A_2	B_2	C_2	D_2	E_2	F_2	R^2
LPBF	CON	0	0	0	0	3.6	0	0.957 (Eq. 63)
	FRM	0	0	0.84	0.0037	0.84	0.017	1 (Eq. 63) 0.998 (Eq. 64) 0.91 (Eq. 65)
	SP3	0	0	0	0	0.6	0.004	1 (Eq. 63) 0.88 (Eq. 64)
LPDF	FRC	4.28	0.0015	1.5	0.0025	0.22	0.0063	1 (Eq. 63) 0.11 (Eq. 64) 0.63 (Eq. 65) 0.75 (Eq. 66)
	WIM	0.28	0.002	0	0	0.8	-0.0016	1 (Eq. 63) 0.82 (Eq. 64) 0.75 (Eq. 65)
	SP2	2.52	0.0032	0	0	1.48	0.0036	1 (Eq. 63) 0.96 (Eq. 64) 0.76 (Eq. 65)
HPBF	FPC(SCH 41-1)	3.98	0.002	0	0	0	0	1 (Eq. 63) 0.97 (Eq. 64)
	FPC (SCH 41-2)	4.26	0.003	0	0	0	0	1 (Eq. 63) 0.99 (Eq. 64)
	FPC (11UP-2)	4.3	0.007	0	0	0	0	1 (Eq. 63) 0.96 (Eq. 64)
	FPG (SEH-1)-ACI	1.6	0.006	0	0	0	0	1 (Eq. 63) 0.96 (Eq. 64)
	FPG (SEH-1)	1.6	0.006	0	0	0	0	1 (Eq. 63) 0.97 (Eq. 64)
	FPG (SEH-2)	2.16	0.002	0	0	0	0	1 (Eq. 63) 0.95 (Eq. 64)
HPDF	SIFC	2.6	0.0014	0.6	0.00345	0.96	0.0028	1 (Eq. 63) 0.74 (Eq. 64) 0.12 (Eq. 65) 0.95 (Eq. 66)

4. Energy Approach to determine ε_{lcr} ¹⁰

ε_{lcr} is obtained from Eq.(V.19), where $U_{sl} = 0$ given that there is no longitudinal steel present.

$$U_{st} = U_{cc} - U_{co} \quad \text{Eq.(V.56)}$$

$$U_{co} = A_c \int_0^{\varepsilon'_c} \sigma_{lc} d\varepsilon_{lc} + A_c(0.003 - \varepsilon'_c) \quad \text{Eq. (V.57)}$$

$$U_{cc} = (A_c + A_{mxxx}) \int_0^{\varepsilon_{lcr}} \sigma_{lc} d\varepsilon_{lc} \quad \text{Eq. (V.58)}$$

$$U_{st} = \rho_s A_c \left(\int_0^{\varepsilon_{lxxxcu}^*} \sigma_{lxxx} d\varepsilon_{lxxx}^* + \int_{\varepsilon_{lxxxcu}^*}^{\varepsilon_{lxxxr}^*} \sigma_{lxxx} d\varepsilon_{lxxx}^* \right) \quad \text{Eq. (V.59)}$$

Where $\rho_s = \frac{A_{lxxx} \pi D_c}{\frac{\pi D_c^2}{4} s_{xxx}}$ is the volumetric ratio of the composite equal to the volume of

the composite divided by the volume of the concrete within the concrete core. σ_{lxxx} is the tensile stress of the composite, ε_{lxxx}^* is the modified tensile strain of the composite, 0.003 is the rupture strain of unconfined concrete, $A_{mxxx} = 0$ for wire mesh confinements and equal to Eq.(V.20) for spirals, ε_{lcr} is the rupture of confined concrete. ε_{lxxxcu}^* and ε_{lxxxr}^* are the modified tensile strains of composite at peak and rupture. All other variables are as defined in the notation list. The confined concrete rupture strain ε_{lcr} is obtained next using Eq.(V.57) and solving for ε_{lcr} . This strain is an indicator of the energy absorption and ductility capacity of the system.

5.1.2 Continuous Confinement (FRM), (FRC), (FPC), (FPG) and (SIFC)

The stress-strain curve model for continuous confinement is derived from the ACI 440⁸ model Eq.(II.5) to (II.8), which define the ascending branch of the curve, i.e. the confinement region and the activation regions. The descending branch of the curve is based on the H. Saadatmanesh et. al¹⁰ model. The following steps in the model development cover the same parameters as for the case of the discrete confinements stated previously. Furthermore, for the SIFC confinements, an additional step is introduced in which multiple cracking mechanism is quantified by determining the number of multiple-cracks.

1. Longitudinal Stress-Strain Curve (Refer to Figures IV (a, b) for ascending branch of curve)

The following definition of the ascending branch is applicable to (FRM), (FRC), (FPC), (FPG) and (SIFC) composites:

$$\sigma_{lc} = E_{lcco} \varepsilon_{lc} - \frac{(E_{lcco} - E_{lc2}) \varepsilon_{cl}^2}{4\sigma'_c} \quad 0 < \varepsilon_{lc} < \varepsilon_{lcco} \quad \text{Eq. (V. 60)}$$

$$\sigma_{lc} = \sigma'_{cc} + E'_{lc2}(\varepsilon_{lc} - \varepsilon_{lcco}) \quad \varepsilon_{lcco} < \varepsilon_{lc} < \varepsilon_{lccu} \quad \text{Eq. (V. 61)}$$

It should be noted that contrary to other composites, FPC and FPG exhibit a brittle failure as soon as the peak stress is reached. Therefore, FPC and FPG do not have a descending branch.

For all other composites (FRM, FRC and SIFC) the descending branch is defined as:

$$\sigma_{lc} = \frac{\sigma_{lccu} r \frac{\varepsilon_{lc}}{\varepsilon_{lccu}}}{r - 1 + \left(\frac{\varepsilon_{lc}}{\varepsilon_{lccu}}\right)^r} \quad \varepsilon_{lccu} < \varepsilon_{lc} < \varepsilon_{lcr} \quad \text{Eq. (V. 62)}$$

$$r = \frac{E_{lcco}}{E_{lcco} - \left(\frac{\sigma_{lccu}}{\varepsilon_{lccu}}\right)} \quad \text{Eq. (V. 63)}$$

where parameters are as previously defined.

$$\sigma'_{cc} = \sigma'_c \frac{A_g}{A_c} = \sigma'_c \frac{\frac{\pi(D_c + 2t_{xxx})^2}{4}}{\frac{\pi D_c^2}{4}} \quad \text{Eq. (V. 64)}$$

Equation (V.64) is satisfied for $\sigma'_c \leq \sigma'_{cc} \leq \sigma_{lcco}$, where $\sigma'_{cc} = \sigma_{lcco}$ for ($t = t_{opt}$) and $\sigma'_{cc} = \sigma'_c$ for ($t = 0$).

a) Peak Stress σ_{lccu} and Strain ε_{lccu}

The peak stress and strain are similar to the ACI 440⁸ equations with modified peak constant factors similar to equations (V.4) and (V.5).

$$\sigma_{lccu} = A_1 \sigma'_{cc} + \psi_f k_a B_1 \sigma_{2cu} \quad \text{Eq. (V. 65)}$$

$$\varepsilon_{lccu} = C_1 \varepsilon'_c + D_1 k_b \frac{\sigma_{2cu} (\varepsilon_{lxxxcu}^*)^{E_1}}{\sigma'_{cc} (\varepsilon'_c)^{F_1}} \quad \text{Eq. (V. 66)}$$

$$\psi_f = 0.95, \quad k_a = k_b = 1$$

Values of A_1 to F_1 are summarized in Table V.1

b) Modified Tensile Strain of Composite ε_{lxxx}^*

The modified strain of the composite ε_{lxxx}^* during the activation region and failure of the composite are determined through efficiency factors similar to the

discrete confinement. Equations (V.9) to (V.16) apply except that the factor $\frac{(\frac{D_c}{2})}{(\frac{D}{2})}$

is not present in the equation since the lateral confinements is applied along the

outside perimeter of the cylinder (i.e. no cover exists) and the factor $\frac{(\frac{D_c}{2})}{(\frac{D}{2})}$ equals

1.

c) Confinement Stress σ_{lcco} , Strain ε_{lcco} and Modulus of Elasticity E_{lcco}

ε_{lcco} can be found by equating the derivative of equation (V.60) to E_{lc2} , refer to

Figure IVa.

$$\frac{d\sigma_{lc}}{d\varepsilon_{lc}} @ \varepsilon_{lcco} = E_{lc2} = \frac{\sigma_{lccu} - \sigma'_c}{\varepsilon_{lccu}} \quad \text{Eq. (V. 67)}$$

From Eq.(V.67) ε_{lcco} equals

$$\varepsilon_{lcco} = \frac{2\sigma'_c}{(E_{lcco} - E_{lc2})} \quad \text{Eq. (V. 68)}$$

σ_{lcco} is obtained by back substituting ε_{lcco} from Eq.(V.68) into the Eq.(V.60).

The slope during activation of the composite is E'_{lc2}

$$E'_{lc2} = \frac{\sigma_{lccu} - \sigma'_{cc}}{\varepsilon_{lccu} - \varepsilon_{lcco}} \quad \text{Eq. (V. 69)}$$

According to Eq(V.64), $\sigma'_{cc} \geq \sigma'_c$ depending on the thickness of the composite layer. All parameters are as defined previously.

The confinement modulus of elasticity equals:

$$E_{lcco} = \frac{E_c A_c + E_{mxxx} A_{mxxx}}{A_c + A_{mxxx}} > E_c \quad \text{Eq. (V. 70)}$$

All parameters are as defined previously.

d) Lateral Stress σ_2

General lateral stress at different points on the curve during activation of composite is based on equilibrium of the tensile force in the composite and lateral force within the concrete core.

$$\sigma_2 = \frac{2\sigma_{lxxx} A_{lxxx}}{A_{cc}} \quad \text{Eq (V. 71)}$$

Since for continuous confinements $A_{lxxx} = t_{xxx} s_{xxx}$ and $A_{cc} = D_c s_{xxx}$

$$\sigma_2 = \frac{2\sigma_{lxxx} t_{xxx}}{D_c} \quad \text{Eq. (V. 72)}$$

Peak lateral stress is obtained from the equation (V.72) above

$$\sigma_{2cu} = \frac{2\sigma_{lxxx} t_{xxx}}{D_c} \quad \text{Eq. (V. 73)}$$

In order to determine σ_{lxxx} and $\sigma_{lxxx} t_{xxx}$, the tensile stress strain equations for the composites are required^{32,36} (summarized in Appendix II), at the location of the plastic centroid within the thickness of the composite.

The plastic centroid, r_{pl} from the center of the cylinder, is the location of the resultant force of the tensile stress distribution of the composite across its thickness as shown in Figure XIII.1 (a) in Appendix IV. The location r_{pl} from the center changes with the state of the tensile stress of the composite across the composite thickness.

$$r_{pl} = \frac{\int_0^{\frac{D_c}{2} + t_{xxx}} r \sigma_{lxxx} A_{lxxx} dr}{\int_0^{\frac{D_c}{2} + t_{xxx}} \sigma_{lxxx} A_{lxxx} dr} \quad \text{Eq. (V. 74)}$$

$$\sigma_{lxxx} = f(\varepsilon_{lxxx}^*) \quad \text{Eq. (V. 75)}$$

$$\varepsilon_{lxxx}^* = \mu_{lxxx} \alpha \varepsilon_{tc} \frac{r}{\left(\frac{D_c}{2} + t_{xxx}\right)} \quad \text{Eq. (V. 76)}$$

Where ε_{lxxx}^* is the modified tensile strain in the composite at location r from the center of the cylinder and σ_{lxxx} is the generalized tensile stress of the composite which is a function of ε_{lxxx}^* based on the tensile stress strain relationship of the composite. σ_{lxxx} is also a function of r as noted from equation (V.76). ε_{tc} is the transverse strain of the confined concrete at the outside circumference of the cylinder. μ_{lxxx} is the efficiency factor of the activation region. All other variables are as defined previously. Refer to Appendix IV for further derivation

In the case of partial confinement for FRM and FRC composites with varying fiber orientation, there is a radial transverse force due to the existing fibers in the transverse direction that reduces the lateral forces within the concrete core. The general lateral stress from equilibrium as shown in Figure XIII (b) in Appendix IV is defined as

$$\sigma_2 = \frac{2\sigma_{lxxx}t_{xxx}}{D_c} - \frac{2\sigma_{txxx}r_{pl}}{D_c} \quad \text{Eq. (V. 77)}$$

The above equations can be generalized for the state at peak with a lateral stress

$$\sigma_{2cu} = \frac{2\sigma_{lxxx}t_{xxx}}{D_c} - \frac{2\sigma_{txxx}r_{pl}}{D_c} \quad \text{Eq. (V. 78)}$$

where σ_{txxcu} represents the transverse tensile stress of the composite at the plastic centroid in the radial direction. All other parameters are as defined previously. Refer to Appendix IV for derivation.

2. Optimization of thickness

The case of optimized thickness is shown in Figure IVa. In general, as the thickness of the composite jacket increases from zero to the optimized value, the point B' in Figure IVa moves upwards towards the point B. However, as the thickness goes beyond the optimal value the point B' remains at the point B, with the stress value being:

$$\sigma_{lcco} = \sigma'_{cc} \geq \sigma'_c \quad \text{Eq. (V. 79)}$$

a) Full Confinement

The value of σ_{lcco} is obtained from equations (V.67) and (V.68) and is substituted in equation (V.79)

$$\sigma_{lcco} = \frac{\sigma'_c(E_{lcco} + E_{lc2})}{(E_{lcco} - E_{lc2})} = \sigma'_{cc} \quad \text{Eq. (V. 80)}$$

The value of the optimal thickness t_{opt} , is finally determined by substituting the value of σ'_{cc} from equation (V.64) into equation (V.80).

In summary:

- $t_{xxx} \leq t_{opt}$ - you get a first peak σ_{lcco} and second peak σ_{lccu}

$$\sigma_{lcco} = \frac{\sigma'_c(E_{lcco} + E_{lc2})}{(E_{lcco} - E_{lc2})} \quad \text{Eq. (V. 81)}$$

$$E_{lc2} = \frac{(\sigma_{lccu} - \sigma'_c)}{\varepsilon_{lccu}} \quad \text{Eq. (V. 82)}$$

$$E'_{lc2} = \frac{(\sigma_{lcco} - \sigma'_{cc})}{(\varepsilon_{lccu} - \varepsilon_{lcco})} \quad \text{Eq. (V. 83)}$$

- $t_{xxx} > t_{opt}$ - one peak only σ_{lccu} exists and $\sigma_{lcco} = \sigma'_{cc}$ from Eq.(V.79)

$$\sigma_{lcco} = \sigma'_{cc} = \frac{\sigma'_c(E_{lcco} + E_{lc2})}{(E_{lcco} - E_{lc2})} \quad \text{Eq. (V.84)}$$

and since the slopes E'_{lc2} and E_{lc2} , based on Figure 3a, match

$$E'_{lc2} = E_{lc2} = \frac{(\sigma_{lccu} - \sigma'_c)}{\varepsilon_{lccu}} \quad \text{Eq. (V.85)}$$

Values for t_{opt} and the corresponding confinement stresses are summarized in TableV-

1.

b) Partial Confinement:

In this case as the modulus of elasticity is negative as shown in Figure IV(b), and therefore as the thickness increases and the point B' approaches the point B, stress σ'_{cc} continuously decreases until it reaches σ_{lcco} at the optimal thickness. A similar but inverse analogy as used for the full confinement can be used here. The slopes E_{lc2} and E'_{lc2} are both negative and the peak stresses are smaller than σ'_c .

3. Longitudinal and Transverse Strains

A regression analysis was performed on the longitudinal versus transverse strains leading to similar equations as equations (V.46), (V.47), (V.48), and (V.49) of discrete composites as defined FigureIV-3(a). Values for A_2 to F_2 are summarized in Table (V.2). The transverse stress-strain model is obtained similar to discrete confinements.

4. Energy Approach to determine ε_{lcr} ¹⁰

Same energy approach as for discrete composites is applicable. Refer to Eq. (V.56)

to (V.78) with a volumetric ratio of $\rho_s = \frac{t_{xxx} s_{xxx} \pi D_c}{\frac{\pi D_c^2}{4} s_{xxx}}$ for continuous confinement.

All parameters are as defined in the notation list.

5. Multiple Cracking in SIFC

In SIFC and from experimental evidence, optimized thickness was reached and $E'_{lc2} = E_{lc2}$ based on Eq.(V.85). The activation region consists of a series of straight lines representing the multiple cracking mechanism as shown in FigureV-2.

The number of cracks can be determined as follows:

For First Crack n=1

$$E_{lc21} = \frac{\sigma_{lccu1} - \sigma'_c}{\varepsilon_{lccu1}} \quad \varepsilon_{lcco} < \varepsilon_{lc} < \varepsilon_{lccu1} \quad \text{Eq. (V. 86)}$$

For Cracks n=2 to n=N

$$(n - 1)\varepsilon_{lccu1} - (n - 2)\varepsilon_{lcco} < \varepsilon_{lc} < n\varepsilon_{lccu1} - (n - 1)\varepsilon_{lcco} \quad \text{Eq. (V. 87)}$$

The multiple crack is

$$E_{lc2n} = \frac{2\sigma_{lccu1} - 2\sigma_{lcco}}{n\varepsilon_{lccu1} - (n - 1)\varepsilon_{lcco}} \quad \text{Eq. (V. 88)}$$

As stated previously, all straight lines in the activation region are approximated by a single line with a slope E_{cl2} which is the average slope. Based on the equations for peak stress, strain and average slope during multiple cracking, the following equations are presented

$$\sigma_{lccu} = n\sigma_{lccu1} - (n - 1) \quad \text{Eq. (V. 89)}$$

$$\varepsilon_{lccu} = n\varepsilon_{lccu1} - (n - 1)\varepsilon_{lcco} \quad \text{Eq. (V. 90)}$$

$$E_{cl2} = \frac{\sum_{i=2}^n \frac{2\sigma_{lccu1} - 2\sigma_{lcco}}{i\varepsilon_{lccu1} - (i - 1)\varepsilon_{lcco}} + \frac{\sigma_{lccu1} - \sigma'_c}{\varepsilon_{lccu1}}}{n} \quad \text{Eq. (V. 91)}$$

where σ_{lccu1} and ε_{lccu1} are the stress and strain of confined concrete at first crack of composite, σ_{lccu} and ε_{lccu} are the peak stress and strain of confined concrete at end of multiple cracking of composite, E_{lc21} and E_{lc2n} are the inelastic moduli for

first crack and n^{th} crack of composite, ε_{lcco} σ_{lcco} are the confinement strain and stress of confined concrete, σ'_{cc} is the strength of confined concrete at start of activation of composite. The number of cracks can be obtained by solving three Eq.(V.89), (V.90), and (V.91) in three unknowns σ_{lccu1} , ε_{lccu1} and the number of the cracks n .

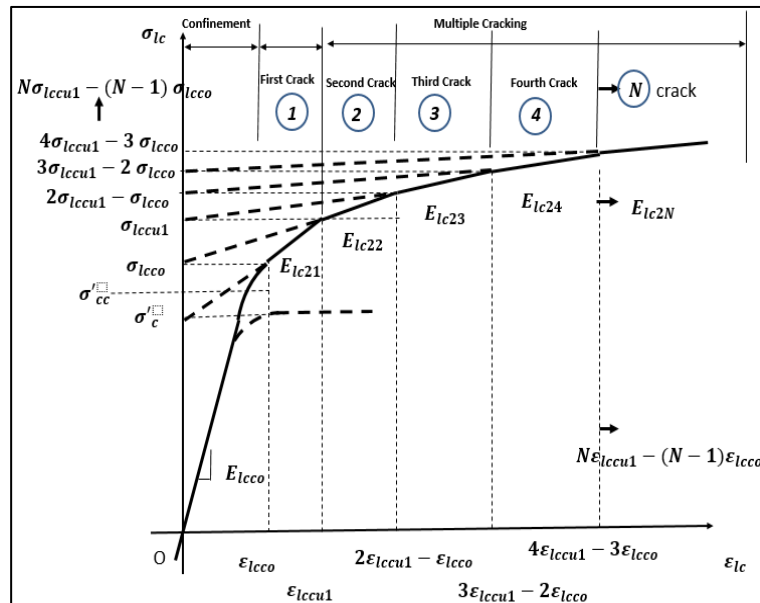


Figure V-2: Multiple cracking model in SIFC

5.2 THEORETICAL RESULTS AND DISCUSSION

Tables V.6, V.7, V.8, and V.9 summarize theoretical pre-peak and post peak stress strain parameters. In the ascending branch, efficiency factors were close to 1 indicating that confined concrete peak stresses were reached when the composite reached its peak stress. In the descending branch, the efficiency factors were larger than 1, indicating that the composite protected the concrete core and it failed after rupture of the composite. WIM composites showed a large value for the efficiency factor in the descending branch-(rupture regions) due to delamination issues between the wire mesh and the concrete surface.

Peak stresses with strain factors, and lateral stresses at peak are listed in Table V.7. It is noted that for FRC and FRM jackets the lateral stress is negative due to partial confinement resulting in lower peak stresses than unconfined concrete. FRP values follow the ACI 440⁸ equations, except that for FPG -1 layer, revised factors have been recommended to predict more accurately the experimental results.

For the case of the full confinement with discrete composites, confinement is continuous and hence, the concept of the optimized spacing is irrelevant. It is noted that points B and B' coincide as shown in Figure V-3a, and are slightly higher than unconfined concrete strength.

For (SP3), the $E_{lc2} = 0$ since the peak stress is equal to that of unconfined concrete and E'_{lc2} does not exist since the strains at peak and at confinement are equal. For (SP2) and (WIM), the slopes $E_{lc2} = E'_{lc2} = 101 \text{ MPa} (1.64 \text{ ksi})$. As for FRM, points B and B' converge no slope E'_{lc2} exists. In FRC the confinement and peak strains are different and $E_{lc2} \neq E'_{lc2} < 0$, represented in TableV.6. As for High performance continuous composites, such as FPC and FPG, optimal thicknesses were not attained resulting in a drop in stress at the transition point and not maximizing the energy absorption of the composite while for SIFC composites; optimal thickness was attained resulting in a maximized energy capacity of the confinement.

Regression constants are presented in Table V.5. These values were obtained using the experimental data. The variation R^2 show values close to 1 indicating good correlation between experimental and theoretical regression lines.

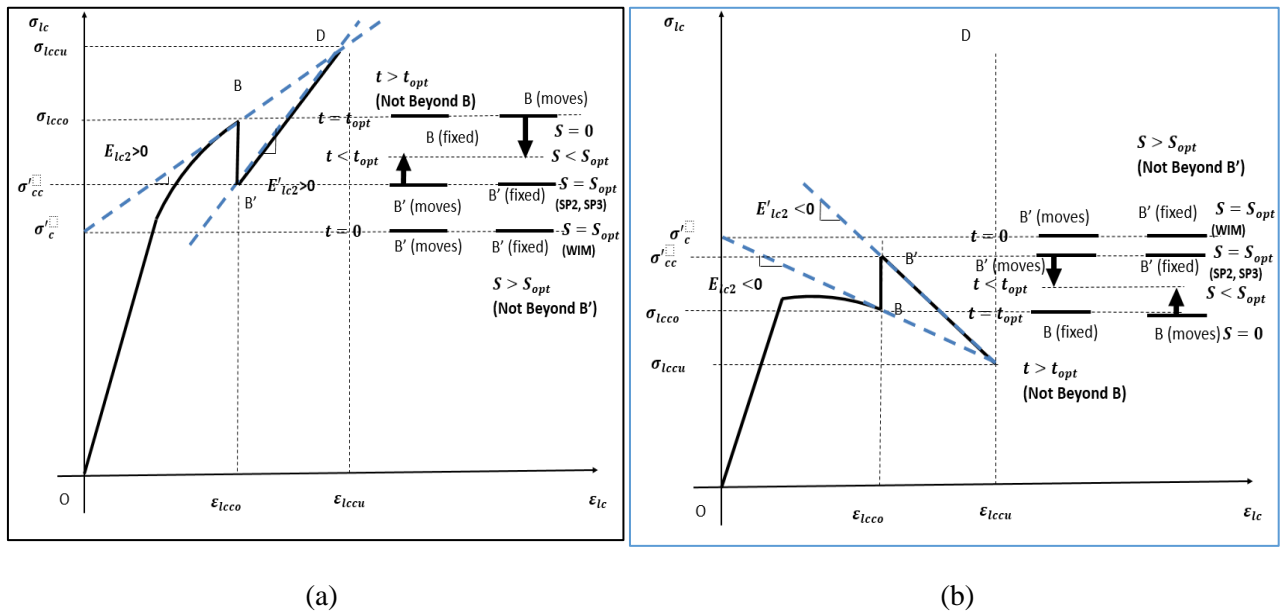


Figure V-3: (a) Ascending portion of the stress-strain curve for full confinement (b) Ascending portion of the stress-strain curve for partial confinement

Table V-6 Pre-peak theoretical data for longitudinal stress and strain of confined concrete (0.15 Ksi=1 MPa)

		E_{lcco} MPa (Ksi)	σ_{lcp} MPa (Ksi)	ϵ_{lcp}	E'_{lc2} MPa (Ksi)	E'_{lc2} MPa (Ksi)	σ_{lcco} MPa (Ksi)	ϵ_{lcco}
LPBF	CON	30460 (4418)	39.6 (5.7)	0.0013	0	0	42 (6)	0.0024
	FRM	23700 (3437)	33.18 (4.8)	0.0014	-4335 (-650)	NA	30.45 (4.4)	0.0031
	SP3	30460 (4418)	39.6 (5.7)	0.0013	0	NA	42 (6)	0.0041
LPDF	FRC	30460 (4418)	30.46 (4.6)	0.001	-4282 (-642)	-24050 (-3607)	32.83 (4.75)	0.0025
	WIM	30460 (4418)	30.46 (4.6)	0.001	101 (14.64)	101 (14.64)	42.418 (6.15)	0.00412
	SP2	30460 (4418)	46.17 (6.7)	0.0015	101 (14.64)	101 (14.64)	42.89 (6.36)	0.0041
HPBF	FPC(SCH 41-1)	32170 (4666)	45.03 (6.5)	0.0014	2304.3 (334.2)	2785 (418)	48.5 (7)	0.0028
	FPC (SCH 41-2)	32170 (4666)	41.82 (6.1)	0.0013	2857 (414)	3385 (508)	49.7 (7.5)	0.0029
	FPC (11UP-2)	31470 (4564)	53.5 (7.76)	0.0017	1575 (228)	1765 (265)	46.4 (6.7)	0.00281
	FPG (SEH-)- ACI	30310 (4396)	45.47 (6.6)	0.0015	1688 (253)	2049 (316)	46.89 (6.8)	0.0029
	FPG (SEH-1)	30310 (4396)	45.465 (6.6)	0.0015	512 (74)	512 (74)	43.4 (6.3)	0.0028
	FPG (SEH-2)	30310 (4396)	45.465 (6.6)	0.0015	1916 (287)	2057 (309)	47.5 (6.9)	0.0029
HPDF	SIFC	23400 (3510)	18.4 (2.7)	0.0008	2742 (411)	2742 (411)	53 (7.7)	0.0041

Table V-7: Post-peak theoretical data for longitudinal stress and strain of confined concrete (symbols in parenthesis represent the relative composite parameters) (0.15 Ksi=1 MPa)

		σ_{lccu} (σ_{lxxxp}) σ_{lxxxcu} MPa (Ksi)	ϵ_{lccu} (ϵ_{lxxxp} , ϵ_{lxxxcu})	σ_{lco} (σ_{lxxxr}) Mpa (Ksi)	ϵ_{lco} (ϵ_{lxxxr})	σ_{lcr} MPa (Ksi)	ϵ_{lcr}	T_l MPa (Ksi)	TI_l
LPBF	CON	42 (6)	0.0024	-	-	32.4 (4.7)	0.005	0.18 (0.026)	1
	FRM	30.45 (4.4)	0.003	27.6 (4)	0.0051	26.5 (3.84)	0.0057	0.149 (0.022)	0.8
	SP3	42 (6)	0.00414	-	-	35.5 (5.33)	0.008	0.19	1.06
LPDF	FRC	30.67 (4.45)	0.00298	26 (3.8)	0.007	19.2 (2.88)	0.016	0.26 (0.06)	1.44
	WIM	42.42 (6.15)	0.00416	-	-	28 (4)	0.011	0.36 (0.05)	2
	SP2	42.9 (6.2)	0.00418	-	-	17.2 (2.5)	0.02	0.57 (0.08)	3.2
HPBF	FPC(SCH 41-1)	74.26 (10.8)	0.014	-	-	54* (8.1)*	0.005*	0.21 (0.03)	1.2
	FPC (SCH 41-2)	82 (12)	0.014	-	-	82 (11.9)	0.014	0.82 (0.12)	4.6
	FPC (11UP-2)	73.5 (10.6)	0.02	-	-	76.6 (11)	0.022	1.25 (0.18)	7
	FPG (SEH-1)-ACI	64 (9.3)	0.013	-	-	67 (10.0)	0.015	0.65 (0.09)	3.61
	FPG (SEH-1)	48.65 (7.3)	0.013	-	-	51 (7.65)	0.018	0.54 (0.08)	1.2
	FPG (SEH-2)	84 (7.1)	0.022	-	-	86 (12.5)	0.023	1.46 (0.2)	8.46
HPDF	SIFC	55.7 (8.1)	0.0051	55.6 (8.1)	0.0054	16.4 (2.4)	0.042	1.23 (0.18)	6.83

Table V-8: Pre-peak theoretical data for longitudinal and transverse strain of confined concrete (symbols in parenthesis represent the relative composite parameters)

		ϵ_{lcp}	ϵ_{tcp}	ϵ_{lcco}	ϵ_{tcco}	ϵ_{lccu} (ϵ_{lxxxp} , ϵ_{lxxxcu})	ϵ_{tccu} (ϵ_{lxxxp} , ϵ_{lxxxcu})
LPBF	CON	0.0013	0.00036	0.0024	0.00064	0.0024	0.00064
	FRM	0.0014	0.00033	0.0031	0.00033	0.003	0.00033
	SP3	0.0013	0	0.0041	0	0.0041	0
LPDF	FRC	0.001	0	0.0025	0.00024	0.00298	0.00035
	WIM	0.001	0	0.00412	0.007	0.00416	0.007
	SP2	0.0015	0	0.0041	0.00036	0.00418	0.00039
HPBF	FPC(SCH 41-1)	0.0014	0	0.0028	0.0002	0.014	0.003
	FPC (SCH 41-2)	0.0013	0	0.0029	0	0.014	0.0025
	FPC (11UP-2)	0.0017	0	0.0028	0	0.02	0.003
	FPG (SEH-1)-ACI	0.0015	0	0.0029	0	0.013	0.0045
	FPG (SEH-1)	0.0015	0	0.0028	0	0.013	0.0045
	FPG (SEH-2)	0.0015	0	0.0029	0.00043	0.022	0.0093
HPDF	SIFC	0.0008	0	0.0041	0.0011	0.0051	0.0028

Table V-9: Post-peak theoretical data for longitudinal and transverse strain of confined concrete (symbols in parenthesis represent the relative composite parameters) (0.15 Ksi=1 MPa)

		ϵ_{lco} (ϵ_{lxxx})	ϵ_{tco} (ϵ_{txxx})	ϵ_{lcr}	ϵ_{tcr}	μ_{lxx}	ζ_{lxx}	ν	T_t MPa (Ksi)	TI_t
LPBF	CON	-	-	0.005	0.0014	-	-	0.28	0.049 (0.007)	1
	FRM	0.0051	0.0016	0.006	0.0024	1	4.7	-	0.055 (0.0085)	1.13
	SP3	-	-	0.008	0.0075	0	1	-	0.313 (0.045)	6.38
LPDF	FRC	0.007	0.0032	0.016	0.046	1	13.1	-	0.38 (0.055)	7.75
	WIM	-	-	0.011	0.016	1	30	-	0.585 (0.09)	12
	SP2	-	-	0.02	0.013	0.007	1	-	0.4 (0.06)	8.15
HPBF	FPC(SCH 41-1)	-	-	0.005	0.0008	0.803	1	-	0.035* (0.005)*	0.72*
	FPC (SCH 41-2)	-	-	0.014	0.0025	1	1.69	-	0.165 (0.025)	3.375
	FPC (11UP-2)	-	-	0.022	0.0035	1	1.67	-	0.215 (0.033)	4.4
	FPG (SEH-1)-ACI	-	-	0.015	0.0045	1	2.67	-	0.25 (0.038)	5.1
	FPG (SEH-1)	-	-	0.018	0.0058	1	2.67	-	0.275 (0.041)	5.61
	FPG (SEH-2)	-	-	0.023	0.0098	1	1.77	-	0.65 (0.1)	13.2
HPDF	SIFC	0.0054	0.013	0.042	0.042	0.4	9.9	-	1.215 (0.183)	24.8

VI. COMPARISON OF EXPERIMENTAL AND ANALYTICAL DATA

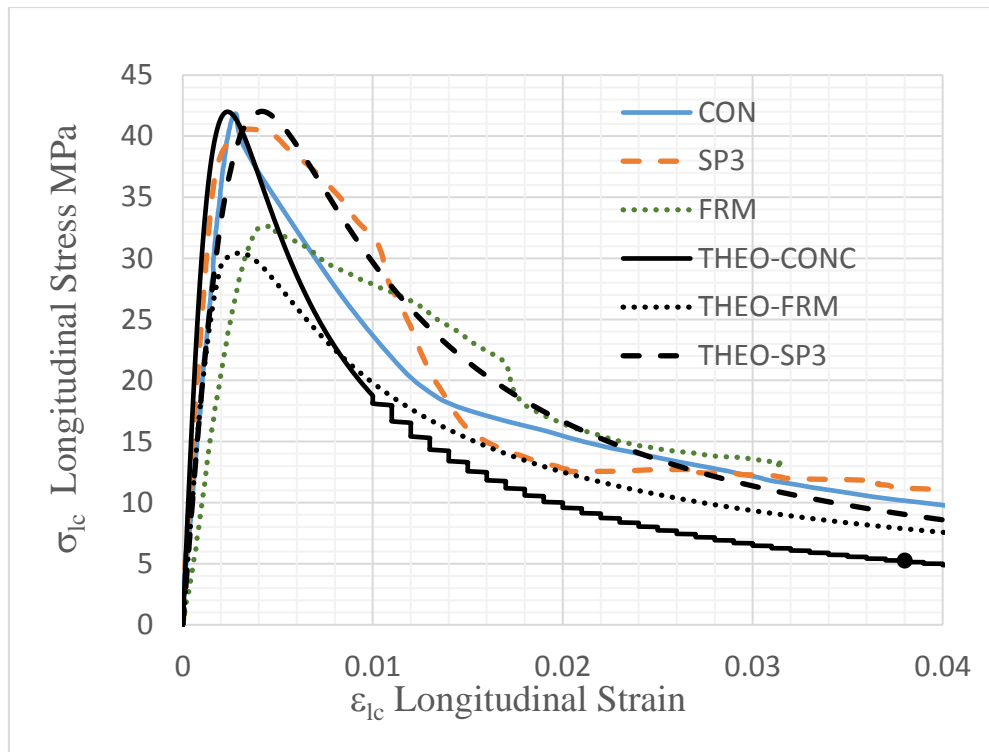
Comparison between experimental and analytical results is shown in Figures VI-1 to VI.5. For low performance (low strength) brittle and ductile composites, good correlation has been noted for pre-peak results. The exception are FRM and FRC which exhibit discrepancy in the post peak region due to the effect of fiber pull out, which was not accounted for in the analytical models. Poisson curves show a higher ratio for FRM and SP3 than for typical concrete which is indicative of a stable system triggered through the activation of the spirals and fibers (steel has higher Poisson's ratio than concrete). Tables V.9 also show discrepancy in the rupture transverse strain for SP3, in which case analytical and experimental values are 0.0075 and 0.001, respectively.

For High performance (high strength) brittle failure composites, good correlation existed except for FPG-1 case where the ACI 440⁸ equations underestimate the experimental values. Furthermore, the energy approach underestimates the rupture strains for most of the FRP cases resulting in (a) lower transverse rupture strains (b) some reduction in the longitudinal and transverse toughness indices. Hence, the energy approach does not adequately predict the post peak failure response of FRP's.

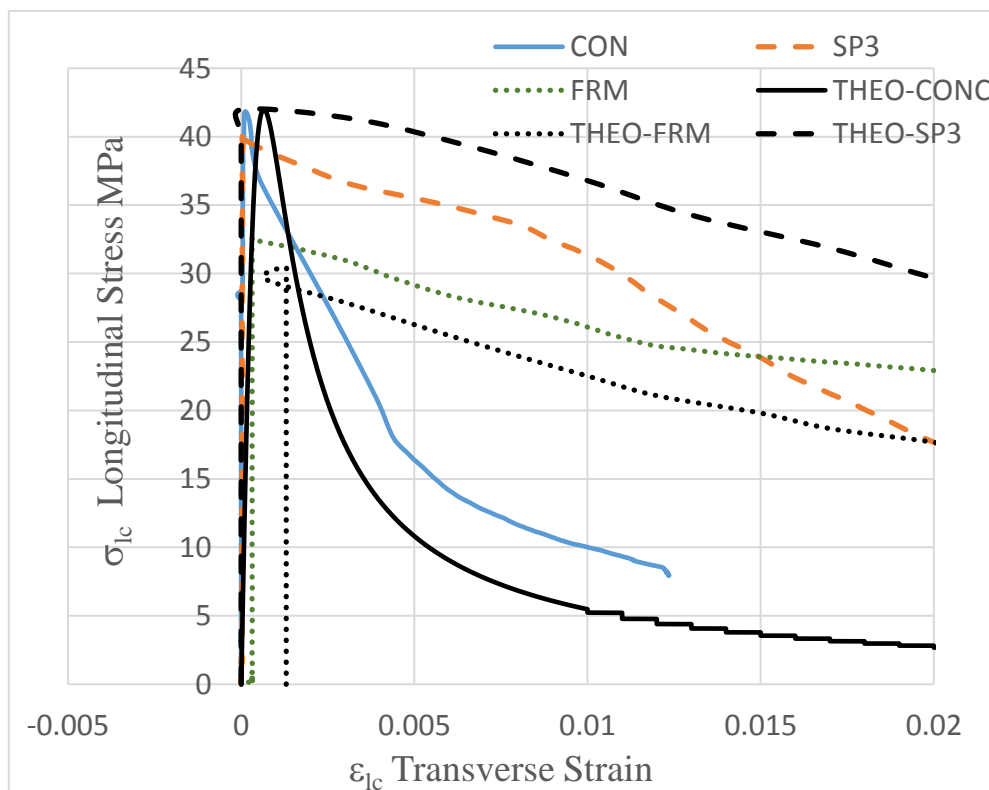
In Tables V.9, for FPC-1 layer, the theoretical rupture stress of 54 MPa was calculated from the rupture strain obtained from the energy equation. The value was below the experimental stress of 70 MPa for similar reasons stated above.

Although the analytical and experimental stress strain curves for High performance (high strength) ductile composites correlate well, as shown in Appendix V, some discrepancies were noted:

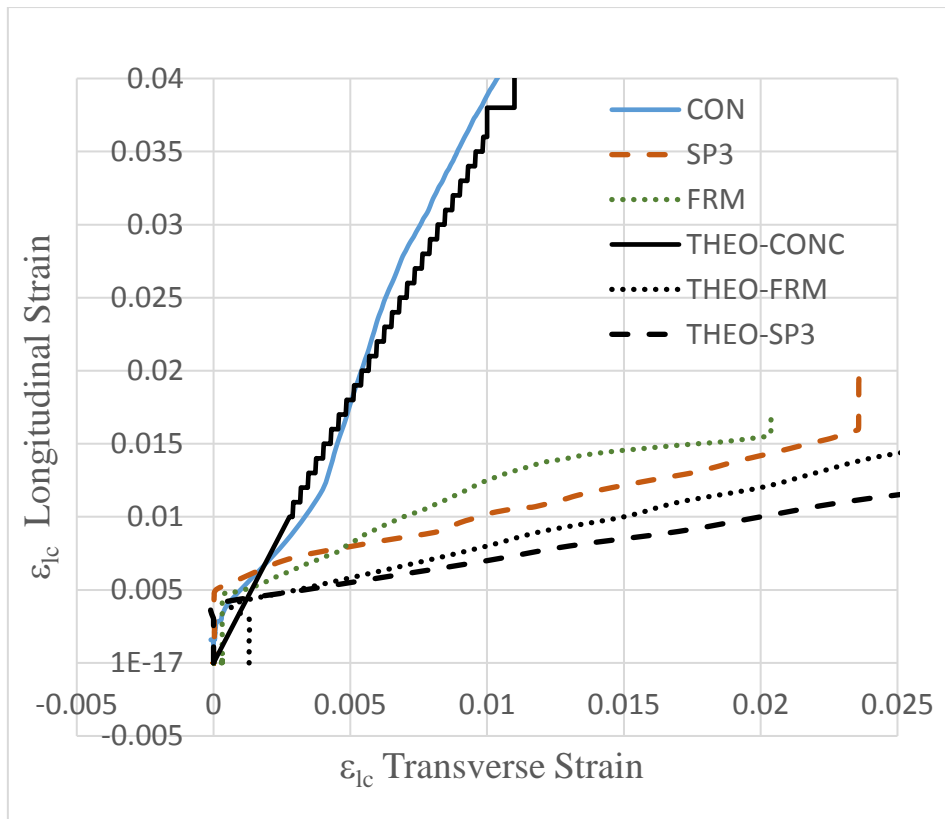
1. The experimental confinement strain of 0.0014 was much lower than the analytically obtained value of 0.004.
2. The experimental transverse rupture strain of 0.016 also differed from the analytical value of 0.042, which led to a higher transverse toughness index of 24.8.



(a)

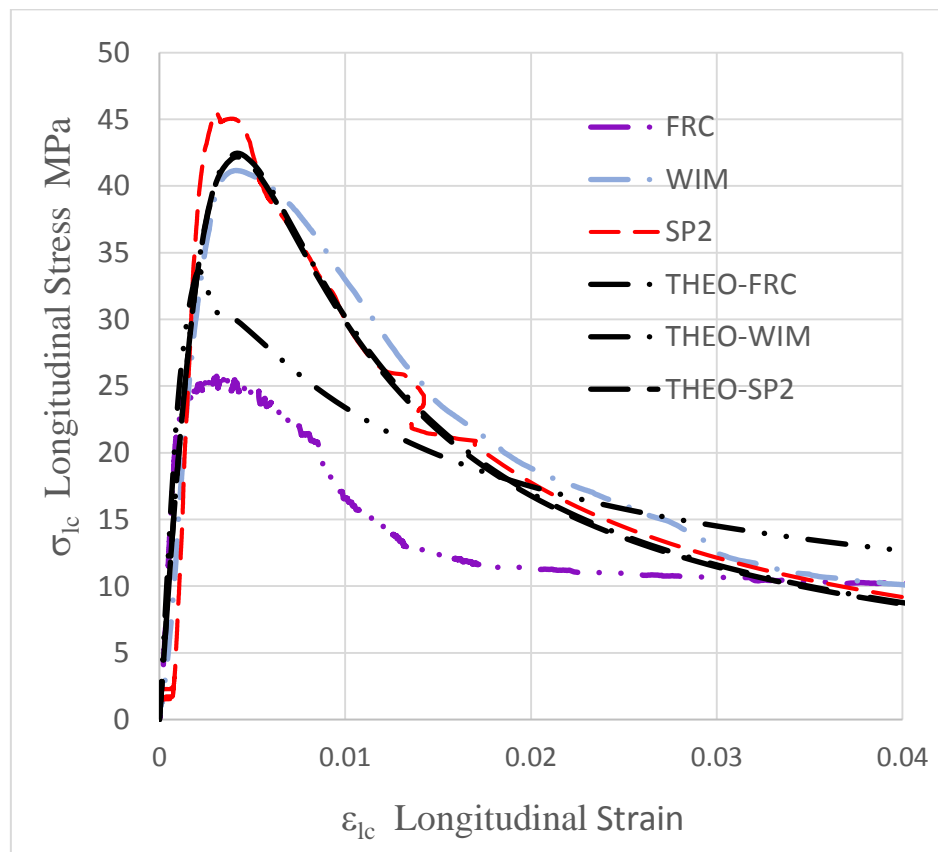


(b)

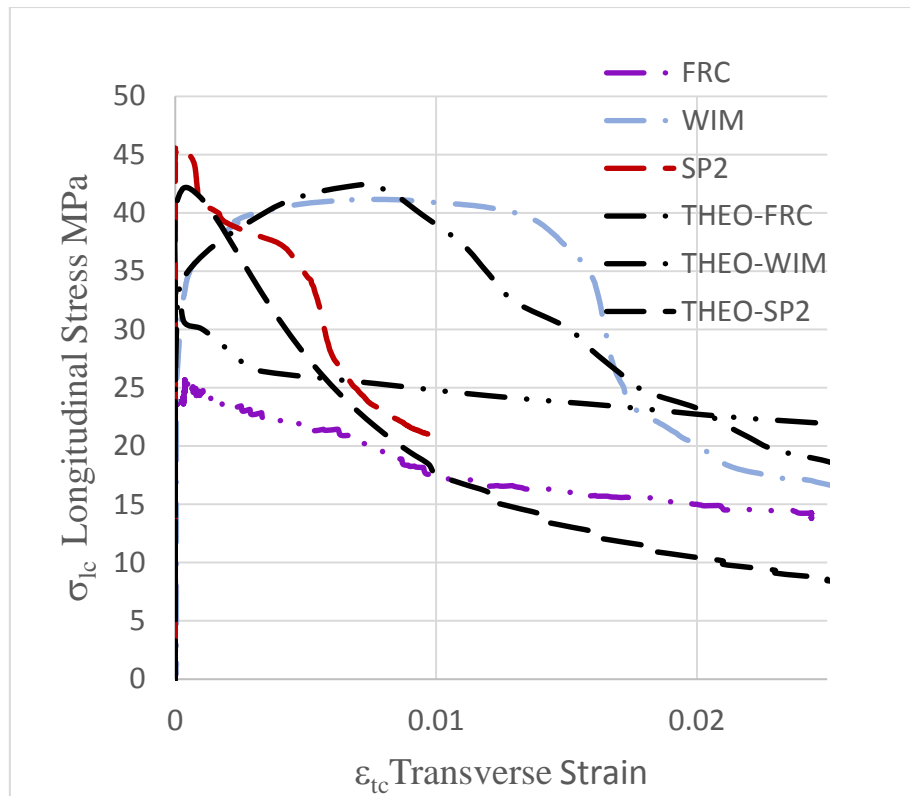


(c)

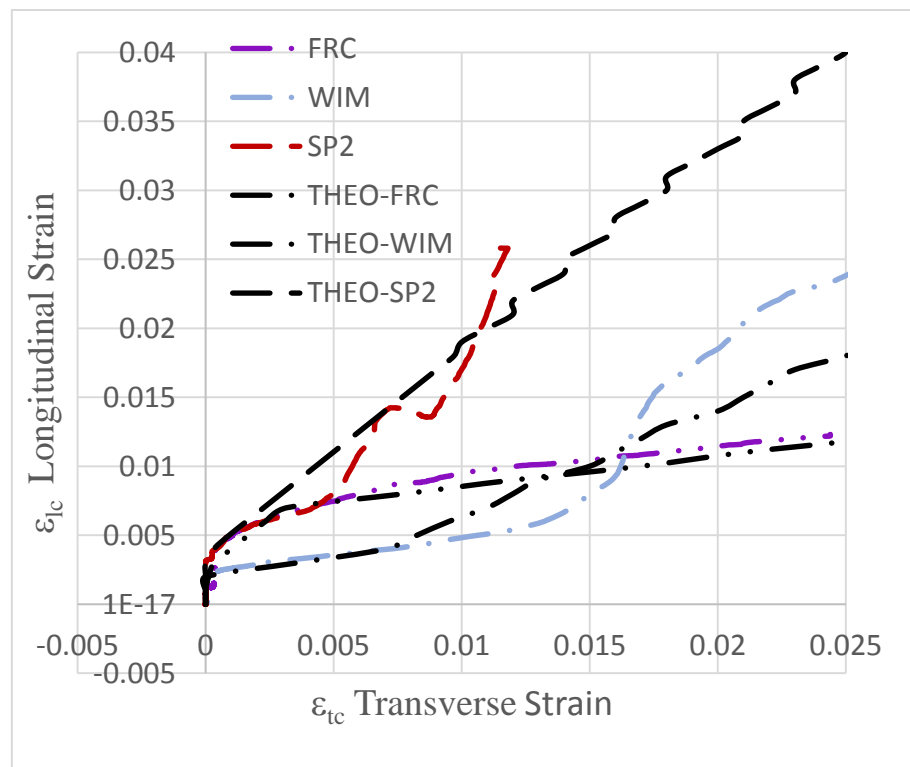
Figure VI-1: (a) Stress versus Longitudinal strain (b) Stress versus Transverse strain (c) Longitudinal versus Transverse strain – LPBF-(THEO+EXP)



(a)

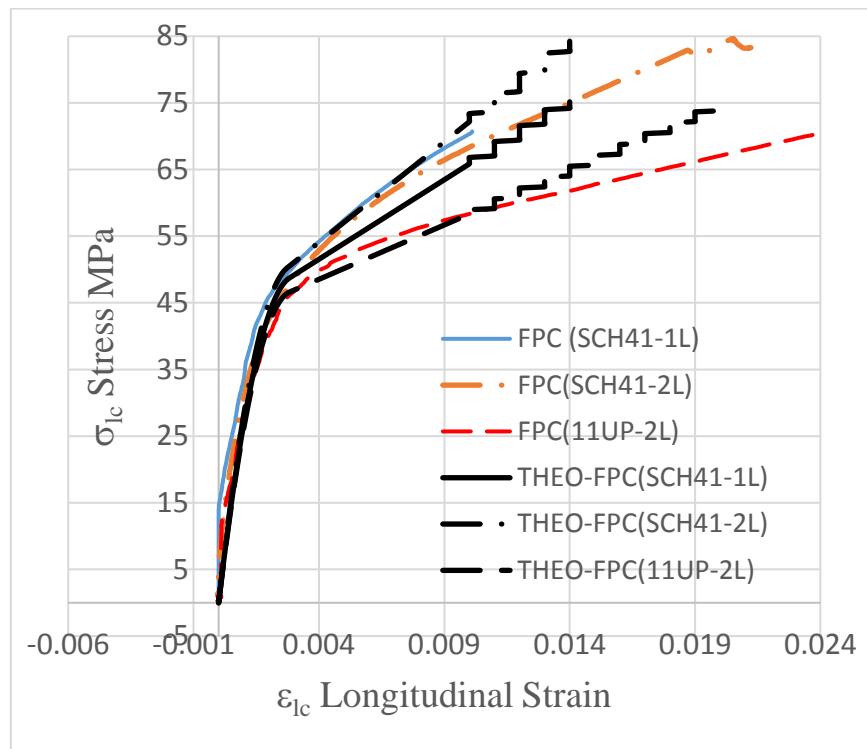


(b)

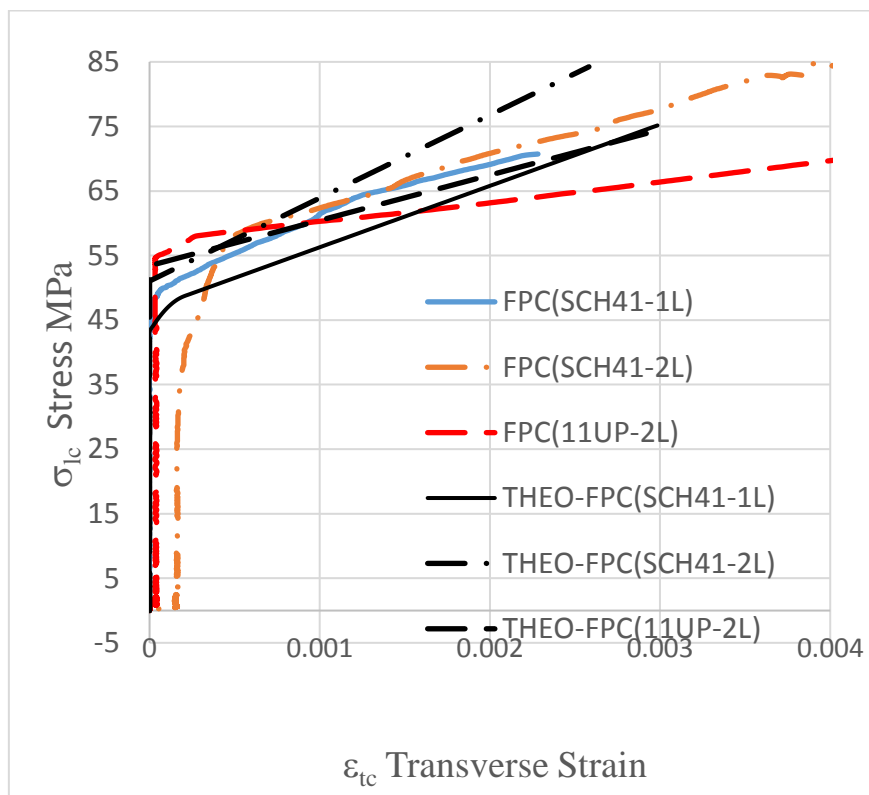


(c)

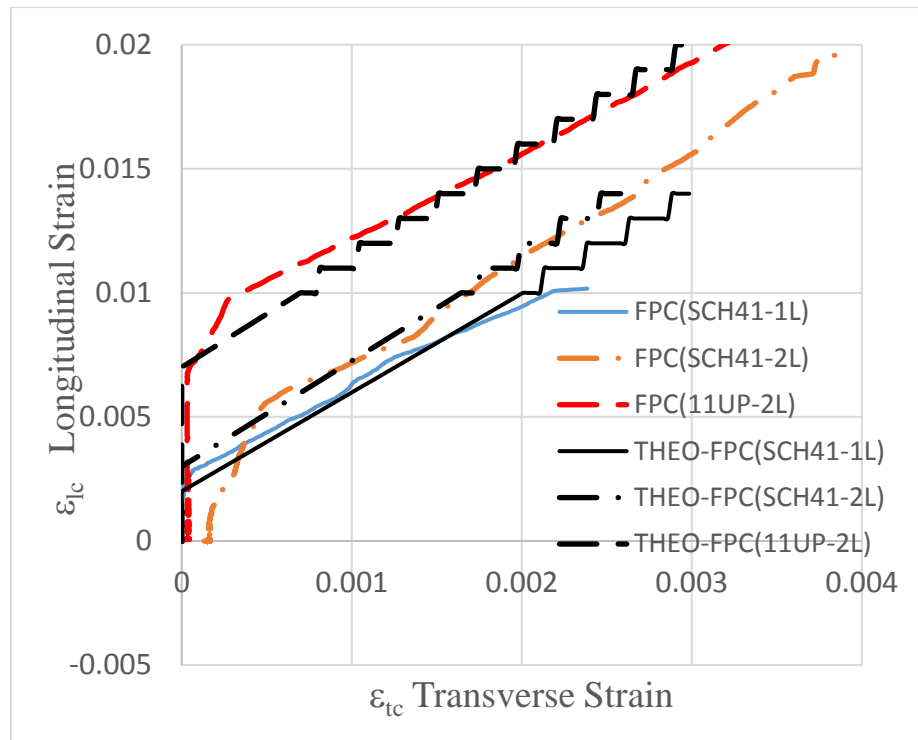
Figure VI-2: (a) Stress versus Longitudinal strain (b) Stress versus Transverse strain (c) Longitudinal versus Transverse strain – LPDF-(THEO+EXP)



(a)

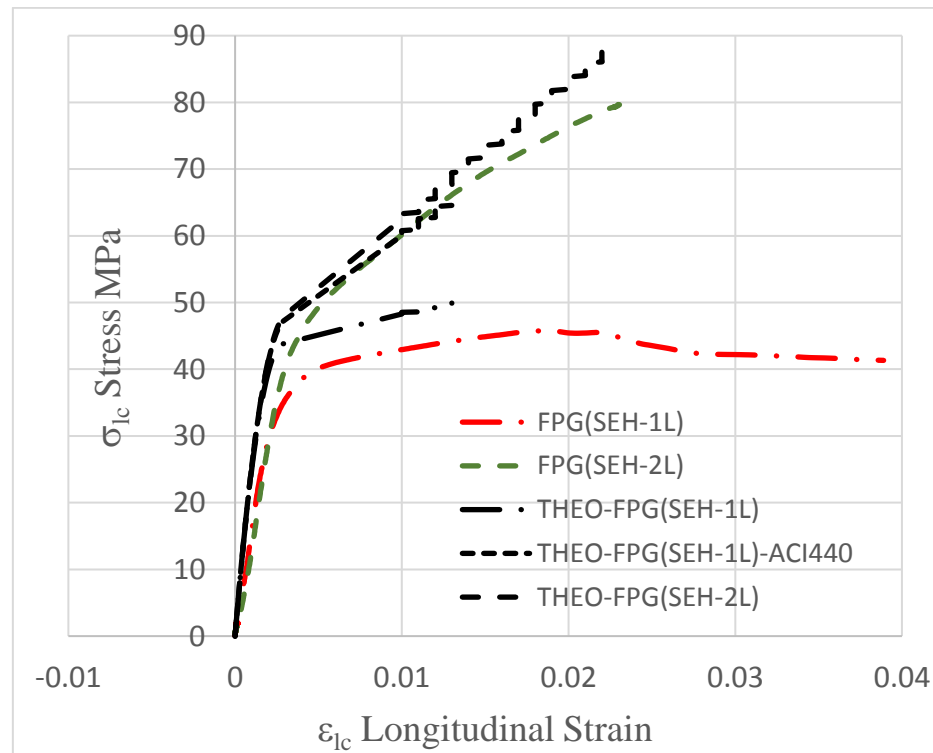


(b)



(c)

Figure VI-3: (a) Stress versus Longitudinal strain (b) Stress versus Transverse strain (c) Longitudinal versus Transverse strain - HPBF (Carbon)-(THEO+EXP)



(a)

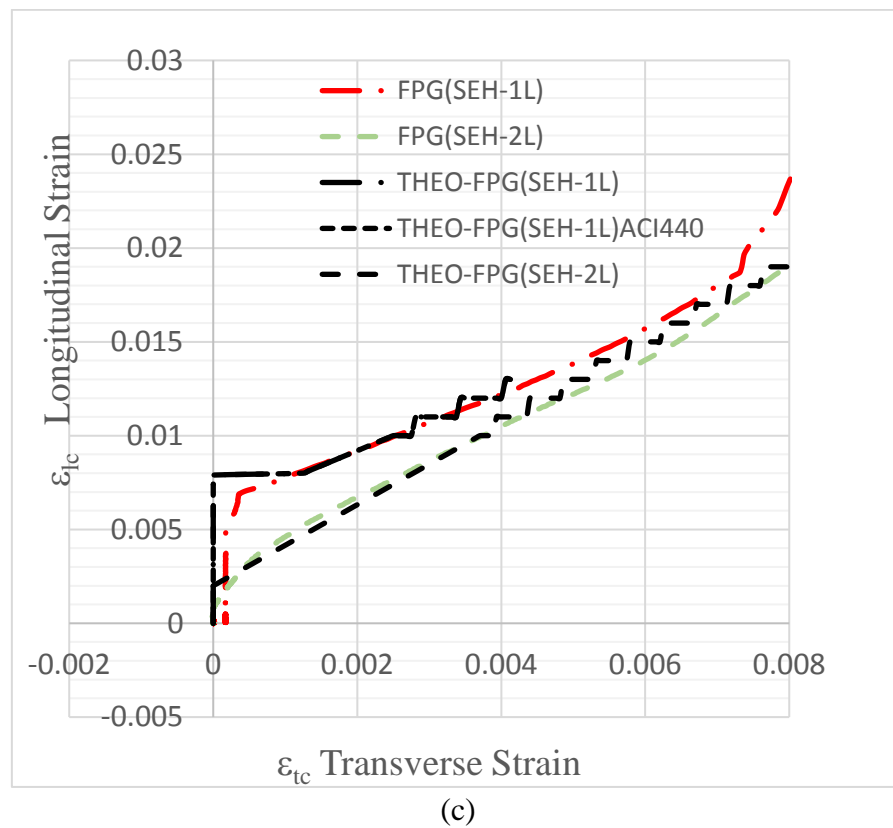
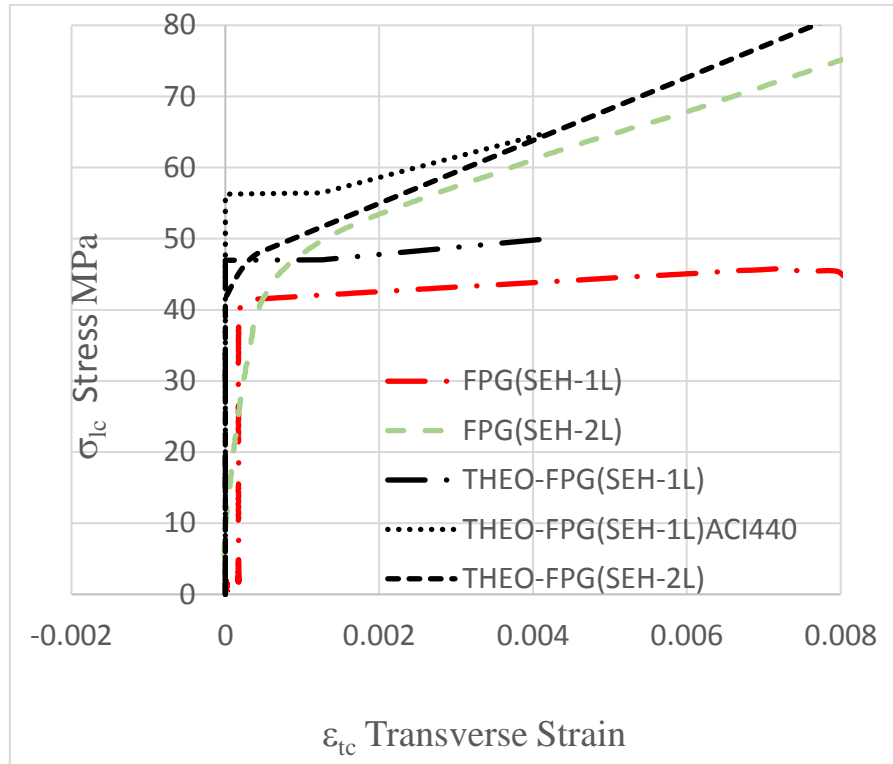
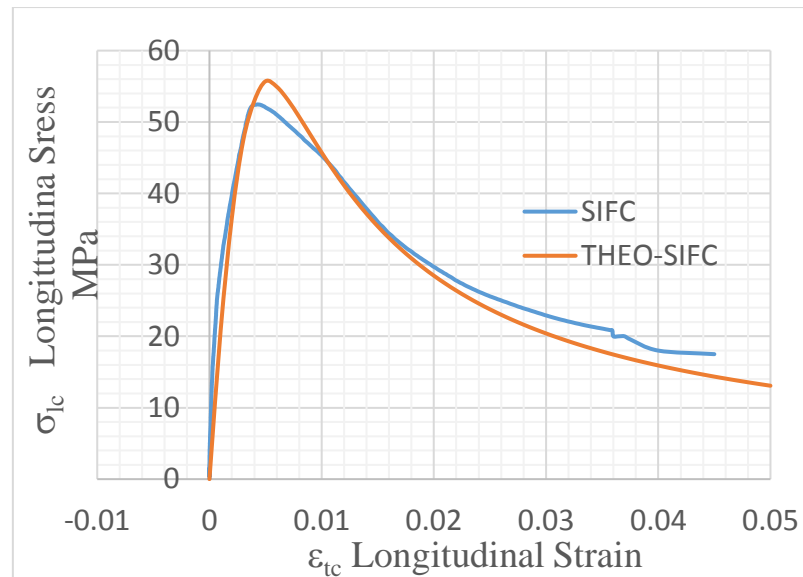
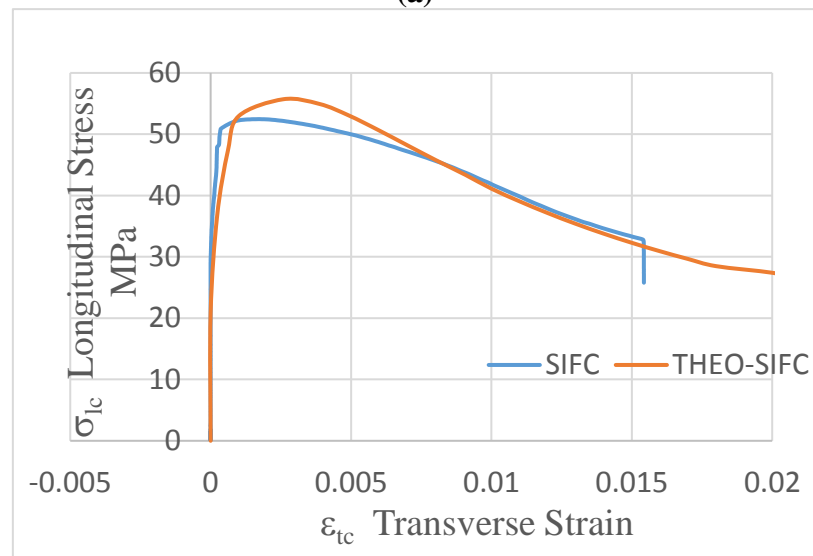


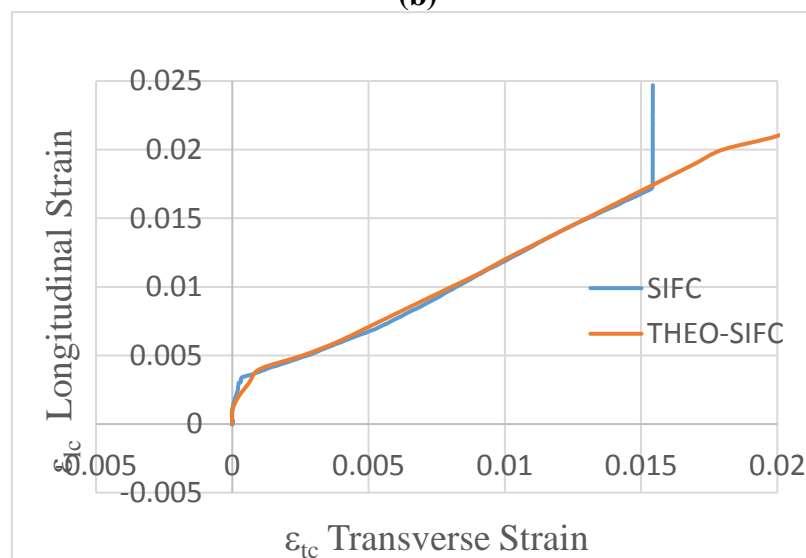
Figure VI-4: (a) Stress versus Longitudinal strain (b) Stress versus Transverse strain (c) Longitudinal versus Transverse strain – HPBF (Glass)-(THEO+EXP)



(a)



(b)



(c)

Figure VI-5: (a) Stress versus Longitudinal strain (b) Stress versus Transverse strain (c) Longitudinal versus Transverse strain – HPDF-(THEO+EXP)

VII. CONCLUSION AND RECOMMENDATION

The objective of the research presented in this paper was to investigate, understand and model (stress-strain curves) the effect of confining columns using continuous jackets made of non-traditional composites such as FRC, FRM, and SIFC; and compare their behavior to existing SP and FRP confinement commonly used in the industry. In addition to considering continuous composite jackets, a case of discrete confinement using wire mesh (WIM) and spirals was also included. The reason for testing WIM confinement was to preliminary understand the effect of varying fiber orientation as well as their interaction (WIM being the “bounding” case with “fibers” being oriented only in the vertical and the horizontal direction). WIM will undergo further investigation (future work)

Comprehensive understanding of the confining effects jackets made of various composite materials have on the concrete strengths is necessary for the field use of these materials in increasing column resistance to various extreme loadings including blast and impact (theoretical standpoint).

Composites are classified based on their:

- 1) Performance Criteria- as high strength (FPC, FPG, SIFC) or low strength (FRC, FRM, SP2, SP3, WIM)
- 2) Failure Criteria-as brittle failure (FPC, FPG, SP3, FRM) or ductile failure (SP2, WIM, FRC, SIFC)
- 3) Continuity- as continuous (FPC, FPG, SIFC, FRC, FRM) or discrete (SP2, SP3, WIM).
- 4) Confining Effectiveness- as partial confined (FRC, FRM) where strengths are lower than that of unconfined concrete or full confined (FPC, FPG, SP2, SP3, WIM, SIFC) where strengths are higher or equal to that of unconfined concrete

Thus, the stress strain response of confined concrete depends on spacing of discrete confinements, and thickness of continuous confinements. Values smaller than the optimal value (the value that renders further increase in confinement ineffective) show the first peak stress, σ_{lcco} , prior to activation of confinement and a second peak stress, σ_{lccu} , at the ultimate load thus not fully utilizing the energy absorption capacity of the composite. Values larger than the optimized value show one peak stress at ultimate σ_{lccu} thus maximizing the energy absorption of the composite. Peak and confinement stresses for full confinement are larger than unconfined concrete strength.

The following can be concluded from the experimental/theoretical investigation herein:

- SP3 and FRM behave similar to unconfined concrete. Cracks are initiated at the outside perimeter and are propagated to the concrete core without any lateral composite resistance. Strengths are maintained at 42 MPa (6.3 ksi) equal to that of concrete. Peak strains and confinement strains are very close indicative of no activation of the composite. Rupture strains are between 0.005 and 0.008 similar to regular concrete. Such retrofits are not recommended for improvement of resistance or energy absorption demands. They are not recommended for confinement.
- FRC, SP2 and WIM provide an improvement in energy absorption due to fiber pullout and yielding of steel but not necessarily in strength especially for FRC's where strength is lower than pure concrete due to partial confinement. The activation of the lateral confinement provides higher strains at peak and rupture thus improving energy absorption with toughness indices of 2 times for WIM and 4 times

for SP2 of unconfined concrete respectively. WIM reinforcement was tested to better understand contribution of fibers placed at two angles to the jacketed column. WIM confinement consists of connected horizontal and vertical wires. Developed model shows that stiffness of vertical wires affects the effectiveness of confinement provided by the horizontal wires. Consequently, more flexible vertical wires lead to an increase in the tensile force in the horizontal wires, thus increasing the confining effects on the concrete core. Inversely, the higher the stiffness of the vertical wires the lower the confining effects. Thus, the stress levels were larger due to the additional resistance of the vertical ties. However, problems with delamination of the wire mesh resulted in much larger stress and strain results at rupture than expected. Such composites: FRC, and WIM can be suited for flexure strength (Longitudinal toughness index) at low loads, dilatation strength (transverse toughness index) at moderate loads, and not suited for axial compression strength (require further investigation for future research)

The observed behavior of FRM and FRC could potentially be attributed to random distribution of fibers, resulting in less effective confinement because not all fibers are oriented in the horizontal (confining) direction, with the least effective fibers being those oriented close to the vertical direction. As expected, this leads to lower confinement effect and lower peak stresses. Due to random distribution and discontinuity, fibers will de-bond and pull-out at lower loads, providing lower level of ductility.

- FRP's (FPC and FPG) show great improvement in strength of up to 84 MPa (12.6 ksi) and can reach high rupture strains with toughness indices at 12. It can be concluded that early confinement strains are close to 0.004 rendering the concrete

core vulnerable. Due to the high tensile strength of the composite, the first crack of the FRP's (no multiple cracking) produce larger rupture strains at 0.032 but brittle failures are expected due to the vulnerability and lack of debonding of the composite with no softening effects after peak. These retrofits are suited for axial compression strength under large loads, flexural strength under low load but dilatation strength under moderate load. Thus, these retrofits could be more applicable to conventional loads rather than blast or impact loads that require softening behaviors at larger strains. FRP's provide ease of application but require fireproofing.

- Fibers in SIFC jackets are perfectly aligned in the transverse direction thus exhibiting multiple cracking with a total number of cracks $n=4$. Therefore, the use of SIFC jackets enhances confinement and more effectively protects the concrete core. SIFC composites have achieved better ductility compared to FRC, SP2 and FRP's. The strength reached 53 MPa (7.95 ksi) which is higher than that of FRC and SP2 but less than that of FRP. High strength retrofit options of structural elements is not necessarily the only solution to resist large load. Resisting large loads can be alternatively mitigated by introducing other redundant structural elements in the overall structure that will resist part of the load. The advantage of SIFC is the larger percentage of aligned fibers leading to a stiffer modulus in the range of 32000 MPa (4800 ksi). The larger percentage of fibers in the transverse direction maintain lower strains at early confinement protecting the concrete core thus produces larger strains at peak due to multiple cracking in lieu of single cracks as in other composites. Continuity of fibers led to higher debonding energies and higher rupture strains at 0.042 and 0.016 in the longitudinal and transverse direction respectively. The toughness indices of 10 were similar to FRP's in the longitudinal

direction and 13 in the transverse direction which are higher than FRP's. This composite is suited for flexural, and dilatation strength under large loads, and axial compression (ultimate strength) under moderate loads. It is theoretically recommended (requires further investigation) for close range blast loads due to multiple cracking and softening effects beyond peak allowing the system to absorb the large deformations. Fibrous confinements also provide protection against cratering and breaching for close stand-offs. Shortcomings of SIFC is the application of the lateral confinement in the field related to fiber placement and follow up pouring. This requires segmental pouring and quality control of fiber installation.

- Transverse strains in all composites are insignificant during confinement prior to activation of the composites. For low performance composites peak strains are in the range between 0.0003 and 0.0006 except for the wire mesh due to delamination. For high performance composites, strains at peak were in the range between 0.002 and 0.009. At rupture, SIFC developed the largest strains at 0.016 due to continuity and debonding of the fibers resulting in the highest transverse toughness index which is essential for blast and impact energy absorption.
- Based on the efficiency factors, fibrous (FRC, FRM, SIFC) and FRP composites were effective in confining the concrete by fully utilizing the tensile stress strain response of the composite at peak and rupture. At rupture, fibers exhibited pull out for FRC and FRM, debonding for SIFC and rupture for FRP. The efficiency factor during the activation region for SP2 and SP3 were low, indicative that the composite did not reach its full capacity by yielding. However, wire mesh (WIM) composites

yielded during the activation region but the efficiency factor at rupture was high due to delamination of the wire mesh. The rupture stresses in WIM were higher due to the additional resistance of the vertical ties.

- Presented models show good correlation with the experimental data. However, it should be noted that the energy approach does not account for energy due to debonding and/or pull-out of fibers. Therefore, for fibrous composites, the energy approach shows discrepancy between analytical and experimental data. For SP3, the theoretical transverse strains compared to experimental at rupture are 0.0075 to 0.001 leading to a toughness index of 6.3 compared to 1.53. For FPC (SCH-41-1 layer), the transverse strains at rupture are 0.0021 compared to 0.0008 leading to a toughness index of 2.60 compared to 0.72. For High performance brittle failure, good correlation existed except for FRG –1 layer where the ACI 440⁸ equations showed over conservative results compared to experimental.

In brief, each retrofit technique has its particular advantage in resisting given load (static or blast/impact). FRC and WIM is suited for flexure strength (Longitudinal toughness index) at low loads, dilatation strength (transverse toughness index) at moderate loads, and not suited for axial compression strength. While, FRM jacketing are not recommended for improvement of strength or energy absorption demands. They are not recommended for confinement. As for SIFC confinement, it is suited for flexural, and dilatation strength under large loads, and axial compression (ultimate strength) under moderate loads. However, FRP suited for axial compression strength under large loads, flexural strength under low load but dilatation strength under moderate load

From a theoretical standpoint, the response behavior of SIFC jacketing in terms of its ductility, softening post peak behavior and multiple cracking could lead to some potential advantages with respect to the retrofitting of concrete columns against large blast loads^{1,2}. The retrofitted structural elements are expected to sustain large strains in both directions which might result in less exhibited damage. At the same time, the presence of high percentage of fibers will prevent the column from breaching and cratering at close stand-off threats.

Thus, Research herein provides alternative solutions using steel fiber composite, other than conventional confinements (FRP tube, Steel, and Concrete Jacketing), for laterally retrofitting existing columns (has construction joints cause weakness in retrofit)

VIII. LIST OF NOTATIONS

xxx is the index designation of the composite type as shown in the list of notations

A	Specimen cross-sectional area
A_e	Area of effectively confined concrete core
A_g	Gross area of concrete
A_{st}	Area of the composite strap
A_{cc}	Effective area enclosed by the composite
A_{fxxx}	Fiber area fraction
A_{mxxx}	Matrix area fraction
A_{lxxx}	Area of composite normal to the lateral force
b	Specimen width
D_c	Diameter of the concrete core (i.e. central portion of the column effectively confined by the composite)
φ_{fxxx}	Diameter of the fiber
ϕ_{xxx}	Diameter of the lateral device
ε_{lur}	Longitudinal Strain at rupture of unconfined concrete,
ε_{lu}	Longitudinal strain of unconfined concrete
ε'_c	Compressive strain at ultimate stress for pure concrete
ε_{lc}	Longitudinal compressive strain for confined concrete
ε_{lcco}	Longitudinal compressive confinement strain for confined concrete
ε_{lcp}	Longitudinal compressive proportional strain for confined concrete
ε_{lccu}	Longitudinal compressive ultimate (peak) strain for confined concrete

ε_{lco}	Longitudinal compressive strain at first crack of concrete concrete core of confined concrete. (Longitudinal strain at end of fiber debonding or pull-out of composite)
ε_{lcr}	Longitudinal compressive strain at rupture of confined concrete
ε_{tcco}	Transverse compressive confinement strain for confined concrete
ε_{tc}	Transverse compressive strain for confined concrete
ε_{tcp}	Transverse compressive proportional strain for confined concrete
ε_{tccu}	Transverse ultimate (peak) compressive strain for confined concrete
ε_{tco}	Transverse compressive strain at first crack of concrete concrete core of confined concrete. (Transverse strain at end of fiber debonding or pull-out of composite)
ε_{tcr}	Transverse compressive strain at rupture of confined concrete
ε_{lxxx}	Longitudinal tensile strain for composite
ε_{lxxxp}	Longitudinal tensile proportional strain (first crack) of composite
ε_{mxxxp}	Longitudinal tensile proportional strain (first crack) of the matrix
ε_{fxxxp}	Longitudinal tensile proportional strain of the fiber
ε_{lxxxcu}	Longitudinal tensile ultimate (peak) strain (end of multiple cracking) for composite
ε_{lxxxr}	Longitudinal tensile strain at rupture for composite
ε_{fxxx}	Longitudinal tensile strain for fiber
ε_{mxxx}	Longitudinal tensile strain for matrix
E_{fxxx}	Longitudinal tensile modulus of elasticity for fiber
E_{mxxx}/E_{mxxx}	Tensile moduli of elasticity of the matrix,
E_c	Modulus of elasticity of unconfined concrete
E_{lcco}	Longitudinal compressive modulus of elasticity for confined concrete

E_{lc2}	In-elastic longitudinal compressive modulus of elasticity for confined concrete
E'_{lc2}	In-elastic longitudinal compressive modulus of elasticity for confined concrete during activation of composite
E_{lxxx}	Longitudinal tensile modulus of elasticity for composite
k_{xxx}	Slip coefficient of the composite
L_{xxx}	Length of the steel fibers
h	Specimen thickness
k_a and k_b are coefficient factors equal to 1 for circular sections	
l_{cxxx}	Critical length of the fiber
l_{oxxx}	Fiber length where bond stress is τ_u
l_{fxxx}	Actual length of the fiber
L	Specimen length
l*	Reference length
n	number of layers of FRP
η'_0	Orientation factor (cracked range)
η_0	Orientation factor in the elastic range.
η_l	Length-efficiency factor
P	Axial load
ρ_{cc}	Ratio of area of longitudinal reinforcement to gross area of concrete
ρ_s	Volumetric ratio of confining strap to concrete core
r	Ratio of fiber cross-sectional area to perimeter
S_{FRP}	Width of FRP strap.
U_{CC}	Ultimate strain energy per unit volume of confined concrete
U_{CO}	Unconfined concrete

U_{sl}	Energy required to maintain yield in longitudinal steel in compression
U_{st}	Ultimate strain energy per unit volume of composite strap
V_{fxxx}	Fiber volume fraction
V_{mxxx}	Matrix volume fraction
ω	Crack width
σ_{lu}	Longitudinal tensile stress of unconfined concrete
σ_{cxxx}	Longitudinal tensile stress of the composite
σ_{fxxx}^*	Fiber stress at the crack in idealized composite
σ_{mxxx}	Longitudinal tensile stress for Matrix Stress
σ_{caxxx}	Longitudinal Average tensile stress of the composite
$\sigma_{LSIFCpl}$	Post-peak plateau stress in compression
σ_{it}	Tensile Stress at inflection point
σ_{txxxcu}	Transverse tensile ultimate (peak) (end of multiple cracking) stress for composite
σ_{fxxx}	Longitudinal tensile stress for fiber = $E_{fxxx}\epsilon_{fxxx}$
σ_{fxxxu}	Longitudinal Ultimate fiber fracture tensile stress
σ_{mxxx}	Longitudinal tensile stress for matrix = $E_{mxxx}\epsilon_{mxxx}$
σ'_c	Compressive strength for pure concrete
σ'_{cc}	Compressive strength of confined concrete at activation of composite
σ_{lc}	Longitudinal compressive stress for confined concrete
σ_{lcco}	Longitudinal compressive confinement stress for confined concrete
σ_{lcp}	Longitudinal compressive proportional stress for confined concrete
σ_{lccu}	Longitudinal compressive ultimate (peak) stress for confined concrete

σ_{lco}	Longitudinal compressive stress at first crack of concrete concrete core of confined concrete. (Longitudinal tensile stress at tensile strain at end of multiple cracking of composite)
σ_{lcr}	Longitudinal compressive stress at rupture of confined concrete
σ_{lxxx}	Longitudinal tensile stress for composite
σ_{lxxxp}	Longitudinal tensile proportional stress (first crack) for composite = $E_{lxxx}\varepsilon_{lxxxp}$
σ_{lxxxcu}	Longitudinal tensile ultimate (peak) (end of multiple cracking) stress for composite
σ_{lxxxr}	Longitudinal tensile stress at rupture for composite
σ_2	Lateral stress within the concrete core
σ_{2cu}	Lateral stress at peak within the concrete core
s_{xxx}	Pitch of the lateral confinement,
T_l	Longitudinal Toughness equal to area under stress strain curve up to rupture point
TI_l	Longitudinal Toughness index equal to ratio of toughness to toughness of pure concrete
T_t	Transverse toughness equal to area under stress strain curve up to rupture point
TI_t	Transverse Toughness index equal to ratio of toughness-to-toughness of pure concrete
t_{xxx}	Thickness of lateral device
$T(x)$	Bond stress at section
τ_{xxxu}	Ultimate shear stress between fiber and matrix
δ	Tensile crack displacement

δ_{it}	Crack displacement at inflection point
ψ_f	Reduction Factor =0.95.
μ_{lxxx}	Strain efficiency factor during activation region = $\frac{\varepsilon_{tccu}}{\varepsilon_{lxxxcu}} = \frac{\varepsilon_{tc}}{\varepsilon_{lxxx}}$
ζ_{lxxx}	Strain efficiency factor during rupture of the composite = $\frac{\varepsilon_{tcr}}{\varepsilon_{lxxxr}} = \frac{\varepsilon_{tc}}{\varepsilon_{lxxx}}$
α	Experimental factor = 4 for high performance composites and = 2 for low performance composites

IX. REFERENCE

- [1] Malak S., Krstulovic-Opara N., “Modeling Material Response of Fiber Composites used for the Retrofit of Existing Concrete Structures under Blast Loadings “ACI Special Publication Oct. 2018, the Dennis Mertz Symposium on Design and Evaluation of Concrete Bridges, ACI Fall Convention 2018, Las Vegas, Nevada
- [2] PDC-TR 06-08, US Army Corps of Engineers Protective Design Center Technical Report, “Single Degree of Freedom Structural Response Limits for Antiterrorism Design”, 7 January 2008*
- [3] A. Meda, S. Mostosi, Z. Rinaldi, P. Riva, “Corroded RC columns repair and strengthening with high performance fiber reinforced concrete jacket”, *Materials and Structures*, 49, 2016, pp. 1967–1978.
- [4] A. Gholampour, R. Hassanli, J.E. Mills, Th. Vincent, M. Kunieda, “Experimental investigation of the performance of concrete columns strengthened with fiber reinforced concrete jacket”, *Construction and Building Materials*. 194, 2019, pp. 51-61
- [5] N. Ganesan and J.V. Ramana Murthy, ‘Strength and Behavior of Confined Steel Fiber Reinforced Concrete Columns’, *ACI Materials Journal*, V. 87, No. 3, May-June 1990, pp. 221-227
- [6] B. Abdollahi, M. Bakhshi, Z. Mirzaee, M. Shekarchi, M. Motavalli,, “SIFCON Strengthening of Concrete Cylinders in Comparison with Conventional GFRP Confinement Method”, *Construction and Building Materials*, 36(2012), pp.765-778
- [7] Sayyed A. D., Davood M., Hadi B., “Strengthening of RC columns by ultra-high performance fiber reinforced concrete (UHPFRC) jacketing”, *Construction and Building Materials*, 235, (2020), 117485
- [8] ACI 440.R-02, Guide for the Design and Construction of Externally Bonded FRP Systems for Strengthening Concrete Structures. American Concrete Institute, Farmington Hills, Michigan, 2018

- [9] Caudio E. Todechine, Albert C. Bianchini and Klyde E. Kesler, "Behavior of Concrete Columns Reinforced with High Strength Steels" *ACI Journal Proceedings*, Vol. 61, No. 6, June 1964, pp. 701-716
- [10] H. Saadatmanesh, M.R. Ehsani, and M.W. Li "Strength and Ductility of Concrete Columns Externally Reinforced with Fiber Composite Straps" *ACI Structural Journal*, V.91, No.4 July-August 1994
- [11] P. Chen, Y. Wang, and C. Liu "Confinement path-dependent analytical model for FRP-confined concrete and concrete-filled steel tube subjected to axial compression" *Composite Structures*, Elsevier, 201, June 2018, pp.234-247
- [12] J.R. Cromwell, K.A. Harries, B.M. Shahrooz, "Environmental durability of externally bonded FRP materials intended for repair of concrete structures", *Construction and Building Materials*. 25, (5), 2011, pp. 2528–2539.
- [13] Houssam A. Toutanji, "Stress-Strain Characteristics of Concrete Columns Externally Confined with Advanced Fiber Composite Sheets," *ACI Material Journal*, V.96, May-June 1999, pp.397-404
- [14] R. Realfonzo, A. Napoli, "Concrete confined by FRP systems: Confined efficiency and design strength models", *Composites: Part B*, 42, 2011, pp.736-755.
- [15] Mohamed Saafi, Houssam A. Toutanji and Zongjin Li, "Behavior of Concrete Columns Confined with Fiber-Reinforced Polymer Tubes", *ACI Materials journal*, V.96, No.4, July-August 1999.
- [16] Canadian Standards Association (CSA). *Canadian Highway Bridge design code – CAN/CSA-S6-06*. Mississauga, Ontario, Canada: CSA; 2006.
- [17] L.A. Bisby, M.F. Green, V.K.R. Kodur, "Response to fire of concrete structures that incorporate FRP", *Prog. Structure Eng. Mater.* 7 (3) (2005), pp. 136–149.
- [18] M.N.S. Hadi, "Behavior of eccentric loading of FRP confined fiber steel reinforced concrete columns", *Construction Building Materials*, 23, (2), (2009), pp. 1102–1108.
- [19] ACI Committee 318. *Building Code Requirements for Structural Concrete (ACI 318–17): An ACI Standard: Commentary on Building Code Requirements for Structural Concrete (ACI 318R–17)*. American Concrete Institute; 2017.
- [20] A.E. Namaan and J.R. Homrich, "Stress-Strain Properties of SIFCON in Uniaxial Compression and Tension", University of Michigan, Ann Arbor, Michigan 48109, Report submitted to the AIR Force Weapons Laboratory, Air Force Systems Command, Kirkland Air Force Base, NM 87117-6008, August 1988
- [21] Marwan N. Youssef, Maria Q. Feng, and Ayman S. Mousallam, "Stress-Strain Model for Concrete Confined by FRP Composites" *Composites: Part B* 38 (2007) 614-628

- [22] Liang Huang, Xiaoxun Sun, Libo Yan, and Deju Zhu, "Compressive Behavior of Concrete Confined with GFRP Tube and Steel Spirals", *Polymers* 2015, 7, 851-875
- [23] Mander J.B., Priestly M.J.N. and Park R. (1988) Theoretical Stress-Strain Model for Confined Concrete, *Journal of Structural Engineering, ASCE*, Vol. 114(8), 1824-1826
- [24] ASTM C469/C469M-14, "Standard Test Method for Static Modulus of Elasticity and Poisson's Ratio of Concrete in Compression" Apr. 28, 2014
- [25] Fyfe Co. LLC, Fyfe Europe S.A. info@fyfe.com, www.fyfec.com
- [26] B. Han, J. Ou, X. Yu, (2005) "Self-Sensing Concrete in Smart Structures", Elsevier
- [27] Katzer J. Steel fibers and steel fiber reinforced concrete in civil engineering. *Pacific Journal of Science and Technology*, 2006;7(1), pp.53-8.
- [28] Bekaert, Dramix, NV Bekaert SA, Bekaerstraat 2-P2222, BE-8550 Zwevegem, Belgium, www.bekaert.com
- [29] ANBAO Corp., Wire & Wire Products, 33 Qinhuangxi Street, Quihuangdao, P.R. China 066000, www.anbao.net, anbao@anbao.com, anbaowire@gmail.com
- [30] Neven Krstulovic-Opara, Sary Malak "Tensile Behavior of Slurry Infiltrated Mat Concrete (SIMCON)", *ACI Materials Journal*, V. 94, No.1 January-February 1997, pp. 39-46
- [31] Sary.A.J. Malak,(1997) "Tensile and compressive behavior of slurry infiltrated mat concrete (SIMCON)", Northeastern University. Ph.D.Thesis
- [32] Lim T.Y., Paramasivam P., and Lee S.L. "Analytical Model for Tensile Behavior of Steel-Fiber Concrete" *ACI Materials Journal*, V. 84, May-June 1988, pp.286-298
- [33] Nammur, G.G., and Naaman, A.E., "Strain Rate Effects on the Tensile Properties of Fiber Reinforced Concrete," in *Cement Based Composites – Strain Rate Effects on Fracture*, S. Mindess, Editor, Materials Research Society, Pittsburgh, PA, 198
- [34] P.Soroushian, C. Lee, "Tensile Strength of Steel Fiber Reinforced Concrete: Correlation with Some Measures of Fiber Spacing", *ACI Materials Journal*, V.87, No.6, 1990, pp.541-546
- [35] Li, V.C. "On Engineered Cementitious Composites (ECC)- A review of the Material and its Application". *J Advanced Concrete Technology*, Vol. I, No.3, 2003, pp.215-230
- [36] Naaman A.E., Homrich J.R. "Tensile Stress-Strain Properties of SIFCON" *ACI Materials Journal*, V. 86, No.3, May-June 1989.

X. APPENDIX I: EXPERIMENTAL RESULTS: GRAPHICAL AND TABULAR RESULTS

1. LPBF TESTED SAMPLES – TABULATED/GRAPHICAL EXPERIMENTAL RESULTS:

Table X-1: Pre peak experimental data for longitudinal stress and strain of LPBF confined concrete specimens (0.15Ksi=1 MPa)

		E'_{lcco}		σ_{lcp}		ϵ_{lcp}		E'_{lc2}		E'_{lc2}		σ_{lcco}		ϵ_{lcco}	
		Mpa(Ksi)	Mpa(Ksi)	Mpa(Ksi)	Mpa(Ksi)		MPa(Ksi)	Mpa (Ksi)	MPa(Ksi)	Mpa (Ksi)	MPa(Ksi)				
LPBF	CON-SP1	2667 (387)	16(2.3)	0.006	0	0	34.4 (5)	0.0012							
	CON-SP2*	27692 (4016)	36 (5.2)	0.0013	0	0	42 (6.1)	0.003							
	CON-SP3	30000 (4351)	18(2.6)	0.0006	0	0	40 (5.8)	0.0024							
	CON-SP4	13334 (1934)	20(2.9)	0.0015	0	0	41.6 (6)	0.004							
	CON-SP5	19000 (2756)	19(2.7)	0.001	0	0	42.4 (6.2)	0.0035							
	CON-SP6	22000 (3191)	22(3.2)	0.001	0	0	38.3 (5.5)	0.003							
	CON-SP7	13000 (1885)	13(1.9)	0.001	0	0	29.3 (4.2)	0.001							
	FRM-SP1*	22857 (3428)	32 (4.5)	0.0014	-2250 (-326)	NA	30 (4.4)	0.004							
	FRM-SP2	19000 (2756)	19(2.7)	0.001	-3800 (-551)	NA	21 (3)	0.005							
	FRM-SP3	17000 (2466)	17(2.5)	0.001	-9000 (-1305)	NA	23 (3.3)	0.002							
	FRM-SP4	15000 (2176)	15(2.2)	0.001	-1200 (-174)	NA	27 (3.9)	0.01							
	FRM-SP5	10000 (1450)	12(1.7)	0.0012	-5667 (-822)	NA	23 (3.3)	0.003							
	FRM-SP6	8000 (1160)	16(2.3)	0.002	-750 (-109)	NA	25 (3.6)	0.02							
	SP3-SP1	12500 (1813)	25(3.6)	0.002	0	0	37 (5.4)	0.003							
	SP3-SP2*	25000 (3626)	35 (5.1)	0.0014	0	0	42.3 (6.13)	0.004							
	SP3-SP3	20000 (2901)	20(2.9)	0.001	0	0	33 (4.8)	0.002							
	SP3-SP4	12940 (1877)	22(3.2)	0.0017	0	0	34 (4.9)	0.0044							
	SP3-SP5	20000 (2901)	20(2.9)	0.001	0	0	35 (5.1)	0.002							
	SP3-SP6	13333 (1934)	20(2.9)	0.0015	0	0	35 (5.1)	0.002							

Table X-2: Post peak experimental data for longitudinal stress and strain of LPBF confined concrete specimens (0.15 Ksi=1 MPa)

		$(\sigma_{lxxxp}, \sigma_{lxxxcu})$	ε_{lccu}	σ_{lco}	ε_{lco}	σ_{lcr}	ε_{lcr}	T_l	TI_l
		MPa(Ksi)	$(\varepsilon_{lxxxp}, \varepsilon_{lxxxcu})$	MPa(Ksi)	(ε_{lxxxr})	MPa(Ksi)		Mpa (Ksi)	
LPBF	CON-SP1	34.4 (5)	0.0125	-	-	27 (3.9)	0.015	0.29 (0.042)	1
	CON-SP2*	42 (6.1)	0.0025	-	-	35 (5.1)	0.005	0.135 (0.019)	1
	CON-SP3	40 (5.8)	0.0024	-	-	12 (1.7)	0.005	0.098 (0.014)	1
	CON-SP4	41.6 (6)	0.004	-	-	34 (4.9)	0.005	0.14 (0.02)	1
	CON-SP5	42.4 (6.2)	0.0035	-	-	41 (5.9)	0.005	0.16 (0.023)	1
	CON-SP6	38.3 (5.5)	0.003	-	-	27 (3.9)	0.005	0.13 (0.019)	1
	CON-SP7	29.3 (4.2)	0.001	-	-	25 (3.6)	0.005	0.15 (0.022)	1
	FRM-SP1*	33 (4.8)	0.004	32 (4.6)	0.0051	31 (4.5)	0.0057	0.14 (0.02)	1.1
	FRM-SP2	23 (3.3)	0.005	23 (3.3)	0.007	21 (3)	0.008	0.32 (0.05)	2.4
	FRM-SP3	24 (3.5)	0.002	19 (2.7)	0.006	18 (2.6)	0.007	0.21 (0.03)	1.6
	FRM-SP4	30 (4.3)	0.01	29 (4.2)	0.013	28 (4.1)	0.015	0.385 (0.06)	2.9
	FRM-SP5	25 (3.6)	0.003	24 (3.5)	0.0041	21 (3.1)	0.005	0.186 (0.03)	1.4
	FRM-SP6	27 (3.9)	0.02	25 (3.6)	0.038	24 (3.5)	0.064	1.57 (0.23)	11.6
	SP3-SP1	37 (5.4)	0.003	-	-	34 (4.9)	0.007	0.19 (0.03)	1.4
	SP3-SP2*	42.3 (6.13)	0.004	-	-	35 (5.1)	0.008	0.17 (0.025)	1.3
	SP3-SP3	33 (4.8)	0.002	-	-	23 (3.3)	0.008	0.21 (0.03)	1.6
	SP3-SP4	34 (4.9)	0.0044	-	-	28 (4.1)	0.01	0.25 (0.04)	1.9
	SP3-SP5	35 (5.1)	0.002	-	-	20 (2.9)	0.007	0.17 (0.02)	1.3
	SP3-SP6	35 (5.1)	0.002	-	-	20 (2.9)	0.004	0.105 (0.015)	0.8

Table X-3: Pre-peak experimental data for longitudinal and transverse strains of LPBF confined concrete specimens (symbols in parenthesis represent the composite parameters)(0.15 Ksi=1 MPa)

		ϵ_{lcp}	ϵ_{tcp}	ϵ_{lcco}	ϵ_{tcco}	ϵ_{lccu}	ϵ_{tccu}
						(ϵ_{lxxxp} , ϵ_{lxxxcu})	(ϵ_{txxxp} , ϵ_{txxxcu})
LPBF	CON-SP1	0.006	0	0.0012	0	0.0125	0
	CON-SP2*	0.0013	0.00039	0.003	0.00075	0.0025	0.00075
	CON-SP3	0.0006	0	0.0024	0.0001	0.0024	0.0001
	CON-SP4	0.0015	0	0.004	0	0.004	0
	CON-SP5	0.001	0	0.0035	0	0.0035	0
	CON-SP6	0.001	0	0.003	0.00038	0.003	0.00038
	CON-SP7	0.001	0	0.001	0	0.001	0
	FRM-SP1*	0.0014	0	0.004	0.00032	0.004	0.00032
	FRM-SP2	0.001	0	0.005	0.003	0.005	0.003
	FRM-SP3	0.001	0	0.002	0.00022	0.002	0.00022
	FRM-SP4	0.001	0	0.01	0.0056	0.01	0.0056
	FRM-SP5	0.0012	0	0.003	0.0009	0.003	0.0009
	FRM-SP6	0.002	0	0.02	0.00028	0.02	0.00028
	SP3-SP1	0.002	0	0.003	0.0001	0.003	0.0001
	SP3-SP2*	0.0014	0.000067	0.004	0.00023	0.004	0.00067
	SP3-SP3	0.001	0.0001	0.002	0.0023	0.002	0.0023
	SP3-SP4	0.0017	0	0.0044	0.0001	0.0044	0.0001
	SP3-SP5	0.001	0.000063	0.002	0.000057	0.002	0.000057
	SP3-SP6	0.0015	0	0.002	0.00075	0.002	0.00075

Table X-4: Post-peak experimental data for longitudinal and transverse strains of LPBF confined concrete specimens (symbols in parenthesis represent the composite parameters)(0.15Ksi=1 MPa)

		ϵ_{lco} (ϵ_{lxxxr})	ϵ_{tco} (ϵ_{txxxr})	ϵ_{lcr}	ϵ_{tcr}	ν	T_t Mpa(Ksi)	TI_t
LPBF	CON-SP1	-	-	0.015	0.004	0.68	0.12 (0.017)	1
	CON-SP2*	-	-	0.005	0.0015	0.3	0.051 (0.00765)	1
	CON-SP3	-	-	0.005	0.012	2.04	0.27 (0.04)	1
	CON-SP4	-	-	0.005	0.0011	0.95	0.042 (0.0061)	1
	CON-SP5	-	-	0.005	0.0008	0.59	0.033 (0.005)	1
	CON-SP6	-	-	0.005	0.004	1.45	0.13 (0.02)	1
	CON-SP7	-	-	0.005	0.0025	0.88	0.07 (0.01)	1
	FRM-SP1*	0.0051	0.0013	0.0057	0.002	-	0.058 (0.0086)	1.14
	FRM-SP2	0.007	0.0058	0.008	0.007	-	0.16 (0.023)	3
	FRM-SP3	0.006	0.008	0.007	0.0087	-	0.18 (0.026)	3.6
	FRM-SP4	0.013	0.0075	0.015	0.0097	-	0.22 (0.03)	4.4
	FRM-SP5	0.0041	0.008	0.005	0.0127	-	0.32 (0.05)	6.35
	FRM-SP6	0.038	0.0062	0.064	0.011	-	0.27 (0.04)	5.5
	SP3-SP1	-	-	0.007	0.0009	0.12	0.05 (0.007)	0.98
	SP3-SP2*	-	-	0.008	0.001	0.1	0.039 (0.0058)	0.76
	SP3-SP3	-	-	0.008	0.002	0.2	0.065 (0.009)	1.27
	SP3-SP4	-	-	0.01	0.0024	0.23	0.072 (0.01)	1.4
	SP3-SP5	-	-	0.007	0.005	0.7	0.1 (0.014)	3
SP3-SP6	-	-	0.004	0.0003	0.08	0.02 (0.003)	0.39	

CONC GRAPHICAL PRESENTATION-ALL SPECIMENS

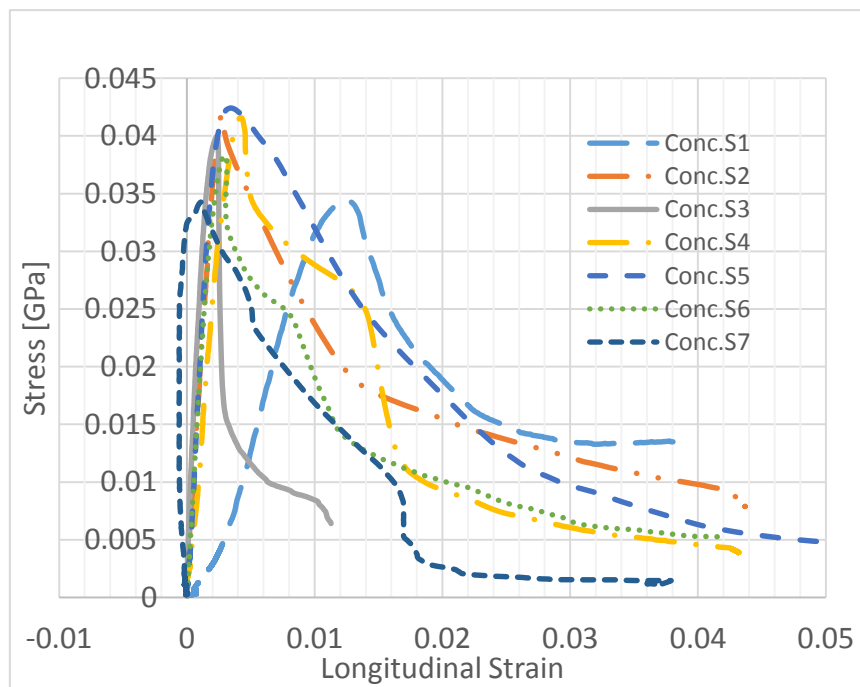


Figure X-1: Stress versus longitudinal strain -7CONC

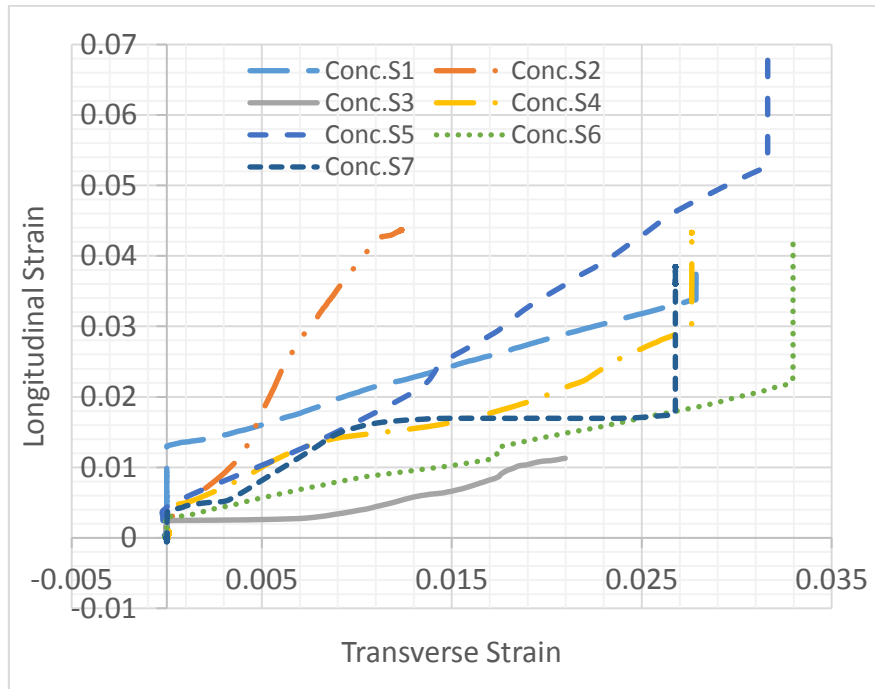


Figure X-2: Longitudinal versus transverse strain -7CONC

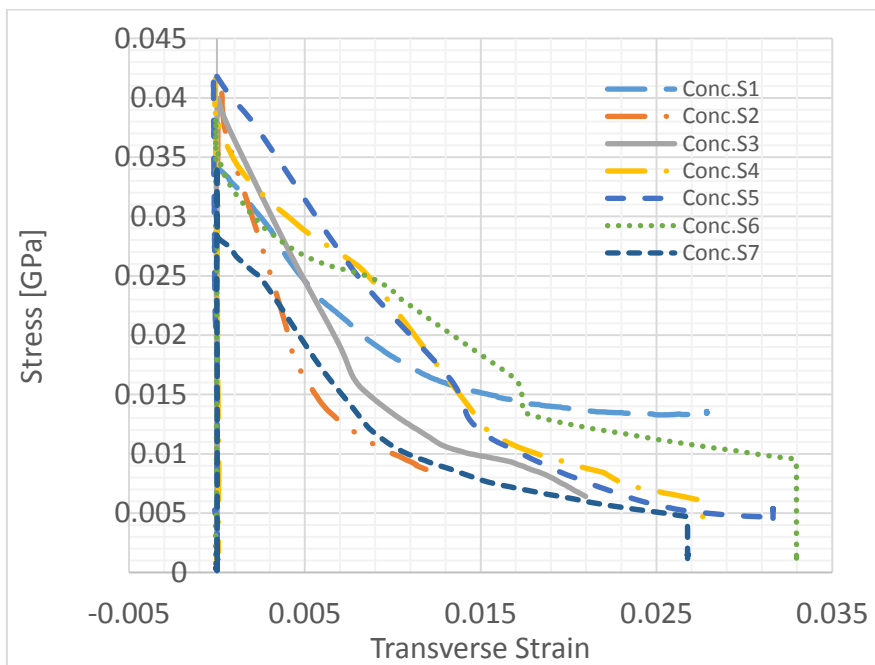


Figure X-3: stress versus transverse strain -7CONC

FRM GRAPHICAL PRESENTATION-ALL SPECIMENS

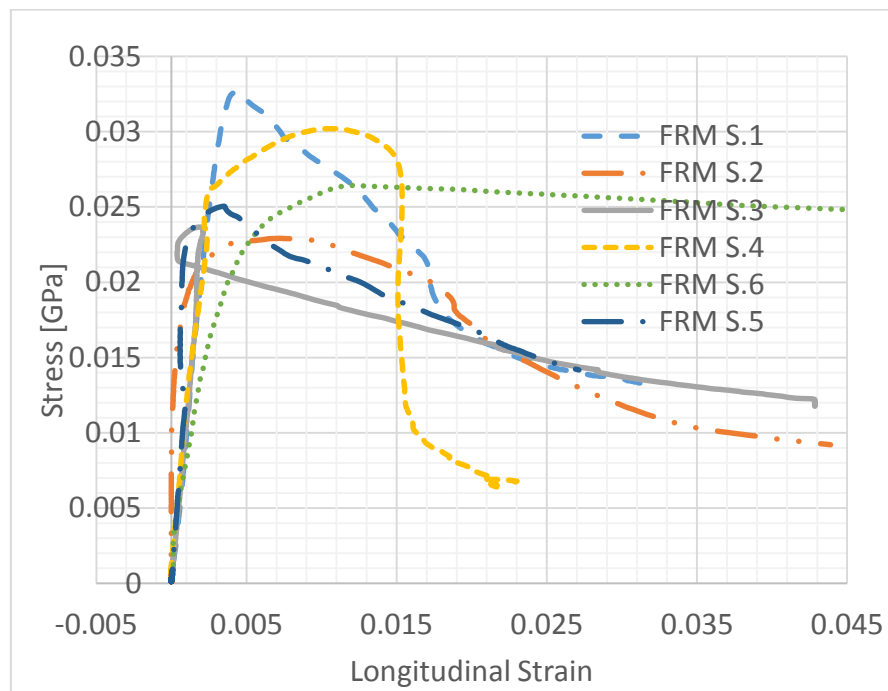


Figure X-4: Stress versus longitudinal strain -6FRM

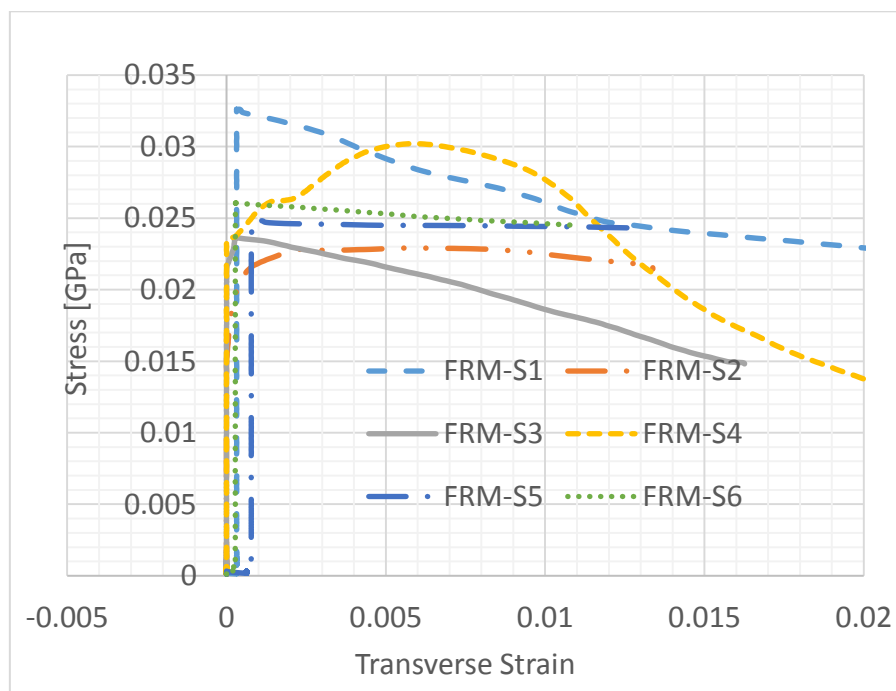


Figure X-5: Stress versus Transverse strain -6FRM

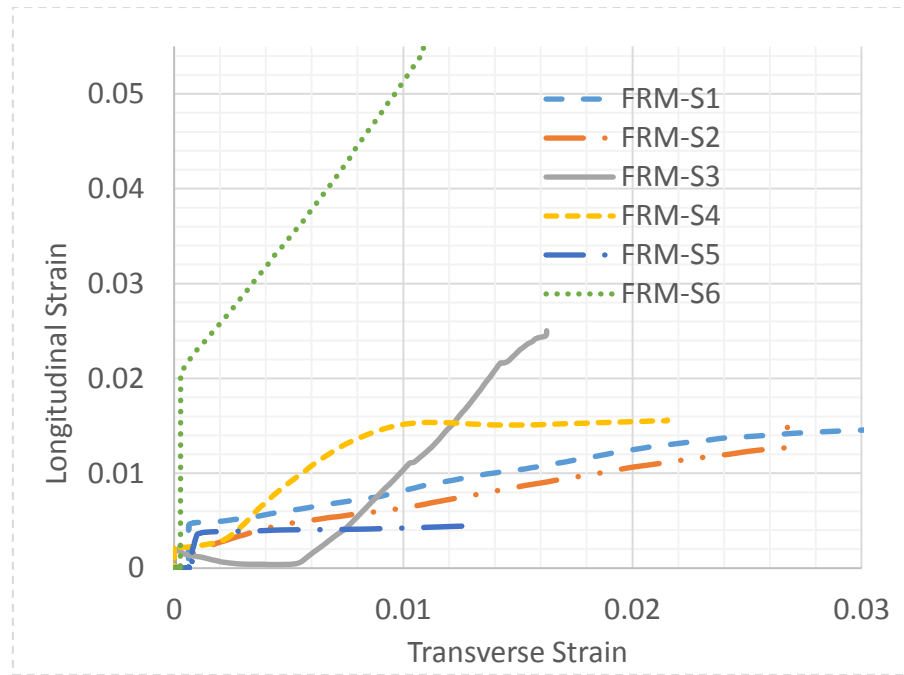


Figure X-6: Longitudinal versus Transverse strain -6FRM

SP3 GRAPHICAL PRESENTATION-ALL SPECIMENS

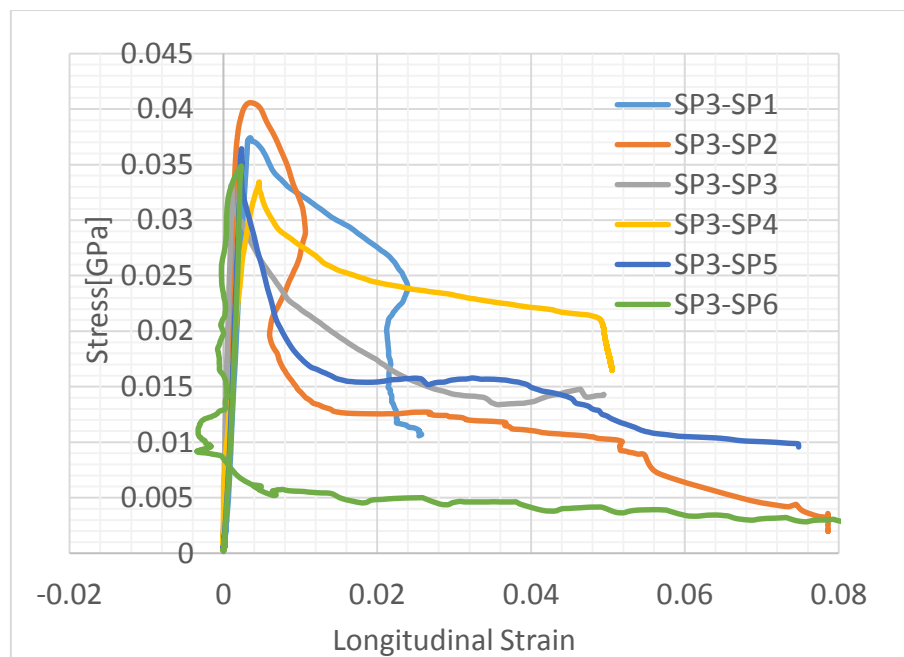


Figure X-7: Stress versus longitudinal strain - 6SP3

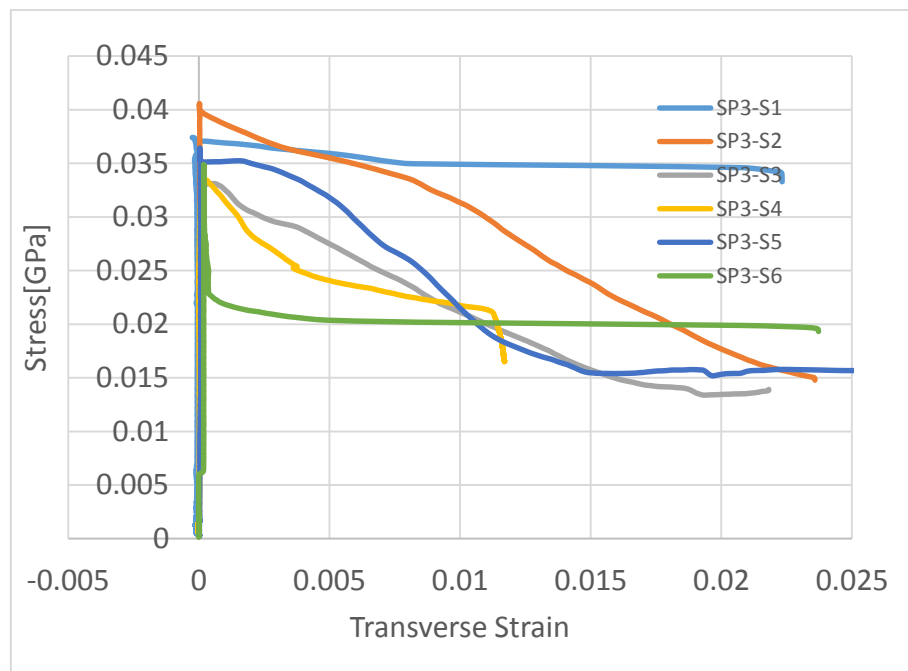


Figure X-8: Stress versus transverse strain - 6SP3

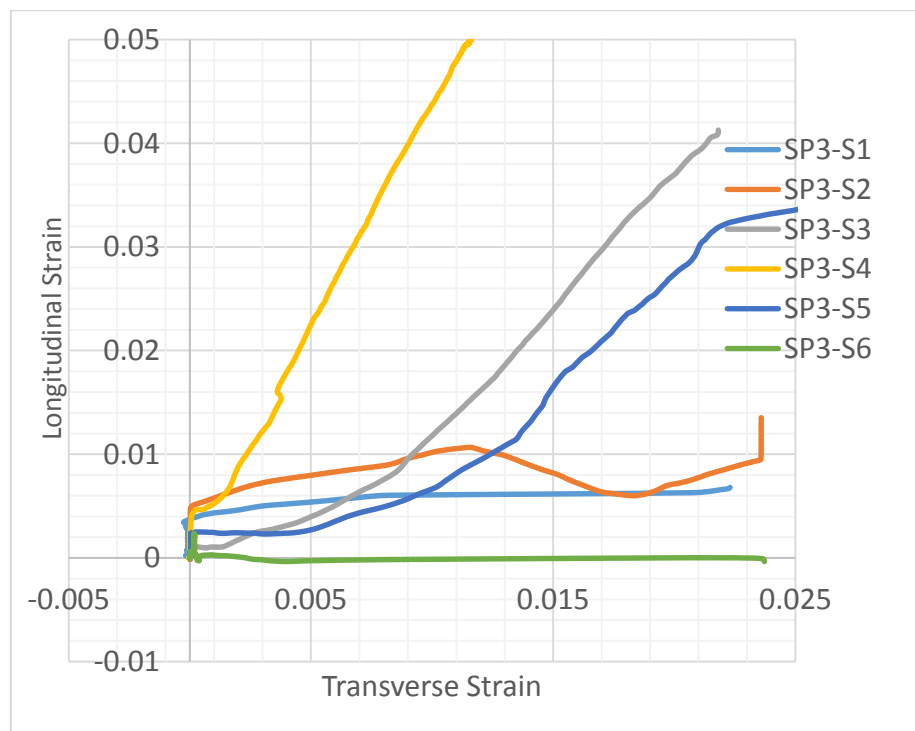


Figure X-9: Longitudinal versus transverse strain - 6SP3

2. LPDF TESTED SAMPLES – TABULATED/GRAPHICAL EXPERIMENTAL RESULTS

Table X-5: Pre peak experimental data for longitudinal stress and strain of LPDF confined concrete specimens (0.15Ksi=1 MPa)

		E_{lcco}	σ_{lcp}	ε_{lcp}	E_{lc2}	E'_{lc2}	σ_{lcco}	ε_{lcco}
		Mpa(Ksi)	Mpa(Ksi)		MPa(Ksi)	Mpa (Ksi)	MPa(Ksi)	
LPDF	FRC-SP1	16000 (2321)	16 (2.3)	0.001	-2778 (-403)	-25000 (-3626)	30 (4.35)	0.0032
	FRC-SP2	23334 (3385)	14 (2.03)	0.0006	-4667 (-677)	-22000 (3191)	25 (3.6)	0.0026
	FRC-SP3	25000 (3626)	15 (2.2)	0.0006	-3913 (-568)	-6000 (-870)	24 (3.5)	0.0008
	FRC-SP4*	23000 (3336)	23 (3.3)	0.001	-5333 (-773.48)	-16000 (-2321)	24 (3.5)	0.002
	FRC-SP5	24286 (3522)	17 (2.5)	0.0007	-4227 (-613)	-45000 (-6527)	32 (4.6)	0.002
	FRC-SP6	27273 (3956)	15 (2.2)	0.00055	-5652 (-820)	-43333 (-6285)	28.5 (4.2)	0.002
	FRC-SP7	18750 (2720)	15 (2.2)	0.0008	-7778 (-1128)	-14000 (-2030)	25 (3.6)	0.0008
	WIM-SP1	25000 (3626)	25 (3.6)	0.001	-1750 (-254)	-1750 (-254)	33 (4.8)	0.003
	WIM-SP2	35000 (5076)	35 (5.1)	0.001	200 (29)	200 (29)	39 (5.7)	0.0018
	WIM-SP3	10000 (1450)	20 (2.9)	0.002	-400 (-58)	-400 (-58)	37 (5.4)	0.008
	WIM-SP4*	26000 (3771)	26 (3.8)	0.001	488 (71)	488 (71)	42.42 (6.15)	0.002
	WIM-SP5	15000 (2176)	30 (4.4)	0.002	286 (41.5)	286 (41.5)	39 (5.7)	0.003
	SP2-SP1	10500 (1523)	21 (3)	0.002	-125 (-18)	-125 (-18)	35 (5.1)	0.002
	SP2-SP2*	24667 (3578)	37 (5.4)	0.0015	698 (101)	698 (101)	43 (6.2)	0.003
	SP2-SP3	15500 (2249)	31 (4.5)	0.002	214 (31)	214 (31)	44 (6.4)	0.012
	SP2-SP4	17000 (2466)	34 (4.9)	0.002	-869 (-126)	-869 (-126)	37 (5.4)	0.003
	SP2-SP5	37500 (5439)	30 (4.3)	0.0008	1500 (217)	1500 (217)	40 (5.8)	0.001
	SP2-SP6	20000 (2901)	20 (2.9)	0.001	-1000 (-145)	-1000 (-145)	34 (4.9)	0.006

Table X-6: Post peak experimental data for longitudinal stress and strain of LPBF confined concrete specimens (0.15 Ksi=1MPa)

		σ_{lccu} (σ_{lxxxp} , σ_{lxxxcu}) MPa(Ksi)	ϵ_{lccu} (ϵ_{lxxxp} , ϵ_{lxxxcu})	σ_{lco} (σ_{lxxxr}) MPa(Ksi)	ϵ_{lco} (ϵ_{lxxxr})	σ_{lcr} MPa(Ksi)	ϵ_{lcr}	T_l Mpa (Ksi)	TI_l
LPDF	FRC-SP1	32 (4.64)	0.0036	21 (3.1)	0.007	13 (1.9)	0.015	0.28 (0.041)	2.07
	FRC-SP2	26.6 (3.86)	0.0033	23 (3.3)	0.0034	8 (1.2)	0.005	0.09 (0.013)	0.67
	FRC-SP3	33 (4.8)	0.0023	22 (3.2)	0.007	13 (1.9)	0.013	0.29 (0.042)	2.14
	FRC-SP4*	26 (3.8)	0.003	25 (3.6)	0.007	16.5 (2.4)	0.016	0.22 (0.03)	1.6
	FRC-SP5	33 (4.8)	0.0022	26 (3.8)	0.0025	20 (3)	0.0032	0.07 (0.01)	0.51
	FRC-SP6	29 (4.2)	0.0023	22 (3.2)	0.007	15 (2.2)	0.008	0.18 (0.026)	1.34
	FRC-SP7	28 (4.1)	0.0018	21 (3.1)	0.007	15 (2.2)	0.015	0.32 (0.046)	2.37
	WIM-SP1	35 (5.1)	0.004	-	-	23 (3.3)	0.01	0.28 (0.041)	2.1
	WIM-SP2	42.5 (6.2)	0.0025	-	-	24 (3.5)	0.012	0.36 (0.05)	2.67
	WIM-SP3	38 (5.5)	0.01	-	-	25 (3.6)	0.022	0.88 (0.13)	6.52
	WIM-SP4*	44 (6.4)	0.0041	-	-	30 (5.2)	0.011	0.26 (0.04)	2
	WIM-SP5	43 (6.24)	0.0035	-	-	20 (3)	0.008	0.22 (0.032)	1.63
	SP2-SP1	39 (5.7)	0.024	-	-	30 (5.2)	0.03	0.76 (0.11)	5.6
	SP2-SP2*	45 (6.5)	0.0043	-	-	20 (2.9)	0.02	0.59 (0.09)	4.4
	SP2-SP3	45 (6.5)	0.014	-	-	31(4.5)	0.03	1.1 (0.16)	8.15
	SP2-SP4	38 (5.5)	0.0046	-	-	29 (4.2)	0.006	0.17 (0.025)	1.26
SP2-SP5	45 (6.5)	0.002	-	-	27 (3.9)	0.012	0.44 (0.064)	3.26	
SP2-SP6	35 (5.1)	0.007	-	-	30 (5.2)	0.015	0.45 (0.065)	3.33	

Table X-7: Pre-peak experimental data for longitudinal and transverse strains of LPDF confined concrete specimens (symbols in parenthesis represent the composite parameters)(0.15 Ksi=1MPa)

		ϵ_{lcp}	ϵ_{tcp}	ϵ_{lcco}	ϵ_{tcco}	ϵ_{tccu}	
						$(\epsilon_{lxxxp}, \epsilon_{lxxxcu})$	$(\epsilon_{txxxp}, \epsilon_{txxxcu})$
LPDF	FRC-SP1	0.001	0	0.0032	0	0.0036	0.005
	FRC-SP2	0.0006	0	0.0026	0	0.0033	0.017
	FRC-SP3	0.0006	0	0.0008	0	0.0023	0.022
	FRC-SP4*	0.001	0	0.002	0	0.003	0.00045
	FRC-SP5	0.0007	0	0.002	0.0005	0.0022	0.0027
	FRC-SP6	0.00055	0	0.002	0.00004	0.0023	0.0013
	FRC-SP7	0.0008	0	0.0008	0	0.0018	0.0068
	WIM-SP1	0.001	0.00001	0.003	0.00084	0.004	0.0035
	WIM-SP2	0.001	0	0.0018	0.0003	0.0025	0.0032
	WIM-SP3	0.002	0	0.008	0.00048	0.01	0.0026
	WIM-SP4*	0.001	0	0.002	0	0.0041	0.0075
	WIM-SP5	0.002	0.00003	0.003	0.00003	0.0035	0.011
	SP2-SP1	0.002	0.00068	0.002	0.00068	0.024	0.00103
	SP2-SP2*	0.0015	0	0.003	0	0.0043	0.0006
	SP2-SP3	0.002	0.0002	0.012	0.0002	0.014	0.0006
	SP2-SP4	0.002	0.00046	0.003	0.0011	0.0046	0.002
	SP2-SP5	0.0008	0.0004	0.001	0.0005	0.002	0.011
	SP2-SP6	0.001	0.00039	0.006	0.00042	0.007	0.0028

Table X-8: Post-peak experimental data for longitudinal and transverse strains of LPDF confined concrete specimens(symbols in parenthesis represent the composite parameters)(0.15 Ksi=1 MPa)

		ϵ_{lco}	ϵ_{tco}	ϵ_{lcr}	ϵ_{tcr}	ν	T_t	TI_t
		(ϵ_{lxxxr})	(ϵ_{txxxr})				Mpa(Ksi)	
LPDF	FRC-SP1	0.007	0.022	0.015	0.026	-	0.7 (0.1)	13.9
	FRC-SP2	0.0034	0.0175	0.005	0.024	-	0.55 (0.08)	10.8
	FRC-SP3	0.007	0.027	0.013	0.027	-	0.6 (0.09)	11.8
	FRC-SP4*	0.007	0.004	0.016	0.012	-	0.33 (0.0368)	6.47
	FRC-SP5	0.0025	0.011	0.0032	0.017	-	0.54 (0.078)	10.7
	FRC-SP6	0.007	0.01	0.008	0.0135	-	0.36 (0.05)	7.05
	FRC-SP7	0.007	0.01	0.015	0.017	-	0.4 (0.058)	7.8
	WIM-SP1	-	-	0.01	0.0074	-	0.26 (0.038)	5.1
	WIM-SP2	-	-	0.012	0.022	-	0.88 (0.13)	17.2
	WIM-SP3	-	-	0.022	0.018	-	0.61 (0.09)	11.9
	WIM-SP4*	-	-	0.011	0.016	-	0.59 (0.089)	11.56
	WIM-SP5	-	-	0.008	0.026	-	0.95 (0.14)	18.6
	SP2-SP1	-	-	0.03	0.008	-	0.26 (0.04)	5.1
	SP2-SP2*	-	-	0.02	0.011	-	0.335 (0.05)	6.62
	SP2-SP3	-	-	0.03	0.0051	-	0.19 (0.027)	4
	SP2-SP4	-	-	0.006	0.018	-	0.56 (0.08)	11.2
	SP2-SP5	-	-	0.012	0.029	-	1.3 (0.19)	25.5
	SP2-SP6	-	-	0.015	0.025	-	0.81 (0.12)	15.9

FRC GRAPHICAL PRESENTATION-ALL SPECIMENS

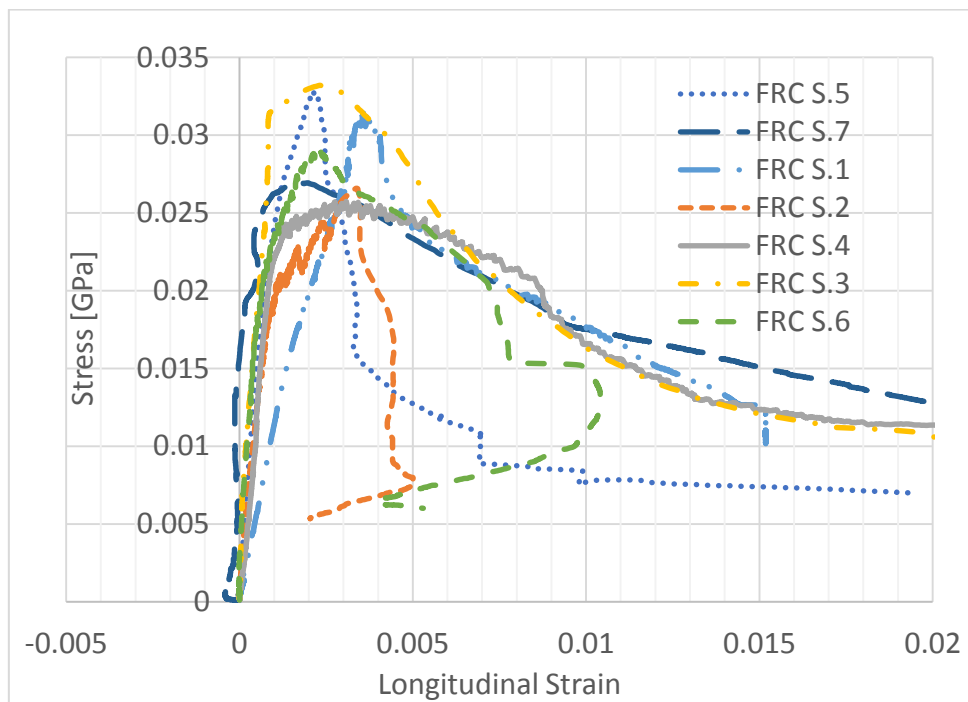


Figure X-10: Stress versus longitudinal strain – 7FRC

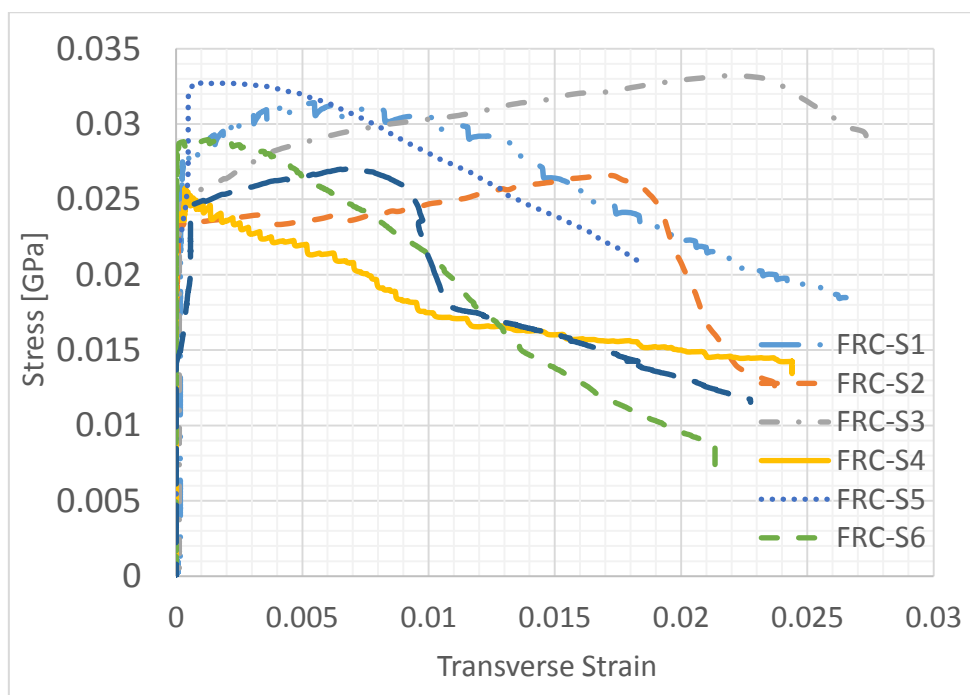


Figure X-11: Stress versus Transverse strain – 7FRC

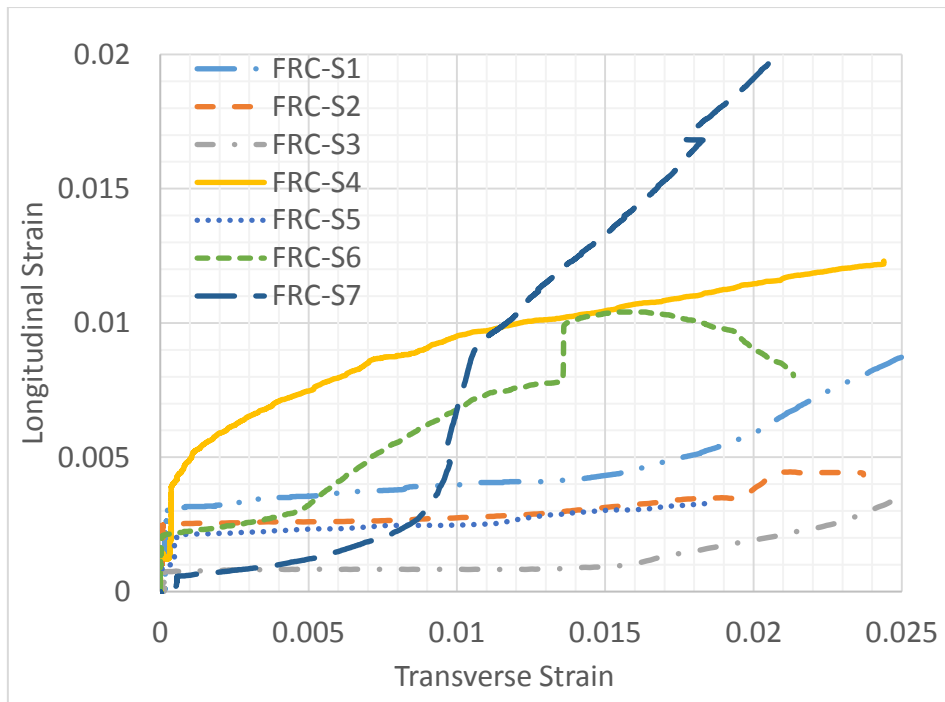


Figure X-12: Longitudinal versus Transverse strain – 7FRC

WIM GRAPHICAL PRESENTATION-ALL SPECIMENS

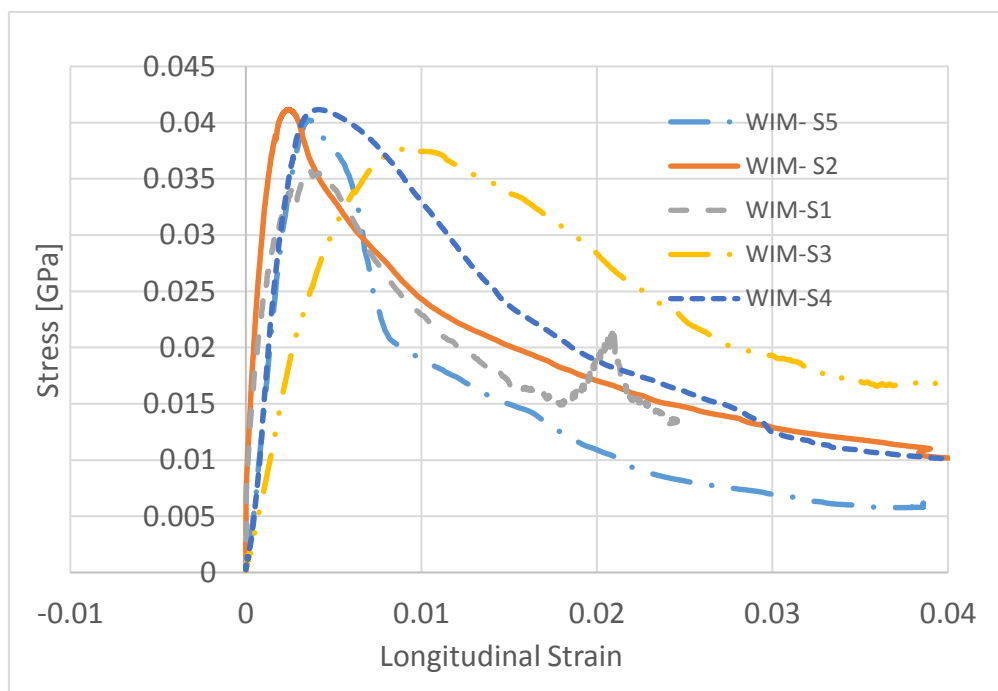


Figure X-13: Stress versus Longitudinal strain – 5MESH

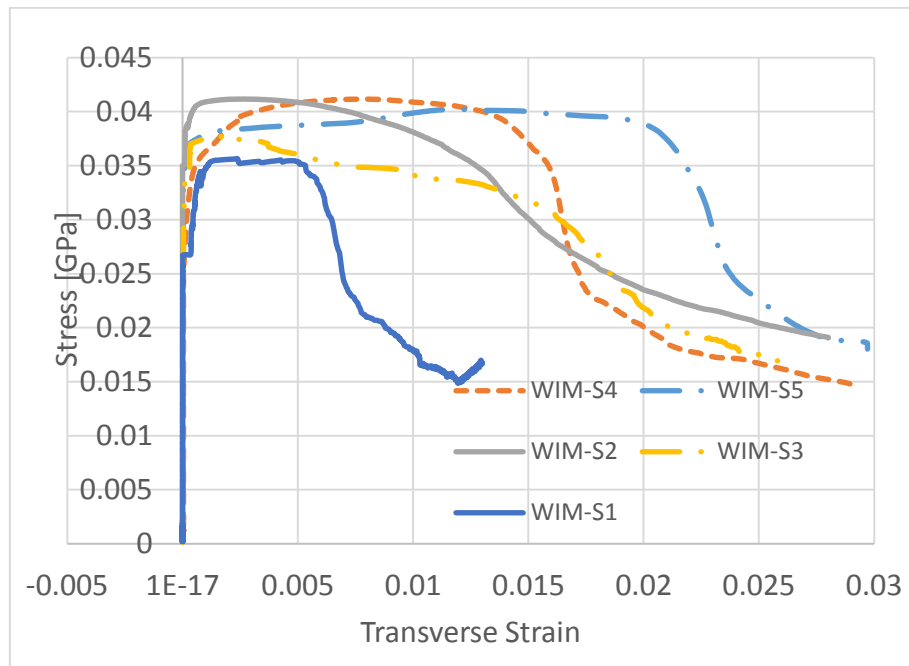


Figure X-14: Stress versus Transverse strain – 5MESH

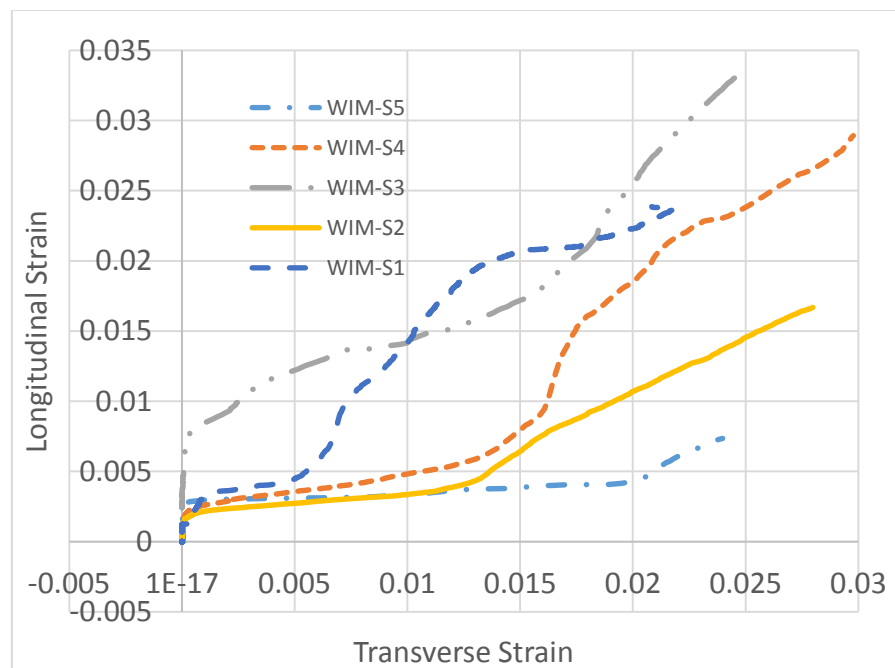


Figure X-15: Longitudinal versus Transverse strain – 5MESH

SP2 GRAPHICAL PRESENTATION-ALL SPECIMENS

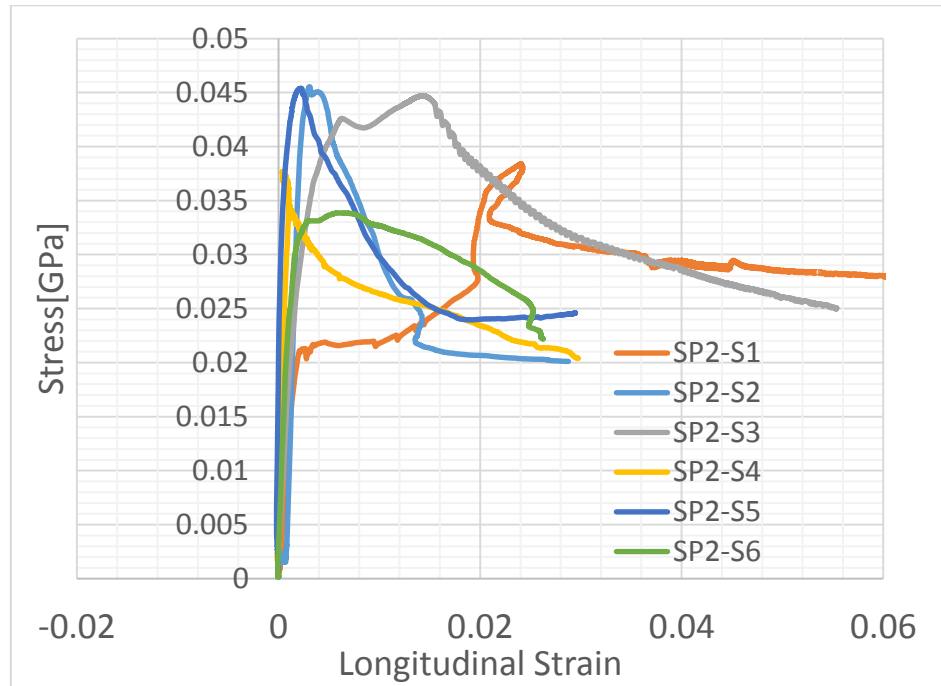


Figure X-16: Stress versus Longitudinal strain – 6SP2

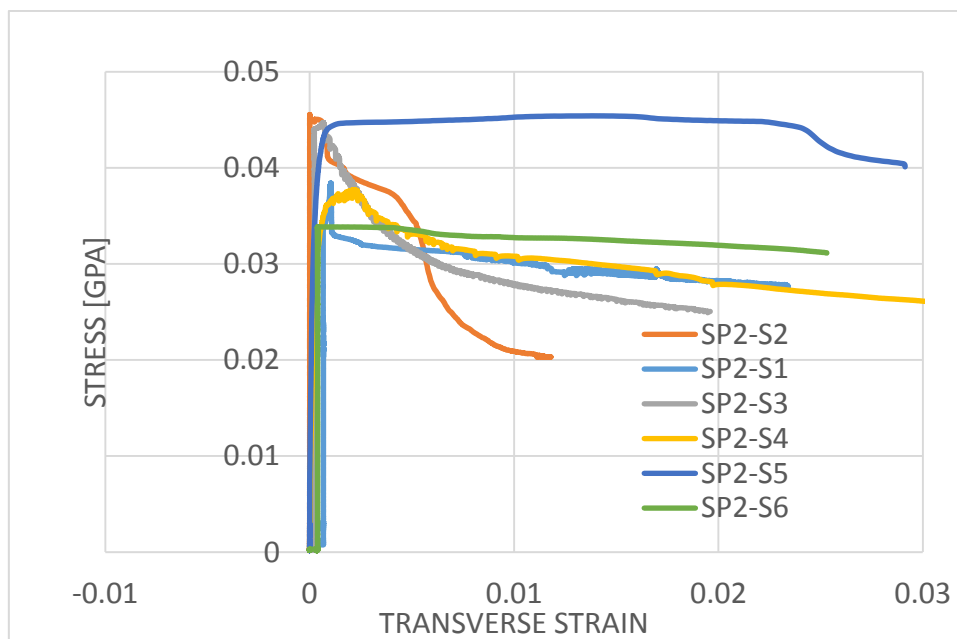


Figure X-17: Stress versus Transverse strain – 6SP2

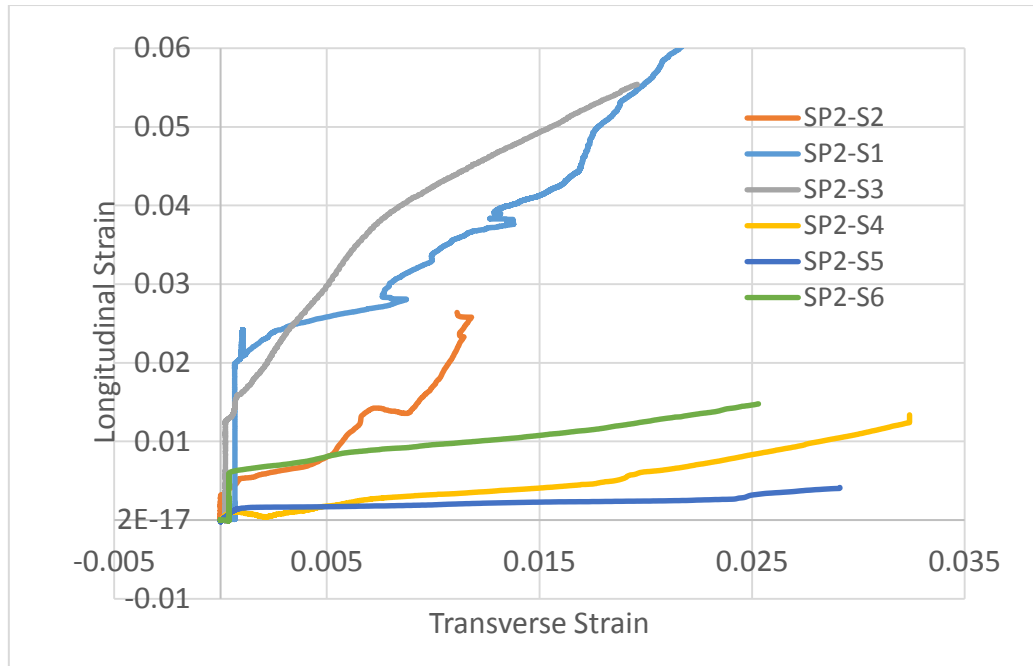


Figure X-18: Longitudinal versus Transverse strain – 6SP2

3. HPBF TESTED SAMPLES – TABULATED/GRAPHICAL EXPERIMENTAL RESULTS

Table X-9: Pre peak experimental data for longitudinal stress and strain of HPBF confined concrete specimens (0.15 Ksi=1 MPa)

		E_{lcco}	σ_{lcp}		ϵ_{lcp}	E_{lc2}	E'_{lc2}	σ_{lcco}	ϵ_{lcco}
			Mpa (Ksi)	Mpa (Ksi)					
HPBF	FPC(SCH 41-1)-S1*	28572 (4144)	40 (5.8)	0.0014	2800 (406)	3500 (508)	46 (6.7)	0.002	
	FPC(SCH 41-1)-S2	22500 (3263)	36 (5.2)	0.0016	1429 (207)	2222 (322)	46 (6.7)	0.005	
	FPC (SCH 41-2)-S1	32000 (4641)	32 (4.6)	0.001	3333 (484)	4651 (675)	58 (8.4)	0.0034	
	FPC (SCH 41-2)-S2*	27693 (4016)	36 (5.2)	0.0013	2000 (290)	2333 (338)	48 (7)	0.003	
	FPC (11UP-2)-S1	22000 (3191)	44 (6.4)	0.002	947 (137)	1162 (168)	56 (8)	0.007	
	FPC (11UP-2)-S2*	26471 (3839)	45 (6.5)	0.0017	1440 (209)	2000 (290)	56 (8)	0.007	
	FPG (SEH-1)-S1*	24667 (3839)	37 (5.4)	0.0015	136 (20)	187 (27)	42 (6.1)	0.006	
	FPG (SEH-1)-S2	5000 (725)	35 (5.1)	0.007	167 (24)	250 (36)	42 (6.1)	0.01	
	FPG (SEH-1)-S3	15600 (2263)	28 (4.1)	0.0018	412 (60)	467 (68)	30 (4.4)	0.002	
	FPG (SEH-2)-S1*	24667 (3839)	37 (5.4)	0.0015	1652 (240)	2000 (290)	48 (7)	0.004	
	FPG (SEH-2)-S2	20000 (2901)	40 (5.8)	0.002	1000 (145)	1186 (172)	50 (7.25)	0.005	

Table X-10: Post peak experimental data for longitudinal stress and strain of HPBF confined concrete specimens (0.15 Ksi=1 MPa)

		σ_{lccu} (σ_{lxxxp} , σ_{lxxxcu}) MPa (Ksi)	ε_{lccu} (ε_{lxxxp} , ε_{lxxxcu})	σ_{lco} (σ_{lxxxr}) MPa(Ksi)	ε_{lco} (ε_{lxxxr})	σ_{lcr} MPa(Ksi)	ε_{lcr}	T_l MPa(Ksi)	TI_l
HPBF	FPC(SCH41-1)-S1*	70 (10)	0.01	-	-	70 (10)	0.01	0.53(0.08)	4
	FPC(SCH41-1)-S2	62 (9)	0.014	-	-	62 (9)	0.014	0.61(0.09)	4.5
	FPC(SCH41-2)-S1	82 (12)	0.012			82 (12)	0.012	0.73(0.1)	5.4
	FPC(SCH41-2)-S2*	84 (12)	0.021	-	-	84 (12)	0.021	1.35(0.19)	10
	FPC (11UP-2)-S1	78 (11.3)	0.038	-	-	78 (11.3)	0.038	2.4(0.35)	18
	FPC (11UP-2)-S2*	78 (11)	0.025	-	-	78 (11)	0.025	1.7(0.25)	12.6
	FPG (SEH-1)-S1*	45 (6.5)	0.022	-	-	45 (6.5)	0.022	0.4(0.058)	3
	FPG (SEH-1)-S2	47 (6.8)	0.03	-	-	47 (6.8)	0.03	1.15(0.17)	8.5
	FPG (SEH-1)-S3	49 (7.1)	0.017	-	-	49 (7.1)	0.017	0.64(0.09)	4.7
	FPG (SEH-2)-S1*	80 (11.6)	0.023	-	-	80 (11.6)	0.023	1.35(0.19)	10
	FPG (SEH-2)-S2	74 (10.7)	0.032	-	-	74 (10.7)	0.032	1.8(0.26)	13

Table X-11: Pre-peak experimental data for longitudinal and transverse strains of HPBF confined concrete specimens(symbols in parenthesis represent the composite parameters)(0.15 Ki=1MPa)

		ε_{lcp}	ε_{tcp}	ε_{lcco}	ε_{tcco}	ε_{lccu} (ε_{lxxxp} , ε_{lxxxcu})	ε_{tccu} (ε_{txxxp} , ε_{txxxcu})
HPBF	FPC(SCH 41-1)-S1*	0.0014	0	0.002	0	0.01	0.0021
	FPC(SCH 41-1)-S2	0.0016	0	0.005	0	0.014	0.004
	FPC (SCH 41-2)-S1	0.001	0	0.0035	0	0.012	0.0028
	FPC (SCH 41-2)-S2*	0.0013	0	0.003	0	0.021	0.004
	FPC (11UP-2)-S1	0.002	0	0.007	0	0.038	0.0067
	FPC (11UP-2)-S2*	0.0017	0	0.0065	0	0.032	0.006
	FPG (SEH-1)-S1*	0.0015	0	0.006	0	0.022	0.0078
	FPG (SEH-1)-S2	0.007	0	0.01	0	0.03	0.01
	FPG (SEH-1)-S3	0.0018	0	0.002	0	0.017	0.0091
	FPG (SEH-2)-S1*	0.0015	0	0.004	0	0.023	0.009
	FPG (SEH-2)-S2	0.002	0	0.005	0	0.032	0.0091

Table X-12: Post-peak experimental data for longitudinal and transverse strains of HPBF confined concrete specimens (symbols in parenthesis represent the composite parameters)
(0.15 Ksi=1MPa)

		ϵ_{lco}	ϵ_{tco}	ϵ_{lcr}	ϵ_{tcr}	ν	T_t Mpa(Ksi)	TI_t
HPBF	FPC(SCH41-1)-S1*	-	-	0.01	0.0021	-	0.133(0.019)	2.60
	FPC(SCH41-1)-S2	-	-	0.014	0.004	-	0.22(0.032)	4.3
	FPC (SCH41-2)-S1	-	-	0.012	0.0028	-	0.2(0.03)	4
	FPC (SCH41-2)-S2*	-	-	0.021	0.004	-	0.267(0.04)	5.24
	FPC (11UP-2)-S1	-	-	0.038	0.0067	-	0.46(0.07)	8.9
	FPC (11UP-2)-S2*	-	-	0.025	0.006	-	0.4(0.06)	7.84
	FPG (SEH-1)-S1*	-	-	0.022	0.0078	-	0.34(0.051)	6.67
	FPG (SEH-1)-S2	-	-	0.03	0.01	-	0.43(0.06)	8.3
	FPG (SEH-1)-S3	-	-	0.017	0.0091	-	0.34(0.049)	6.7
	FPG (SEH-2)-S1*	-	-	0.023	0.009	-	0.54(0.081)	10.64
	FPG (SEH-2)-S2	-	-	0.032	0.0091	-	0.56(0.08)	10.9

FPC GRAPHICAL PRESENTATION-ALL SPECIMENS

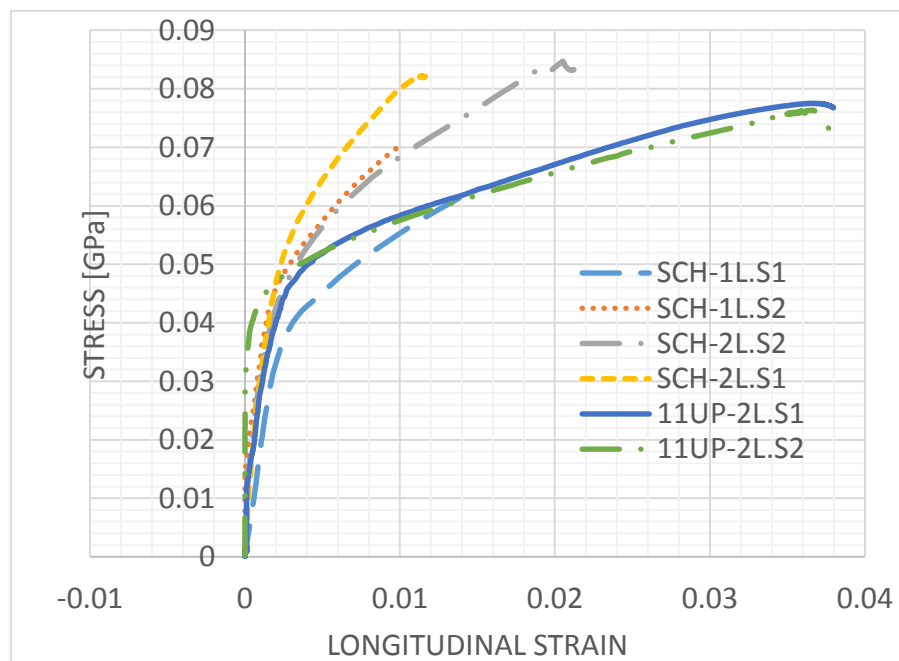


Figure X-19: Stress versus Longitudinal strain – 6FPC

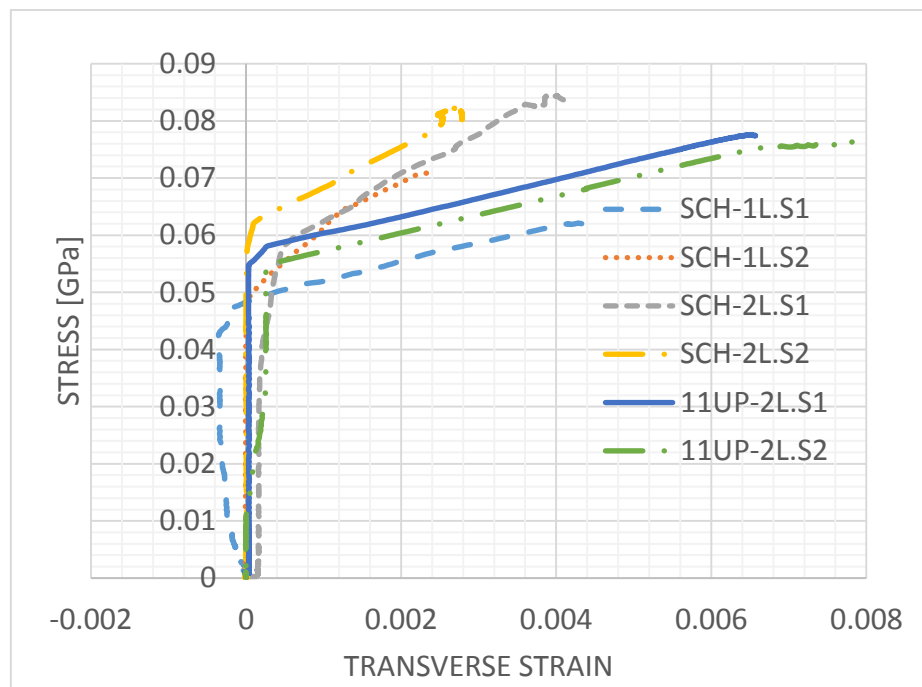


Figure X-20: Stress versus Transverse strain – 6FPC

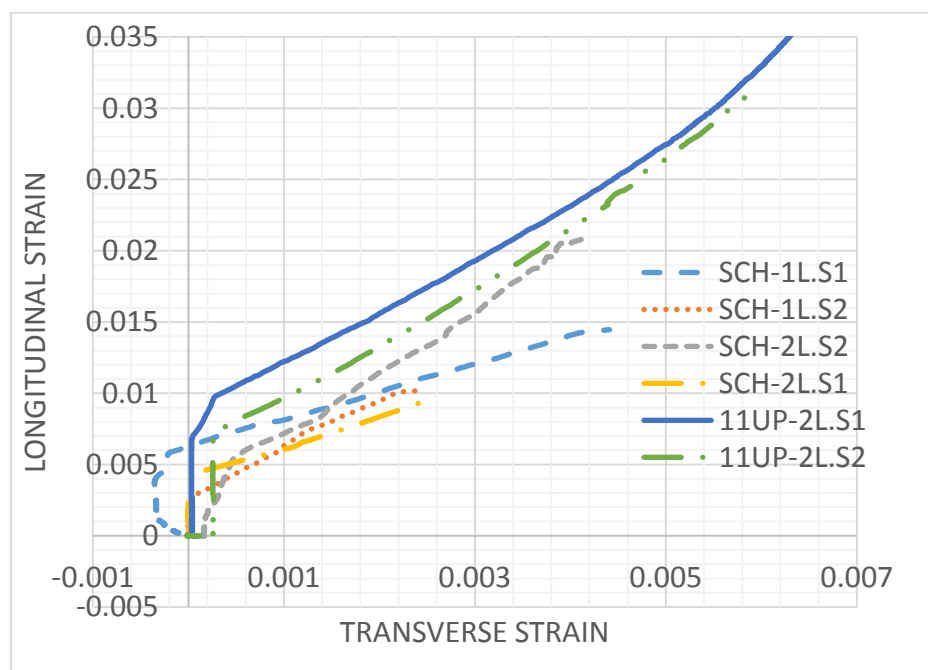


Figure X-21: Longitudinal versus Transverse strain – 6FPC

FPG GRAPHICAL PRESENTATION-ALL SPECIMENS

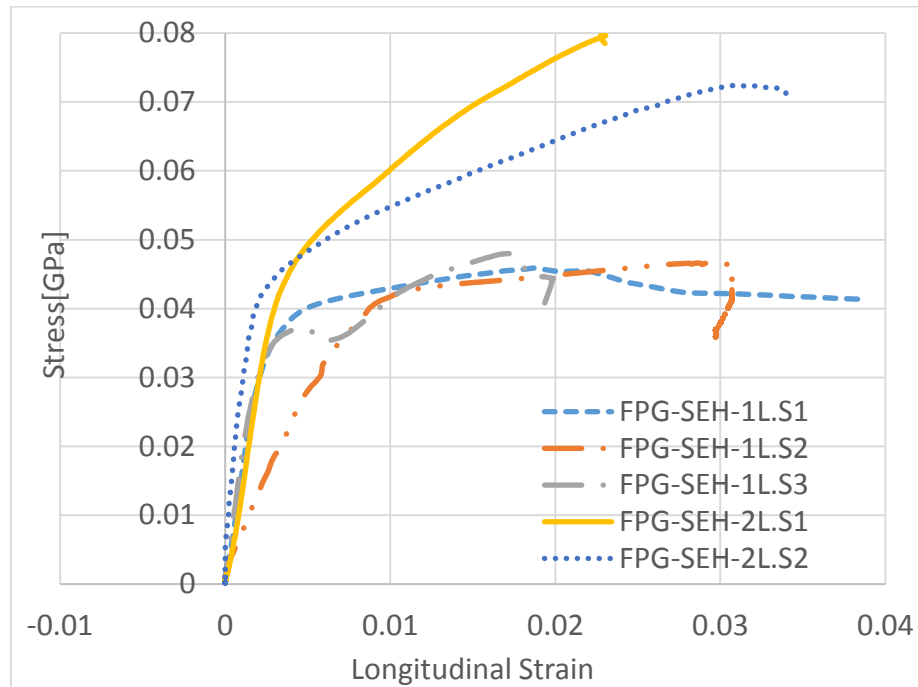


Figure X-22: Stress versus Longitudinal strain – 5FPG

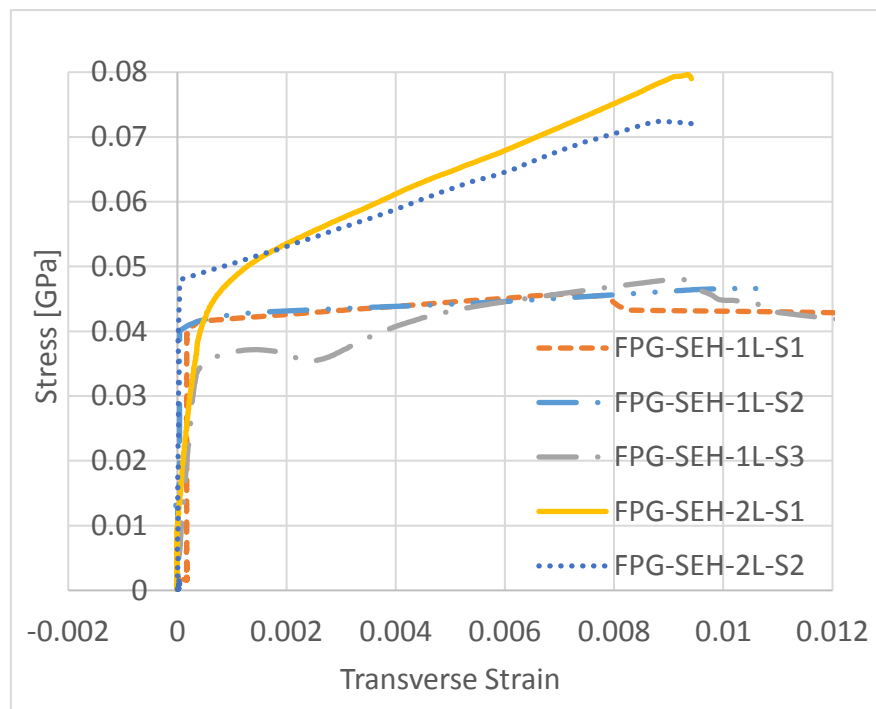


Figure X-23: Stress versus Transverse strain – 5FPG

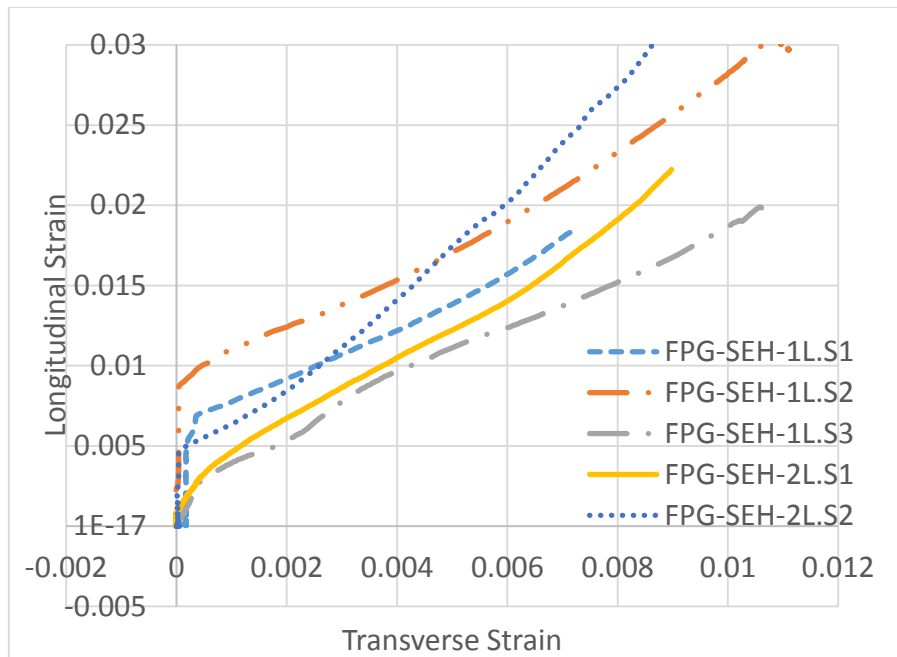


Figure X-24: Longitudinal versus Transverse strain – 5FPG

4. HPDF TESTED SAMPLES – TABULATED/GRAPHICAL EXPERIMENTAL RESULTS

Table X-13: Pre peak experimental data for longitudinal stress and strain of HPDF confined concrete specimens (0.15Ksi=1 MPa)

		E_{lcco}	σ_{lcp}	ϵ_{lcp}	E_{lc2}	E'_{lc2}	σ_{lcco}	ϵ_{lcco}
		Mpa(Ksi)	Mpa(Ksi)		Mpa(Ksi)	Mpa (Ksi)	Mpa(Ksi)	
HPDF	SIFC-S1*	32500 (4714)	26 (3.8)	0.0008	2500 (363)	2500 (363)	42 (6.1)	0.0014
	SIFC-S2	30000 (4351)	30 (4.3)	0.001	572 (83)	572 (83)	35 (5.1)	0.002
	SIFC-S3	20000 (2900)	20 (2.9)	0.001	-3600 (-522)	-3600 (-522)	25 (3.6)	0.0015
	SIFC-S4	15000 (2176)	30 (4.3)	0.002	715 (104)	715 (104)	44 (6.4)	0.005
	SIFC-S5	25000 (3626)	25 (3.6)	0.001	-1000 (-145)	-1000 (-145)	33 (4.8)	0.0018
	SIFC-S6	11000 (1595)	22 (3.2)	0.002	-1000 (-145)	-1000 (-145)	26 (3.8)	0.0028

Table X-14: Post- peak experimental data for longitudinal stress and strain of HPDF confined concrete specimens (0.15 Ksi=1 MPa)

		σ_{lccu} (σ_{lxxxp} , σ_{lxxxcu}) MPa(Ksi)	ε_{lccu} (ε_{lxxxp} , ε_{lxxxcu})	σ_{lco} (σ_{lxxxr}) MPa (Ksi)	ε_{lco} (ε_{lxxxr})	σ_{lcr} MPa (Ksi)	ε_{lcr}	T_t MPa (Ksi)	TI_t
HPDF	SIFC-S1*	52 (7.5)	0.004	50 (7.2)	0.0054	20 (2.9)	0.042	1.28 (0.18)	10
	SIFC-S2	44 (6.4)	0.0035	34 (4.9)	0.009	19 (2.7)	0.037	1.03 (0.15)	7.6
	SIFC-S3	33 (4.8)	0.0025	32 (4.6)	0.004	20 (2.9)	0.04	1.03 (0.15)	7.6
	SIFC-S4	47 (6.8)	0.007	39 (5.6)	0.015	23 (3.3)	0.054	1.82 (0.26)	13.5
	SIFC-S5	40 (5.8)	0.002	29 (4.2)	0.015	26 (3.8)	0.021	0.67 (0.09)	5
	SIFC-S6	37 (5.4)	0.005	35 (5.1)	0.012	24 (3.5)	0.026	0.77(0.11)	5.7

Table X-15: Pre-peak experimental data for longitudinal and transverse strains of HPDF confined concrete specimens (symbols in parenthesis represent the composite parameters)(0.15 Ksi=1 MPa)

		ε_{lcp}	ε_{tcp}	ε_{lcco}	ε_{tcco}	ε_{lccu} (ε_{lxxxp} , ε_{lxxxcu})	ε_{tccu} (ε_{txxxp} , ε_{txxxcu})
HPDF	SIFC-S1*	0.0008	0	0.0014	0	0.004	0.0013
	SIFC-S2	0.001	0	0.002	0	0.0035	0.00051
	SIFC-S3	0.001	0	0.0015	0	0.0025	0.0002
	SIFC-S4	0.002	0	0.005	0	0.007	0.00051
	SIFC-S5	0.001	0	0.0018	0	0.002	0.0005
	SIFC-S6	0.002	0	0.0028	0	0.005	0.0006

Table X-16: Post-peak experimental data for longitudinal and transverse strains of HPDF confined concrete specimens (symbols in parenthesis represent the composite parameters)(0.15Ksi=1 MPa)

		ε_{lco}	ε_{tco}	ε_{lcr}	ε_{tcr}	ν	T_t Mpa(Ksi)	TI_t
HPDF	SIFC-S1*	0.0054	0.003	0.042	0.016	-	0.685(0.103)	13.43
	SIFC-S2	0.009	0.006	0.037	0.016	-	0.52(0.075)	10.2
	SIFC-S3	0.004	0.0058	0.04	0.0075	-	0.24(0.035)	4.7
	SIFC-S4	0.015	0.006	0.054	0.019	-	0.68(0.098)	13.4
	SIFC-S5	0.015	0.002	0.021	0.005	-	0.16(0.023)	3.1
	SIFC-S6	0.012	0.0079	0.026	0.017	-	0.58(0.084)	11.3

SIFC GRAPHICAL PRESENTATION-ALL SPECIMENS

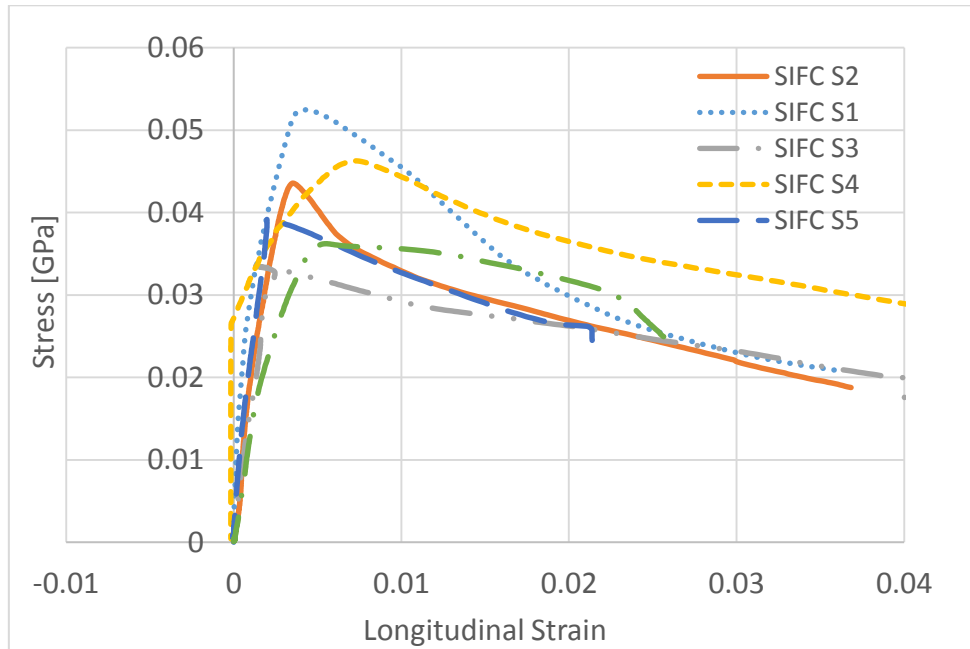


Figure X-25: Stress versus Longitudinal strain – 6SIFC

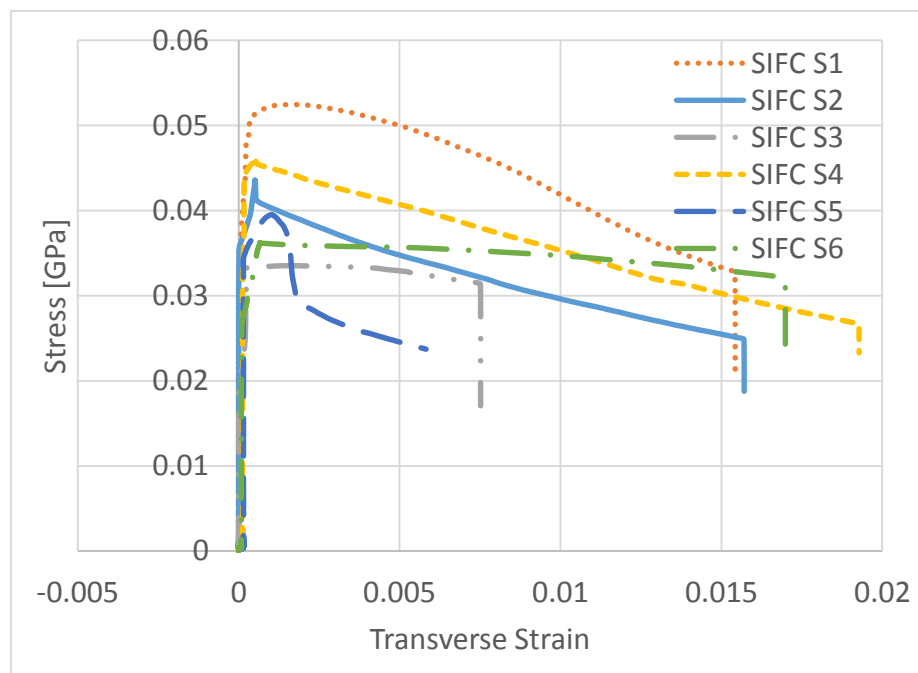


Figure X-26: Stress versus Transverse strain – 6SIFC

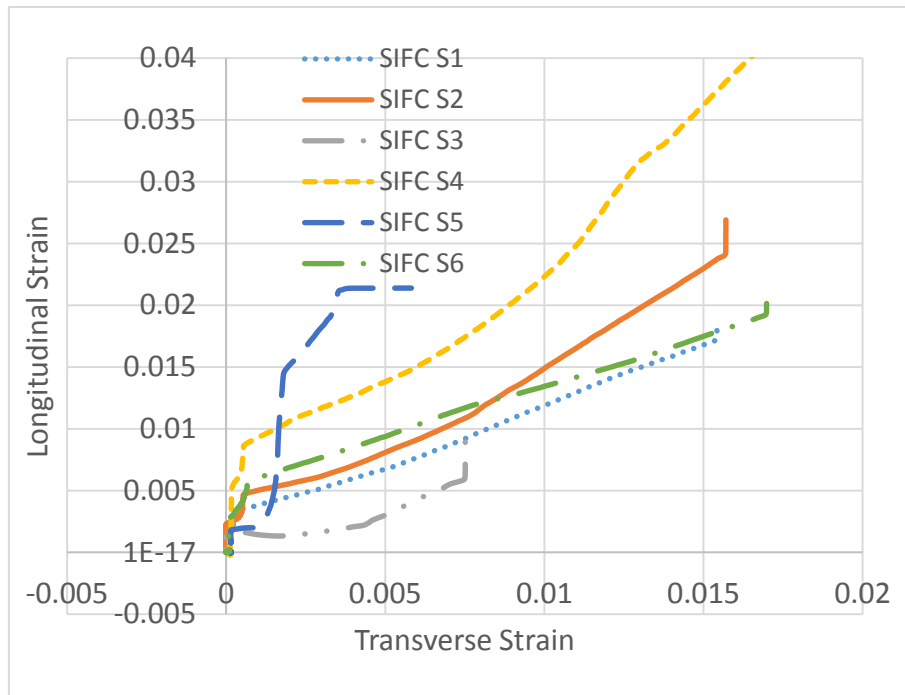


Figure X-27: Longitudinal versus Transverse strain – 6SIFC

XI. APPENDIX II: TENSILE STRESS STRAIN EQUATIONS FOR FIBROUS COMPOSITE CONFINEMENTS

All stresses and strains are applied at the plastic centroid r_{pl} of the composite from the center of the cylinder. Refer to Appendix IV for the location of the plastic centroid r_{pl} . Strains in the equations represent the modified strains to represent the composite response during confinement.

Proceeding equations are based on study done by Lee. Et.al³² for FRM, FRC and Naaman et.al³⁶ for SIFC, where analytical models for tensile behavior of steel-fiber concrete and slurry infiltrated fiber concrete were introduced. Some modification were done to the existing equations to take into account the actual tensile strain of the composite; in addition to relating the radial transverse strain to the tangential strain using the modified tensile strain of the composite.

FRM and FRC³²

$$\sigma_{lxxx} = E_{lxxx} \varepsilon_{lxxx}^* \quad 0 < \varepsilon_{lxxx}^* < \varepsilon_{lxxxp}^* \quad \text{Eq. (XI. 1)}$$

$$\sigma_{lxxx} = E_{lxxx} \left(\varepsilon_{lxxx}^* - \frac{\omega}{L} \right) \quad \varepsilon_{lxxxp}^* < \varepsilon_{lxxx}^* < \varepsilon_{lxxxcu}^* \quad \text{Eq. (XI. 2)}$$

$$\sigma_{lxxx} = \sigma_{lxxxcu} \frac{(0.1\varepsilon_{lxxx}^* + 1)}{(0.1\varepsilon_{lxxx}^* - 1)^2} \quad \varepsilon_{lxxxcu}^* < \varepsilon_{lxxx}^* < \varepsilon_{lxxxr}^* \quad \text{Eq. (XI. 3)}$$

$$E_{lxxx} = E_{mxxx} V_{mxxx} + E_{fxxx} V_{fxxx} \eta_l \eta_o \quad \text{Eq. (XI. 4)}$$

$$\varepsilon_{lxxxp} = \eta_l \eta_o' V_{fxxx} (\varepsilon_{fxxxp} - \varepsilon_{mxxxp}) + \varepsilon_{mxxxp} \quad \text{Eq. (XI. 5)}$$

$$\varepsilon_{lxxxp}^* = \mu_{lxxx} \varepsilon_{lxxxp} \quad \text{Eq. (XI. 6)}$$

$$\sigma_{lxxxcu} = \eta_l \eta_o' V_{fxxx} L_{xxx} \frac{\tau_{lxxx}}{2r_{xxx}} \quad \text{Eq. (XI. 7)}$$

$L = D_c$ and ω is the crack width that is determined from Eq. (XI.2) by iterations and the load deflection curves.

$$\varepsilon_{lxxxr} = \frac{\left(\frac{L_{xxx}}{16} \right)}{L^*} \quad \text{Eq. (XI. 8)}$$

$$\varepsilon_{lxxxr}^* = \zeta_{lxxx} \frac{\left(\frac{L_{xxx}}{16}\right)}{L^*} \quad \text{Eq. (XI. 9)}$$

L^* is the average crack spacing equal to πD_c since it is a single crack. μ_{lxxx} is the efficiency factor of the ascending branch related to the modified strain of Eq. (XI.1) and (XI.2), while ζ_{lxxx} is the efficiency factor of the descending branch related to the modified strain of Eq.(XI.3) and xxx is the index designation for (FRM) or (FRC) σ_{lxxx} and ε_{lxxx} is the tensile stress and strain of the composite at plastic centroid location, E_{lxxx} is the tensile composite modulus of elasticity, ε_{lxxxp} is the tensile strain at first crack or proportional limit, ε_{lxxxp}^* , ε_{lxxxcu}^* , ε_{lxxxr}^* are the modified first crack, peak and rupture strains of the composite at plastic centroid, E_{mxxx} and E_{fxxx} are the moduli of the matrix and fibers, V_{mxxx} and V_{fxxx} are the volume fractions of the matrix and fibers, ε_{fxxxp} and ε_{mxxxp} are the proportional limit strains of the fibers and matrix, ε_{lxxxp} is the first crack of the composite, η_l , η_o and η'_o are distribution factors of fiber orientation, L_{xxx} and r_{xxx} are the length and radius of the fibers, τ_{uxxx} is the ultimate elastic shear between matrix and fibers.

SIFC³⁶

$$\sigma_{lSIFC} = \sigma_{lSIFCcu} \left(1 - \left(1 - \left(\frac{\varepsilon_{lSIFC}^*}{\varepsilon_{lSIFCcu}^*} \right)^{D_{SIFC}} \right) \right) \quad 0 < \varepsilon_{lSIFC}^* < \varepsilon_{lSIFCcu}^* \quad \text{Eq. (XI. 10)}$$

$$\sigma_{lSIFC} = a e^{(-b(\varepsilon_{lSIFC}^* \left(\frac{L_{SIFC}}{2}\right)^m)} - c \left(\varepsilon_{lSIFC}^* \frac{L_{SIFC}}{2} \right)^n \quad \varepsilon_{lSIFCcu}^* < \varepsilon_{lSIFC}^* \quad \text{Eq. (XI. 11)}$$

$$a = \sigma_{lSIFCcu} \quad \text{Eq. (XI. 12)}$$

$$c = 2 \frac{e^{(-b\left(\left(\frac{L_{SIFC}}{2}\right)^m)} - \sigma_{lSIFCcu}}{L_{SIFC}} \quad \text{Eq. (XI. 13)}$$

$$b = \frac{(m-1)}{m\delta_{it}^m} \quad \text{Eq. (XI. 14)}$$

$$m = \frac{1}{\left[1 + \ln \left[\frac{\sigma_{it}}{\sigma_{lSIFCcu}} + c\delta_{it} \right] \right]} \quad \text{Eq. (XI. 15)}$$

$$\sigma_{it} = 0.6\sigma_{ISIFCCu} \text{ and } \delta_{it} = \frac{0.01V_{fSIFC}L_{SIFC}^2}{\phi_{SIFC}} \quad \text{Eq. (XI. 16)}$$

$$\sigma_{ISIFCCu} = \frac{V_{fSIFC}L_{SIFC}}{d_f} \frac{(200 + 8\sqrt{f_o})}{3} \quad (US) \quad \text{Eq. (XI. 17)}$$

$$\sigma_{ISIFCCu} = \frac{V_{fSIFC}l_{SIFC}}{d_f} \frac{(1.4 + 0.66\sqrt{f_o})}{3} \quad (METRIC) \quad \text{Eq. (XI. 18)}$$

$$E_{ISIFC} = E_{mSIFC}V_{mSIFC} + \frac{E_{fSIFC}V_{fSIFC}}{30} \quad \text{Eq. (XI. 19)}$$

$$\varepsilon_{ISIFCCu} = \varepsilon_{lmSIFCCu} + 0.00174 \frac{V_{fSIFC}L_{SIFC}}{\phi_{SIFC}} \quad \text{Eq. (XI. 20)}$$

$$\varepsilon_{ISIFCCu}^* = \mu_{ISIFC}\varepsilon_{ISIFCCu} \quad \text{Eq. (XI. 21)}$$

$$D_{SIFC} = E_{ISIFC} \frac{\varepsilon_{ISIFCCu}^*}{\sigma_{ISIFCCu}} \quad \text{Eq. (XI. 22)}$$

$$\varepsilon_{ISIFCr} = \frac{\left(\frac{L_{cr}}{16}\right)}{L^*} \text{ and } \varepsilon_{ISIFCr}^* = \zeta_{ISIFC} \frac{\left(\frac{L_{cr}}{16}\right)}{L^*} \quad \text{Eq. (XI. 23)}$$

$$L_{cr} = \frac{\sigma_{lfSIFCCu}\phi_{SIFC}}{2\tau_{uSIFC}} \quad \text{Eq. (XI. 24)}$$

$L^* = \pi \frac{D_c}{4}$ since there are 4 cracks as obtained from the main paper. μ_{ISIFC} is the efficiency factor of the ascending branch related to the modified strain of Eq (XI.10), while ζ_{ISIFC} is the efficiency factor of the descending branch related to the modified strain of Eq (XI.11)

σ_{ISIFC} and ε_{ISIFC} are the tensile stress and strain of (SIFC) at plastic centroid location, E_{ISIF} is the tensile composite modulus of elasticity, f_o is the compressive strength of SIFC, $\varepsilon_{ISIFCCu}^*$ ε_{ISIFCr}^* are the modified peak and rupture strains of the composite, $\sigma_{ISIFCCu}$ and σ_{ISIFCr} are the stresses of the composite at peak and rupture, E_{mSIFC} and E_{fSIFC} are the moduli of the matrix and fibers, V_{mSIFC} and V_{fSIFC} are the volume fractions of the matrix and fibers, L_{SIFC} and ϕ_{SIFC} are the length and diameter of the

fibers, τ_{uSIFC} is the ultimate elastic shear between matrix and fibers, L_{cr} is the critical length at debonding of the fibers and ε_{SIFC}^* is the modified tensile strain of the composite.

XII. APPENDIX III: GENERAL STRESS STRAIN MODEL FOR DISCRETE AND CONTINUOUS CONFINEMENTS

In the composite activation region, the stress-strain relationship of confined concrete consists of a series of straight lines following the tensile behavior of the composite and the concept of Mohr Circles for stress and strain as shown in Figures XII-1 (a) and (b). For spirals, wire mesh, FRP's, the activation region is represented by one straight line based on the tensile stress-strain linear relationship of the composite. For FRM and FRC, the activation region is represented by two lines: (1) one corresponding to the response prior to the tensile first crack of the composite and (2) the other for the tensile response between the first crack and the peak composite stress. For SIFC, the activation region consists of a series of straight lines representing the multiple cracking mechanism.

Behavior in this region is simplified by a straight line stress-strain curve derived from ACI 440⁸ using the generalized constants A_1 through F_1 :

$$\sigma_{lc} = A_1 \sigma'_{cc} + \psi_f k_a B_1 \sigma_2 \quad \text{Eq. (XII. 1)}$$

$$\varepsilon_{lc} = C_1 \varepsilon'_c + D_1 k_b \frac{\sigma_2 (\varepsilon_{lxxx}^*)^{E_1}}{\sigma'_{cc} (\varepsilon'_c)^{F_1}} \quad \text{Eq. (XII. 2)}$$

$$\sigma_2 = f(\sigma_{lxxx}) = \frac{2\sigma_{lxxx} A_{lxxx}}{A_{cc}} \quad \text{Eq. (XII. 3)}$$

where A_{lxxx} is the area of the composite, and D_c is the core diameter, σ_{lxxx} and ε_{lxxx}^* are the corresponding tensile stress and modified strain of the composite (details of the modified strain are explained in the subsequent text). σ_2 is the general lateral stress (function of the composite tensile stress). $A_{cc} = D_c s_{xxx}$ is the effective area of concrete enclosed by the composite, s_{xxx} is spacing of lateral confinement (i.e., spirals or wire mesh), and σ'_{cc} is the compressive stress of the concrete core at

the start of composite activation (start of lateral expansion and initiation of tensile stresses in composite).

xxx index designates type of the composite as defined in the list of notations.

$$\sigma'_{cc} = \sigma'_c \frac{A_g}{A_c} = \sigma'_c \frac{\frac{\pi(D_c + 2t_{xxx})^2}{4}}{\frac{\pi D_c^2}{4}} \quad \text{Eq. (XII. 4)}$$

Equation (XII.4) represents the compressive stress in the concrete core at the start of lateral expansion and activation of the composite. The composite and concrete core act independently where the ultimate unconfined peak load of concrete $\sigma'_c A_g$ is now resisted only by the concrete core.

A_g is the gross area of the cylinder, A_c is the concrete core area, and t_{xxx} is thickness of the composite member for continuous composites or cover for spirals.

$\sigma'_{cc} = \sigma'_c$ for wire mesh composites since the outside thickness is insignificant ($t_{xxx} = 0$). $\sigma'_{cc} > \sigma'_c$ for spirals, fibrous composites and FRP's, based on equation (XII.4), where t_{xxx} is the cover to the spirals or thickness of the composites.

Each value of stress and strain of confined concrete in the activation region has an associated set of constants A_1 through F_1 for each composite type presented in, Table V.1. These constants represent different experimentally obtained factors corresponding to different confinement levels. As shown in equations (XII.1) and (XII.2), factors A_1, C_1, F_1 depend only on the strength of unconfined concrete. Hence, these factors are independent of the composite type or the stress level. Factors $B_1, D_1,$ and E_1 depend on the composite type, but are also stress independent. $k_a = k_b = 1$ and $\psi_f = 0.95$.

Concept of Mohr Circle of Stress and Strain in the Activation Region

Based on the ACI 440⁸, the peak stress and strain curves in the activation region are approximated by the following equations:

$$\sigma_{lc} = \sigma'_{cc} \pm f(\sigma_{lxxx}) \quad \text{Eq. (XII. 5)}$$

$$\varepsilon_{lc} = 1.5\varepsilon'_c \pm f(\varepsilon_{lxxx}) \quad \text{Eq. (XII. 6)}$$

where σ_{lc} and ε_{lc} are the principal stresses and strains of confined concrete in the activation region, σ'_{cc} is the stress in the concrete core at the start of activation of composite, σ_{lxxx} and ε_{lxxx} are the tensile stresses of the composite, and ε'_c is the strain at peak of unconfined concrete. The (+) sign is for full confinement while the (-) is for partial confinement since the composite stresses reduce the confinement effects. As shown in Figures XII.1 (a) and (b), during confinement, the Mohr circles remain fixed at the origin until the diameter equals σ'_{cc} or $1.5\varepsilon'_c$. During activation of the composite the Mohr circles push to the right for full confinement or to the left for partial confinement with a constant diameter of σ'_{cc} or $1.5\varepsilon'_c$. Each position of the Mohr circle represents a level of tensile stress and strain of the composite until reaching peak where the stresses and strains at peak of confined concrete are presented by:

$$\sigma_{lccu} = \sigma'_{cc} \pm f(\sigma_{lxxxcu}) \quad \text{Eq. (XII. 5. a)}$$

$$\varepsilon_{lccu} = 1.5\varepsilon'_c \pm f(\varepsilon_{lxxxcu}) \quad \text{Eq. (XII. 6. a)}$$

Derivation of Peak Stress and Strain Factors for Discrete Confinements

The peak stress and strain based on the developed model in this work are presented by the following equations:

$$\sigma_{lccu} = A_1\sigma'_{cc} + \psi_f k_a B_1 \sigma_{2cu} \quad \text{Eq. (XII. 7)}$$

$$\varepsilon_{lccu} = C_1\varepsilon'_c + D_1 k_b \frac{\sigma_{2cu}}{\sigma'_c} \frac{(\varepsilon_{lxxxcu}^*)^{E_1}}{(\varepsilon'_c)^{F_1}} \quad \text{Eq. (XII. 8)}$$

$$\psi_f = 0.95, \quad k_a = k_b = 1 \quad \text{Eq. (XII. 9)}$$

The Todechini⁹ peak stress and strain are presented by equations (XII.10) and (XII.11)

$$\sigma_{lccu} = \sigma'_c + 4.1\sigma_{2cu} \quad \text{Eq. (XII. 10)}$$

$$\varepsilon_{lccu} = \frac{G_1\sigma_{lccu}}{E_{lcco}} \quad \text{Eq. (XII. 11)}$$

A_1 to F_1 are the factors, σ_{2cu} is the lateral stress at peak and ε_{lxxxcu}^* is the modified peak strain of the composite.

The constants A_1 to G_1 are determined by equating equations (XII.7) and (XII.8) to the stress and strain equations (XII.10) and (XII.11).

$$\sigma_{lccu} = \sigma'_c + 4.1\sigma_{2cu} \quad \Rightarrow \quad A_1 = 1 \quad \text{Eq. (XII. 12)}$$

$$4.1 = \psi_f k_a B_1 \quad \text{Eq. (XII. 13)}$$

$$B_1 = \frac{4.1}{\psi_f k_a} = 4.32 \quad \text{Eq. (XII. 14)}$$

$$\varepsilon_{lccu} = \frac{G_1\sigma_{lccu}}{E_c} = \frac{G_1(\sigma'_c + 4.1\sigma_{2cu})}{E_c} \quad \text{Eq. (XII. 15)}$$

$$\varepsilon_{lccu} = \frac{G_1(\sigma'_c)}{E_c} + \frac{G_1(4.1)\sigma_{2cu}}{E_c} \quad \text{Eq. (XII. 16)}$$

Since $E_{ci} = 0.58E_c$ is the inelastic modulus of concrete¹⁹ and substituting in Eq. (XII.16)

$$\varepsilon_{lccu} = \frac{G_1(\sigma'_c)}{1.71E_{ci}} + \frac{G_1(4.1)\sigma_{2cu}}{1.71E_{ci}} \quad \text{Eq. (XII. 17)}$$

and

$$E_{ci} = \frac{\sigma'_c}{\varepsilon'_c} \quad \text{Eq. (XII. 18)}$$

Substituting equation (XII.18) in equation (XII.17)

$$\varepsilon_{lccu} = \frac{G_1(\varepsilon'_c)}{1.71} + \frac{G_1(4.1)\sigma_{2cu}\varepsilon'_c}{1.71\sigma'_c} \quad \text{Eq. (XII. 19)}$$

$$\varepsilon_{lccu} = \frac{G_1(\varepsilon'_c)}{1.71} + 2.52G_1\psi_f k_b \frac{\sigma_{2cu}}{\sigma'_c} \frac{(\varepsilon_{lxxxcu}^*)^0}{(\varepsilon'_c)^{-1}} \quad \text{Eq. (XII. 20)}$$

$$C_1 = \frac{G_1}{1.71} \quad \text{Eq. (XII. 21)}$$

$$D_1 = 2.52G_1 \quad \text{Eq. (XII. 22)}$$

$E_1 = 0$ and $F_1 = -1$. So the only factors that are variables with the different composite types are B_1 , D_1 and E_1 but remain constant for the different stress levels during the activation region for each particular composite type. $G_1 = 3$ for discrete confined concrete and $G_1 = 1.71$ for unconfined concrete based on the Todechini model⁹.

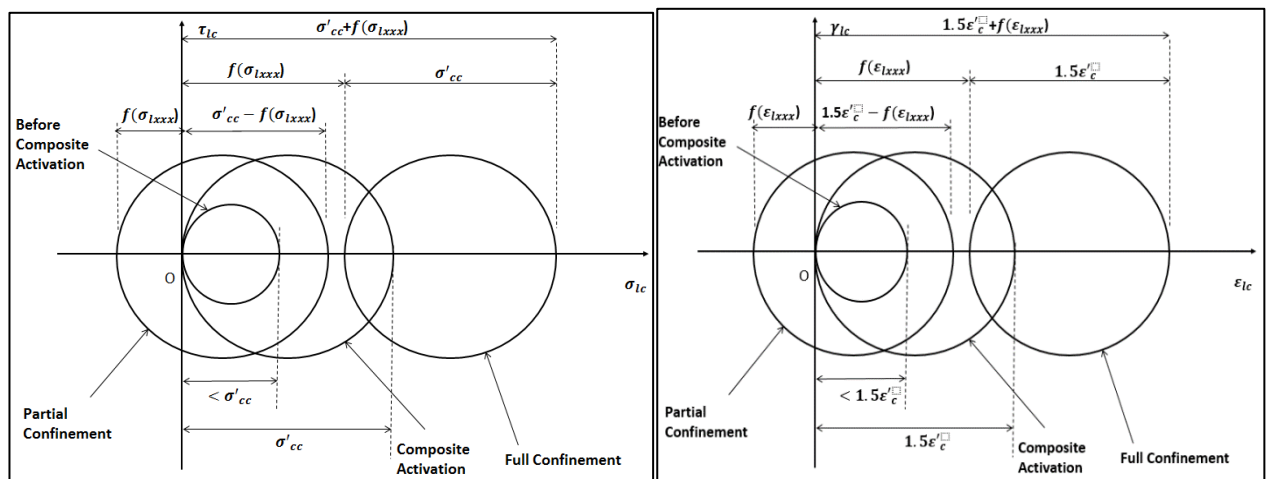


Figure XII-1: (a) Mohr circle for lateral confining stresses (b) Mohr circle for lateral confining Strains

XIII. APPENDIX IV: LOCATION OF THE PLASTIC CENTROID AND LATERAL STRESS FOR PARTIAL CONFINEMENT

Location of Plastic Centroid (Refer to Figure XIII.1a): The location of the plastic centroid and the tensile stress of the composite at that location is required. Plastic centroid is the location of the resultant of the tensile composite stress distribution across its thickness. The tensile strain of the composite at a location r can be defined as linear with the radius of the column.

$$\varepsilon_{lxxx}^* = \mu_{lxxx} \alpha \varepsilon_{tc} \frac{r}{\left(\frac{D_c}{2} + t_{xxx}\right)} \quad \text{Eq. (XIII. 1)}$$

Where r represents the radius from center of cylinder to a point within the composite, ε_{tc} is the transverse strain at the circumference, and ε_{lxxx}^* is the modified circumferential strain of composite at location r from the center. The stress is a function of strain

$$\sigma_{lxxx} = f(\varepsilon_{lxxx}^*) \quad \text{Eq. (XIII. 2)}$$

σ_{lxxx} is the tensile stress of the composite as a function of the modified tensile strain ε_{lxxx}^* based on the stress-strain relationship of the composite. Since ε_{lxxx}^* is a function of the radius r , σ_{lxxx} is a function of r . The plastic centroid location can be obtained as follows:

$$r_{pl} = \frac{\int_0^{\frac{D_c}{2} + t_{xxx}} r \sigma_{lxxx} A_{lxxx} dr}{\int_0^{\frac{D_c}{2} + t_{xxx}} \sigma_{lxxx} A_{lxxx} dr} \quad \text{Eq. (XIII. 3)}$$

r_{pl} is the location of the plastic centroid within the composite where the resultant stress is applied. A_{lxxx} is the area of the composite normal to the applied tensile stress.

At different points of the ascending portion of the stress strain curve (activation region), the generalized strain at the plastic centroid is

$$\varepsilon_{lxxx}^* = \mu_{lxxx} \alpha \varepsilon_{tc} \frac{r_{pl}}{\left(\frac{D_c}{2} + t_{xxx}\right)} \quad \text{Eq. (XIII. 4)}$$

Lateral Stress at peak at the plastic centroid is obtained from equation (XIII.2)

$$\text{Where } \sigma_{lxxxcu} = f(\varepsilon_{lxxxcu}^*) \quad \text{Eq. (XIII. 5)}$$

Lateral Strain at peak at the plastic centroid is obtained from equation (XIII.4)

$$\varepsilon_{lxxxcu}^* = \mu_{lxxx} \varepsilon_{lxxxcu} \quad \text{Eq. (XIII. 6)}$$

$$\varepsilon_{lxxxcu}^* = \mu_{lxxx} \alpha \varepsilon_{tcu} \frac{r_{pl}}{\left(\frac{D_c}{2} + t_{xxx}\right)} \quad \text{Eq. (XIII. 7)}$$

σ_{lxxxcu} and σ_{lxxx} , are obtained from the tensile stress strain equations for the composites.

- Stress strain equations for Composite (FPC) and (FPG)

$$\sigma_{lxxx} = E_{lxxx} \varepsilon_{lxxx}^* \quad \text{Generalized} \quad \text{Eq. (XIII. 8)}$$

$$\sigma_{lxxxcu} = E_{lxxx} \varepsilon_{lxxxcu}^* \quad \text{At peak} \quad \text{Eq. (XIII. 9)}$$

- Stress strain equations for Composite (FRM) and (FRC)³²

Refer to appendix II for the equations of stress and strain in tension for (FRM) and (FRC)

- Stress strain equations for (SIFC)³⁶

Refer to appendix II for the equations of stress and strain in tension for (SIFC)

Lateral Stress for Partial Confinement (Refer to Figure XIII.1(b)): For the case of partial confinement²¹, there is a radial transverse force in the composite due to the fibers in the transverse direction as shown in Figure XIII.1(b) that reduce the lateral force within the concrete core. Based on equilibrium, following equations can be obtained:

$\sigma_{txxx} r_{pl} d\theta s_{xxx}$ can be resolved into two components $\sigma_{txxx} r_{pl} d\theta s_{xxx} \cos(\theta)$ and $\sigma_{txxx} r_{pl} d\theta s_{xxx} \sin(\theta)$ where r_{pl} is the location of the plastic centroid σ_{txxx} is the

transverse tensile stress of the composite at the plastic centroid, s_{xxx} is the spacing of the composite and θ is the angle that the stress makes with the horizontal axis.

Using equilibrium and from Figure XIII.1 (b)

$$s_{xxx}\sigma_2 D_c + \int_0^\pi \sigma_{txxx} r_{pl} d\theta (s_{xxx}) \sin(\theta) = 2\sigma_{lxxx} t_{xxx} s_{xxx} \quad \text{Eq. (XIII. 10)}$$

$$\sigma_2 = \frac{2\sigma_{lxxx} t_{xxx}}{D_c} - \frac{2\sigma_{txxx} r_{pl}}{D_c} \quad \text{Eq. (XIII. 11)}$$

σ_{lxxx} is the tangential tensile stress of the composite. Equation (XIII.11) leads to negative values for the σ_2 resulting in partial confinement and stress at peak lower than that of unconfined concrete. The above equations can be generalized for the state at peak with a lateral stress σ_{2cu} .

$$\sigma_{2cu} = \frac{2\sigma_{lxxx} t_{xxx}}{D_c} - \frac{2\sigma_{txxx} r_{pl}}{D_c} \quad \text{Eq. (XIII. 12)}$$

where σ_{txxxcu} represents the transverse tensile stress of the composite in the radial direction. The value of σ_{txxxcu} is determined using Eq.(XIII.13) below and by multiplying (a) the modulus of elasticity in the transverse direction, with (b) the peak tensile strain of the composite³⁶

$$\sigma_{txxxcu} = E_{fxxx} V_{fxxx} (1 - \eta_l) (1 - \eta_o) \varepsilon_{lxxx}^* \quad \text{Eq. (XIII. 13)}$$

where E_{fxxx} is the modulus in tension of the fibers, V_{fxxx} is the volume fraction of the fibers, ε_{lxxx}^* is the modified peak strain of composite at plastic centroid, while η_l and η_o are fiber distribution factors.

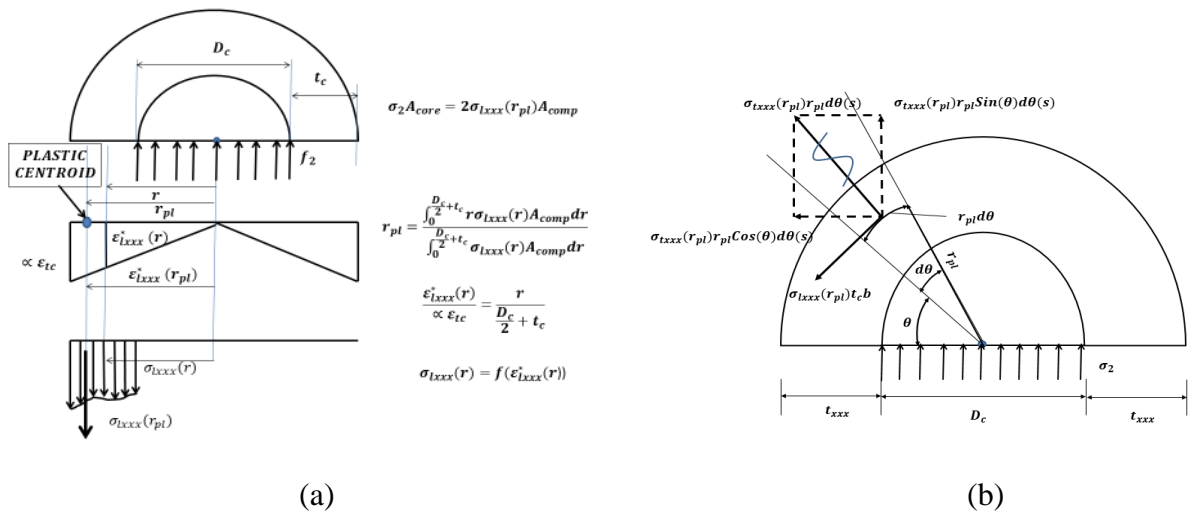


Figure XIII-1: (a) Location of plastic centroid of composite (b) Partial confinement stresses in FRM and FRC

$$\sigma_2 A_{core} = 2\sigma_{lxxx}(r_{pl})A_{comp}$$

$$r_{pl} = \frac{\int_0^{\frac{D_c}{2}+t_c} r\sigma_{lxxx}(r)A_{comp}dr}{\int_0^{\frac{D_c}{2}+t_c} \sigma_{lxxx}(r)A_{comp}dr}$$

$$\frac{\epsilon_{lxxx}^c(r)}{\propto \epsilon_{tc}} = \frac{r}{\frac{D_c}{2} + t_c}$$

$$\sigma_{lxxx}(r) = f(\epsilon_{lxxx}^c(r))$$